


2009

Analytical Modeling of Tree Vibration Generated during Cutting Process

Payman Karvanirabori

University of Massachusetts Amherst, paymaan@gmail.com

Follow this and additional works at: <http://scholarworks.umass.edu/theses>

 Part of the [Civil and Environmental Engineering Commons](#), [Computational Engineering Commons](#), [Mechanical Engineering Commons](#), and the [Other Engineering Commons](#)

Karvanirabori, Payman, "Analytical Modeling of Tree Vibration Generated during Cutting Process" (2009). *Masters Theses 1911 - February 2014*. 358.

<http://scholarworks.umass.edu/theses/358>

This thesis is brought to you for free and open access by the Dissertations and Theses at ScholarWorks@UMass Amherst. It has been accepted for inclusion in Masters Theses 1911 - February 2014 by an authorized administrator of ScholarWorks@UMass Amherst. For more information, please contact scholarworks@library.umass.edu.

ANALYTICAL MODELING OF TREE VIBRATION GENERATED
DURING CUTTING PROCESS

A Thesis Presented
by
PAYMAN KARVANIRABORI

Submitted to the Graduate School of the
University of Massachusetts Amherst in partial fulfillment
of the requirements for the degree of

MASTER OF SCIENCE IN CIVIL ENGINEERING

SEPTEMBER 2009

Civil and Environmental Engineering Department
Structural Engineering and Mechanics

ANALYTICAL MODELING OF TREE VIBRATION GENERATED
DURING CUTTING PROCESS

A Thesis Presented
by
PAYMAN KARVANIRABORI

Approved as to style and content by:

Sergio F. Brena, Chair

Thomas J. Lardner, Member

Brian Kane, Member

Richard N. Palmer, Department Head
Civil and Environmental Engineering Department

ACKNOWLEDGMENTS

I would like to thank my advisor, Sergio F. Brena, for his guidance and support. I would also like to extend my gratitude to the members of my committee, Thomas J. Lardner and Brian Kane for their helpful comments and suggestions on all stages of this project.

Special thanks to all those whose support and friendship helped me to stay focused on the project and provided me with the encouragement to continue when the going got tough.

ABSTRACT

ANALYTICAL MODELING OF TREE VIBRATION GENERATED DURING CUTTING PROCESS

SEPTEMBER 2009

PAYMAN KARVANIRABORI, B.S., SHARIF UNIVERSITY OF TECHNOLOGY
M.S.C.E., UNIVERSITY OF MASSACHUSETTS AMHERST

Directed by: Professor Sergio F. Brena

There are several ways to cut down a tree. The piece by piece cutting method is studied in this research. By modeling the cutting process into simple dynamic models and obtaining governing equations of motion of tree and cut piece in each model, the forces during cutting process were calculated. The method was then applied to a set of real data and tree vibrations were compared with field measurements. The study is very rare in the case of the variety of the topics it covers from dynamics and mechanics to finite element modeling of a biological system.

CONTENTS

	Page
ACKNOWLEDGMENTS.....	iii
ABSTRACT.....	iv
LIST OF TABLES.....	viii
LIST OF FIGURES.....	x
CHAPTER	
1. INTRODUCTION	1
1.1. Technical Background	1
1.2. Objectives	3
1.3. Significance of the Research.....	4
1.4. Literature Review.....	6
1.4.1. Mathematical Modeling.....	6
1.4.2. Free Vibration Experiments.....	7
1.4.3. Factor of Safety.....	9
1.5. Field Measurements	10
1.6. Scope of Thesis	16
2. MOTION FUNCTION OF CUT PIECE AND INDUCED APICAL LOADS DUE TO CUTTING PROCESS.....	18
2.1. Modeling of Stages A, B and C	20
2.1.1. Simplified Method (Modeling of Stages A, B and C)	25
2.1.2. Results (Modeling of Stages A, B and C).....	29
2.1.3. Verification of Results by the Energy Method	39
2.2. Modeling of Stage D.....	41
2.2.1. Results (Modeling of Stage D)	47
2.2.2. Verification of Results by the Energy Method	53
2.3. Modeling of Stage E	54
2.3.1. Simplified Method (Modeling of Stage E)	61
2.3.2. Results (Detailed modeling of Stage E).....	65

2.3.3. Verification of Results by the Energy Method	70
2.4. Modeling of Stage F.....	72
2.4.1. Results (Modeling of Stage F)	74
2.5. Summary of Results.....	76
3. VERIFICATION OF CALCULATED APICAL LOAD FUNCTION WITH EXPERIMENTAL DATA.....	80
3.1. Finite Element Modeling	80
3.1.1. Modal Analysis and Verification of Finite Element Model.....	81
3.1.2. Effect of Dimension and Material Parameters on Dynamic Properties of Tree.....	86
3.1.3. Modification of Finite Element Model.....	98
3.1.4. Dynamic Analysis of FE Model under Apical Forces during Cutting Process	100
3.2. Simplification of FE model.....	106
3.3. Analytical Method to Obtain Axial Strain near the Bottom of the Tree from Displacement of Tree Top	109
4. SENSITIVITY STUDY OF THE CALCULATION OF CUT PIECE MOTION AND APPLIED FORCE	113
4.1. Initial Rotation of Cut Piece.....	114
4.2. Linear Velocity (V_{Δ})	119
4.3. Height of Tree Trunk	124
4.4. Mass of Cut Piece	130
4.5. Diameter of Tree Trunk	136
5. CONCLUSION.....	143
5.1. Future research on the topic.....	147
APPENDICES	
A. CALCULATING M, K AND C OF THE TRUNK SIMPLIFIED MODEL	148
B. STUDY OF THE MODELING OF TREE TRUNK AS A SIMPLIFIED DYNAMIC MODEL	151
C. PULLEY AND ROPE MODELING	158
D. RUNGE KUTTA METHOD OF ORDER FOUR (RK4).....	159

E.	LAGRANGIAN APPROACH	158
F.	INFORMATION ABOUT RED PINE	160
G.	TREE NO.7 MEASUREMENTS AND DATA	162
H.	TRUNK DEFECTS WHICH MAY CAUSE FAILURE.....	163
I.	CODES WRITTEN IN C++	164
	BIBLIOGRAPHY.....	173

LIST OF TABLES

TABLE	Page
1.1. Typical data collected during field cutting	12
1.2. Calculation of damping ratio (Refer to equation 1.1)	15
2.1. Motion initial condition: Stage A, B and C	29
2.2. Motion initial condition: Stage A, B and C	33
2.3. Summary of results: Stage A, B and C	36
2.4. Motion initial condition: Stage D	47
2.5. Summary of results: Stage D	51
2.6. Final condition of motion at end of stage D	52
2.7. Motion initial condition: Stage E	65
2.8. Analysis results: Stage E	65
2.9. Motion final condition: Stage E	69
2.10. Impact condition (Stage F)	74
3.1. Tree No.7 field parameters	81
3.2. FEM modal analysis result for tree No.7	83
3.3. Defect Dimensions	93
3.4. Amount of error required to cause 31% error in natural frequency	98
3.5. Comparison of axial strain from FEM and field measurements (Refer to Figure 3.20)	102
3.6. Comparison of axial strain from FEM and field measurements (Refer to Figure 3.23)	104
3.7. Modeling with beam element	106

4.1.Parameters of motion of the cut piece and applied force function during cutting process.....	118
4.2.Parameters of motion of the cut piece and applied force function during cutting process	122
4.3.Variation of dynamic properties of tree trunk with height	124
4.4.Parameters of motion of the cut piece and applied force function during cutting process.....	128
4.5.Parameters of motion of the cut piece and applied force function during cutting process.....	134
4.6.Variation of dynamic properties of tree trunk with height	136
4.7.Parameters of motion of the cut piece and applied force function during cutting process.....	141
5.1.Sensitivity of maximum force to each parameter.....	145
B.1.Tree No.7 dynamic properties from Appendix A.....	152
G.1.Field Measurement Data.....	162

LIST OF FIGURES

FIGURE	Page
1.1.Cutting process (Adapted from a drawing of tree shapes by USFS-TAMU).....	1
1.2.Location of probes on tree trunk.....	10
1.3.Measurements - tree dimensions.....	11
1.4.Variation of axial strain with time (Probe 2 is in the direction of fall).....	13
2.1.Cutting process modeling	18
2.2.Stages A, B and C model sketch: (a, c) Geometry (b, d) Forces	21
2.3.Free diagram of cut piece.....	23
2.4.Sketch of stages A, B and C simplified model	25
2.5.Accelerations - simplified model of stages A, B and C.....	27
2.6.Variation of piece angle (θ) with time	30
2.7.Variation of horizontal acceleration of the CG of the piece with time.....	30
2.8.Variation of horizontal force with time	31
2.9.Variation of deflection and velocity of tree top with time during stages A, B, C	32
2.10.Variation of horizontal force applied to the tree top with time.....	34
2.11.Variation of angle and angular velocity of piece (θ , $\dot{\theta}$) with time.....	34
2.12.Variation of deflection and velocity of tree top with time during stages A, B, C ...	35
2.13.Variation of horizontal force with time during stage A, B, C.....	37
2.14.Variation of deflection of tree top with time during stages A, B, C.....	38
2.15.Variation of velocity of tree top with time during stages A, B, C.....	38
2.16.Variation of energy terms with time in stages A, B, C.....	39
2.17.Variation of energy terms with time in stages A, B, C.....	40

2.18. Release moment (end of stage C)	41
2.19. Velocity of falling piece a moment after release instant.....	43
2.20. Modeling of stage D–Movement of CG of the piece.....	44
2.21. Variation of displacement of tree top with time during stage D.....	48
2.22. Variation of displacement of tree top with time during stages A, B, C and D	48
2.23. Variation of velocity of tree top with time during stage D.....	49
2.24. Variation of deflection and velocity of tree top with time during stages A, B, C and D.....	49
2.25. Stage D results– Motion trajectory of the CG of the piece.....	50
2.26. Variation of energy terms with time in stage D.....	53
2.27. Stage E model	54
2.28. Stage E model .Geometry	55
2.29. Stage E model - Forces	57
2.30. Simplified model of stage E - Parameters.....	61
2.31. Simplified model of stage E - Forces.....	62
2.32. Variation of α (in radian) with time -as described before.....	66
2.33. Variation of β (in radian) with time -as described before.....	66
2.34. Variation of α angular velocity (in radian/s) with time - as described before	67
2.35. Variation of β angular velocity (in radian/s) with time - as described before	67
2.36. Variation of deflection of tree top (m) with time.....	68
2.37. Variation of velocity of tree top (m/s) with time	68
2.38. Variation of energy terms with time in stage E	70
2.39. Variation of energy terms with time in stage E	71
2.40. Stage F model - Impact.....	72

2.41. Variation of uniformly distributed impact force, ω_{impact} , as a function of impact time (Δt).....	75
2.42. Variation of displacement of tree top with time during.....	79
2.43. Cutting process loads	79
3.1. FEM meshing of tree trunk	82
3.2. Variation of axial strain with time (time domain graph)	84
3.3. Fourier amplitudes for axial strains as a function of frequency.....	84
3.4. Variation of frequency of the first three modes of vibration with height	88
3.5. Variation of natural frequency with height and the trend line	88
3.6. Variation of frequency of the first three modes of vibration with average diameter.	89
3.7. Variation of natural frequency with average diameter and its trend line.....	90
3.8. Variation of frequency of the first three modes of vibration with modulus of elasticity	91
3.9. Variation of natural frequency with modulus of elasticity and its trend line.....	91
3.10. Common type of decay in tree trunk.....	92
3.11. Meshing around decay zone.....	93
3.12. Variation of frequency of the 1st mode with defect length	94
3.13. Variation of frequency of the 2 nd mode with defect length	94
3.14. Variation of frequency of the 3 rd mode with defect length.....	95
3.15. Variation of frequency of axial mode (mode 7) with defect length.....	95
3.16. Variation of frequency of different modes (mode 1, 2, 3 and 7) with defect length	96
3.17. Mode shapes of vibration of tree No.7 (height=15.52m)	97
3.18. Radial meshing and actual dimension of an element.....	100
3.19. Cutting process loads	101

3.20. Axial strain time history at the location of probe 2 in FE model.....	102
3.21. Axial strain in frequency domain at the location of probe 2 in FE model.....	103
3.22. Variation of displacement with time of tree top in FE model.....	103
3.23. Variation of axial strain at the location of probe 2 in modified FE model with time.....	104
3.24. Axial strain in frequency domain at the location of probe 2 in modified FE model	105
3.25. Variation of displacement of tree top with time in modified FE model	105
3.26. Sample of meshing tree trunk with beam element.....	106
3.27. Variation of moment with time in a frame at the location of probe 2	107
3.28. Variation of axial strain with time at the location of probe 2 in FE model meshed with beam and solid elements	107
3.29. Axial strain (in frequency domain) at the location of probe 2 in FE model meshed with beam and solid elements	108
3.30. Tree horizontal displacement and shape function.....	109
3.31. Verification of axial strain at the location of probe 2	111
3.32. Comparison of axial strain at the location of probe 2.....	112
4.1. Variation of piece angle (θ) with time for two different initial rotations–Stages A, B and C	114
4.2. Apical force induced during cutting process to the tree for two different initial rotations.....	115
4.3. Variation of displacement of tree top with time for two different initial rotations..	116
4.4. Movement trajectory of the CG of the piece for two different initial rotations – Stage D	117
4.5. Apical force induced during cutting process to the tree	119

4.6. Variation of displacement of tree top with time	120
4.7. Movement trajectory of the CG of the piece – Stage D.....	121
4.8. Variation of piece angle (θ) with time for three different tree heights – Stages A, B and C.....	125
4.9. Apical force induced during cutting process to the tree for three different tree heights.....	125
4.10. Variation of displacement of tree top with time for three different tree heights ...	126
4.11. Movement trajectory of the CG of the piece for three different tree heights – Stage D.....	126
4.12. Maximum force ratio vs. Height of tree ratio	127
4.13. Variation of piece angle (θ) with time for three different mass values–Stages A, B and C	130
4.14. Apical force induced during cutting process to the tree for three different mass values.....	131
4.15. Variation of displacement of tree top with time for three different mass values...	131
4.16. Movement trajectory of the CG of the piece for three different mass values – Stage D	132
4.17. Maximum force ratio vs. Mass of cut piece ratio	133
4.18. Variation of piece angle (θ) with time for three different diameters – Stages A, B and C	137
4.19. Apical force induced during cutting process to the tree for three different diameters.....	138
4.20. Variation of displacement of tree top with time for three different diameters	138
4.21. Movement trajectory of the CG of the piece for three different diameters – Stage D.....	139
4.22. Maximum force ratio vs. Diameter of tree ratio	140

A.1.Tree trunk simplified dynamic model.....	149
B.1.Simplified Model of Tree Trunk.....	151
B.2.Applied force function.....	153
B.3.Displacement of tree top from FE model and Simplified dynamic model.....	154
B.4.Applied force function.....	154
B.5.Displacement of tree top from FE model and Simplified dynamic model.....	155
C.1.Pulley and rope.....	156
F.1.Old tree in Itasca State Park, Minnesota.....	160
F.2.Distribution map (USGS 1999)	160
F.3.Pollen cones of <i>Pinus resinosa</i> in spring.....	161
F.4.Old-growth red pine, Algoma Highlands, Ontario.....	161

CHAPTER 1

INTRODUCTION

1.1. Technical Background

Cutting down a tree can be done in various ways. The method that is studied in this research is cutting down a tree piece by piece using a rigging tool that connects the cut piece to the trunk (Figure 1.1). To cut the tree piece by piece, a worker cuts predefined location on the trunk then pushes the top of the tree until the cut section breaks. Thus the cut piece falls after the worker pushes it and, while it is connected to the tree by rigging tools, may hit the trunk abruptly or after some swinging. Because of the large dynamic forces generated during this process tree failure is very possible.

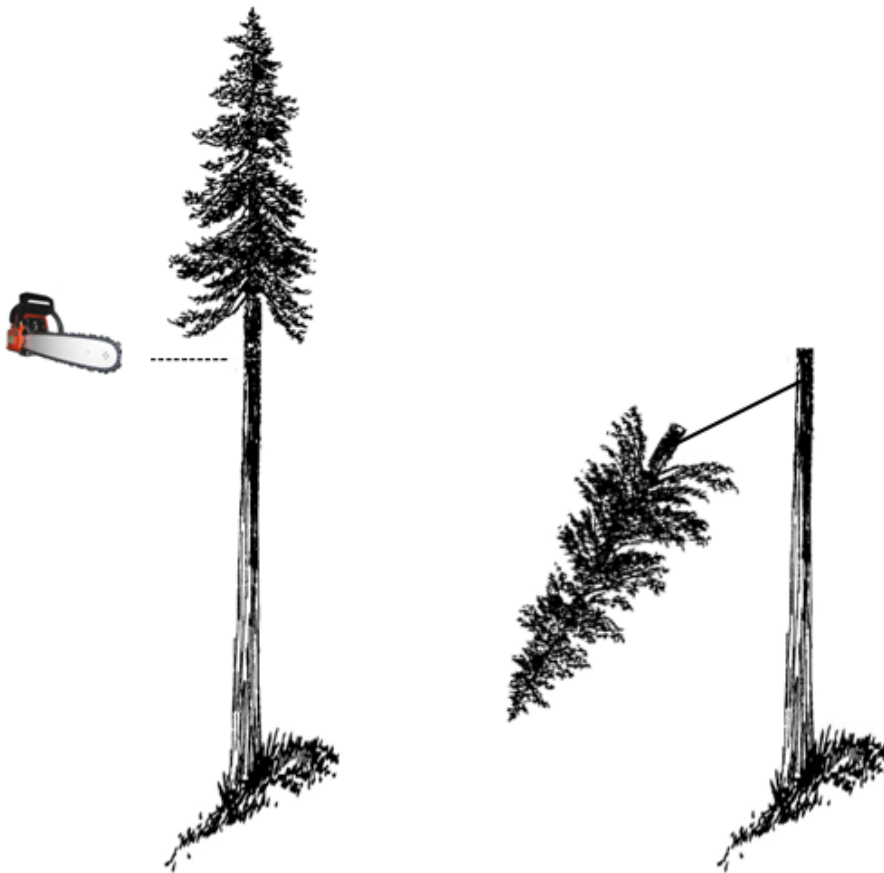


Figure 1.1 - Cutting process (Adapted from a drawing of tree shapes by USFS-TAMU)

Tree breakage during cutting process, especially in urban areas and recreation areas, may result in property damage or personal injury. While many of these failures are predictable, there remains a lack of engineering-based research to study exact influence of the cutting process on structure of tree as well as the importance of specific tree structural defects, site disturbances, and other events associated with failures. The objectives of this research are to develop information to better understand tree performance during cutting processes to enhance public safety and minimize damage risk.

Two major failure modes in trees during cutting are trunk and root failure. Trunk failure happens on the part of the trunk loaded above ground. It includes breakage of the trunk above the root collar, even if the root collar and lower trunk are below ground [17]. Common defects that are associated with trunk failures are shown in Appendix H.

Failure of the roots may happen even if they are above ground, as well as failures that involve both roots and a portion of the lower trunk. Root failure includes broken roots, cut roots, and root plate lifting out of the ground [17].

Defects in trunk and root may cause failure during cutting process which can cause damage to nearby properties, vehicles and houses or personal injuries, fire and power outage.

1.2. Objectives

The main goal of the research is to provide analytical tools to investigate vibration characteristics of trees during cutting operation. This objective is accomplished through completion of the following research activities:

- a) Develop an accurate model of the motion of cut/falling piece and predict the induced apical forces.
- b) Create a finite element model of the tree consisting of trunk and possible defects in tree.
- c) Determine the dynamic behavior of the tree during cutting process and compute stresses and strains along the height of the trunk using the FE model.
- d) Compare finite element results with experimental data measured during the cutting process.
- e) Conduct a parametric study to develop a simplified model of the phenomenon that captures the important characteristics of the dynamic behavior of the tree. In each chapter simplified models are proposed and compared with accurate models.

1.3. Significance of the Research

“Tree stability and failure are very important issues in urban areas where there can be risks of damage to people and property and in forests where damage may cause economic loss. Tree failure may cause severe damages to nearby properties, vehicles and houses. In addition, trees standing next to highways, school yards, picnic grounds or homes are of particular concern. They may also cause fire and/or power outage.” [12]

Indeed, the amount of effort and cost to fix damages generated after tree failure is very substantial. The average costs associated with property damage, repair and clean up for failures reported in the CTFRP¹ database for 550 cases was \$1650, with a standard deviation of \$6485. Costs ranged from 0 to \$100,000 [19]. Also money lost in damage claims exceeds the cost to fund tree hazard inspections. For the death of a man in a National Park Service campground, a court in Wyoming awarded over \$43,000. He was hit by a tree with physical defects that failed in the absence of unusual weather conditions. Damage awards are increasing each year so the relative cost of tree failure evaluations and maintenances is minimal. [20]

Current methods of managing trees are mostly based on visual inspection or the experience of people such as trained arborists and only limited data are available to evaluate tree strength and stability. Recent research on the measurement of dynamic loads and its effect on tree stability is providing a better understanding of how different trees withstand dynamic loads. The importance of the present research is that it is the first research of this kind which studies tree dynamic behavior under unusual cutting process forces. Most of recent research just study effects of unusual weather conditions and wind

¹ California Tree Failure Report Program (CTFRP)

load on trees. On the other hand, considering tree defects in a finite element modeling context is a new investigation that will be done in this research. Parametric study of the tree dynamic behavior and suggestion of a simplified model capturing the basic tree behavior are also innovative ideas that are accomplished in this research.

1.4. Literature Review

Oscillation of trees have widely been studied by Milne (1991), Peltola (1996), Bruchert et al. (2003), Moore and Maguire (2004), James et al. (2006), Spatz et al. (2006) and theoretically analyzed by Kerzenmacher and Gardiner (1997), Bruchert et al. (2003). In addition, Moore and Maguire (2008) provided a theoretical description of these oscillations through finite element analysis. In this section, studies done on vibration of trees are categorized into three topics and are described.

1.4.1. Mathematical Modeling

Mathematical modeling of tree dynamic behavior was conducted by Kerzenmacher and Gardiner (1997). A mathematical dynamic model of a spruce tree was created and studied against measurements of the movement of a tree within a forest. The model tree was divided into sections each with stiffness, mass and damping parameter then equations were written for each segment. These equations were formulated to evaluate the response of every section forming a system of coupled differential equations. With the aid of matrices, these equations were solved and the transfer function of the tree was found from the resulting modes and used to calculate the deflection of the tree in the wind. Transfer functions were used to obtain the response of a tree which had been divided into small segments. Also the model had been developed to calculate the time dependent response of a tree to turbulent wind loading in addition to the frequency response. The research was an extension on previous research by Gardiner about tree vibrations. However, unlike Gardiner (1992) the new model did not need any further assumptions to be made about the tree dynamic behavior and measurable physical characteristics of the

tree were the only inputs. Methods comparing modeled vibration with measured data are described comprehensively in this paper.

Another theoretical analysis of tree vibration was presented by Bruchert et al. (2003). Free vibration of plant stems was modeled by formulizing equilibrium between bending moments and moments of inertial. A comprehensive analytical solution of differential equations with appropriate boundary conditions was proposed for plant stems with top loads and negligible mass of the stem and for stems with finite mass but without apical loading.

1.4.2. Free Vibration Experiments

Free vibration experiments known as ‘pull and release’, which give information about modal frequencies and damping ratios in relation to the architecture of plants have been carried on by the following researches: Speck and Spatz (2004), Sellier and Fourcaud (2005), Spatz et al. (2007). Most of these studies focus on the effect of branches and wind forces which are not the main issue of this research. But these works contain correlations of architectural parameters in trees and typical material properties. Also, good observations on free vibration experiments have been made to estimate damping ratio and natural frequency of vibrations. Natural frequency and damping characteristics of a tree are important parameters for a dynamic modeling. These two dynamic properties are described in detail in the following sections.

1.4.2.1. Damping Ratio

Damping of trees is categorized into internal and external damping [9]. Internal damping is because of energy dissipation in the stem-ground connection system and internal friction within the wood material of the stem and the branch system [11], [10]. External damping is as a result of aerodynamic drag of the crown and due to collision with neighboring trees [11].

A damping model can simply describe energy dissipation in a dynamic system. Defining a damping model for a natural system like a tree is complex and difficult, as the dissipation mechanisms are not completely understood. Therefore, damping coefficient is simply assumed to be proportional to the velocity, so-called viscous damping and with this assumption, the damping ratio can be obtained with experimental methods like the logarithmic decrement, the resonant amplification, and the half-power. The simplest and most common method to evaluate the damping is the logarithmic decrement. In this method, the damping is obtained in the time-domain and evaluated between two adjacent amplitude peaks in the measured signal. With the resonant amplification method and the half-power method, the damping is evaluated in the frequency-domain.

1.4.2.2. Natural Frequencies

Natural frequencies of a tree are important parameters for a dynamic modeling. A tree responds to dynamic loads like a distributed mass system and absorbs energy at all its natural frequencies; however, energy is mostly absorbed at the tree's first natural frequency [13]. The studies indicate that the relationship between the natural frequencies

of the tree and the frequency of the acting load provides information on how a tree copes with apical loads.

1.4.3. Factor of Safety

Factor of safety in trees has not been studied in detail except by Niklas and Spatz (1999). Factor of safety is the concept that indicates how much a structure is capable of withstanding unprecedented loads without failure. This factor can be estimated for individual structures or for a population of structures differing in their load capabilities. “Objective methods for quantifying factors of safety for biological structures are difficult to devise because (1) actual loads are defined by conditions that can vary widely, (2) breaking loads of otherwise mechanically equivalent structures can likewise vary as a result of developmental variation, and (3) specific criteria for failure must be determined.”[6]

Niklas and Spatz (1999) proposed two methods for calculating factors of safety for plants. The first method called individual approach approximate the potential for survival of an individual stem or plant. The disadvantage of this method is that it does not consider natural variation among plants. The second method which is a population approach estimates the probability of survival of a population in a particular environment and is useful when dealing with a population of plants.

1.5. Field Measurements

Some field data are used to assess the accuracy and validity of the proposed models presented in this thesis. Field measurements have been carried out by Professor Brian Kane [23] on *Pinus Resinosa*, Red Pine, trees (Appendix F – Information about Red Pine). A number of these trees have been cut down piece by piece while two probes were situated on their trunk in the direction of fall (probe 2) and normal to the direction of fall (probe 1) approximately one meter above ground (Figure 1.2). The gauges were positioned to record axial strain.

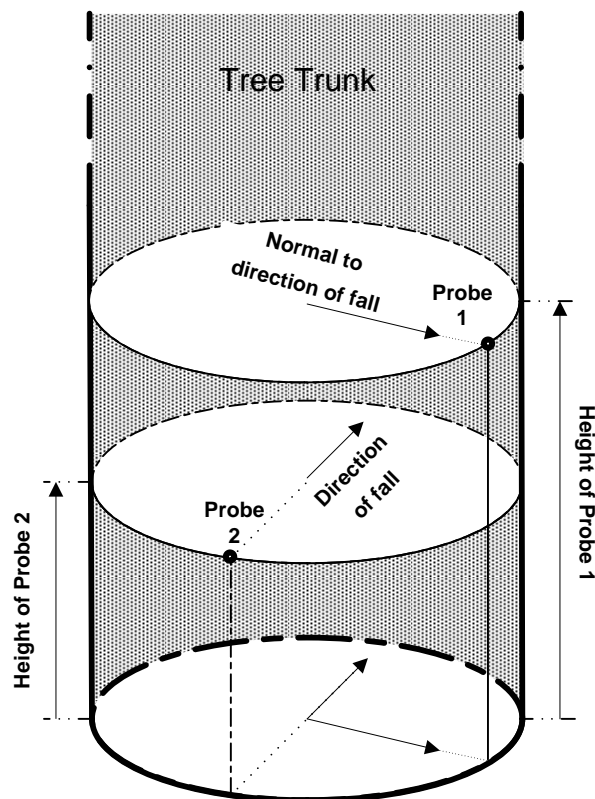


Figure 1.2 - Location of probes on tree trunk

For each experiment a set of data is available showing the tree dimensions and weights.

Figure 1.3 shows measured dimensions of a tree and a typical piece cut from the top.

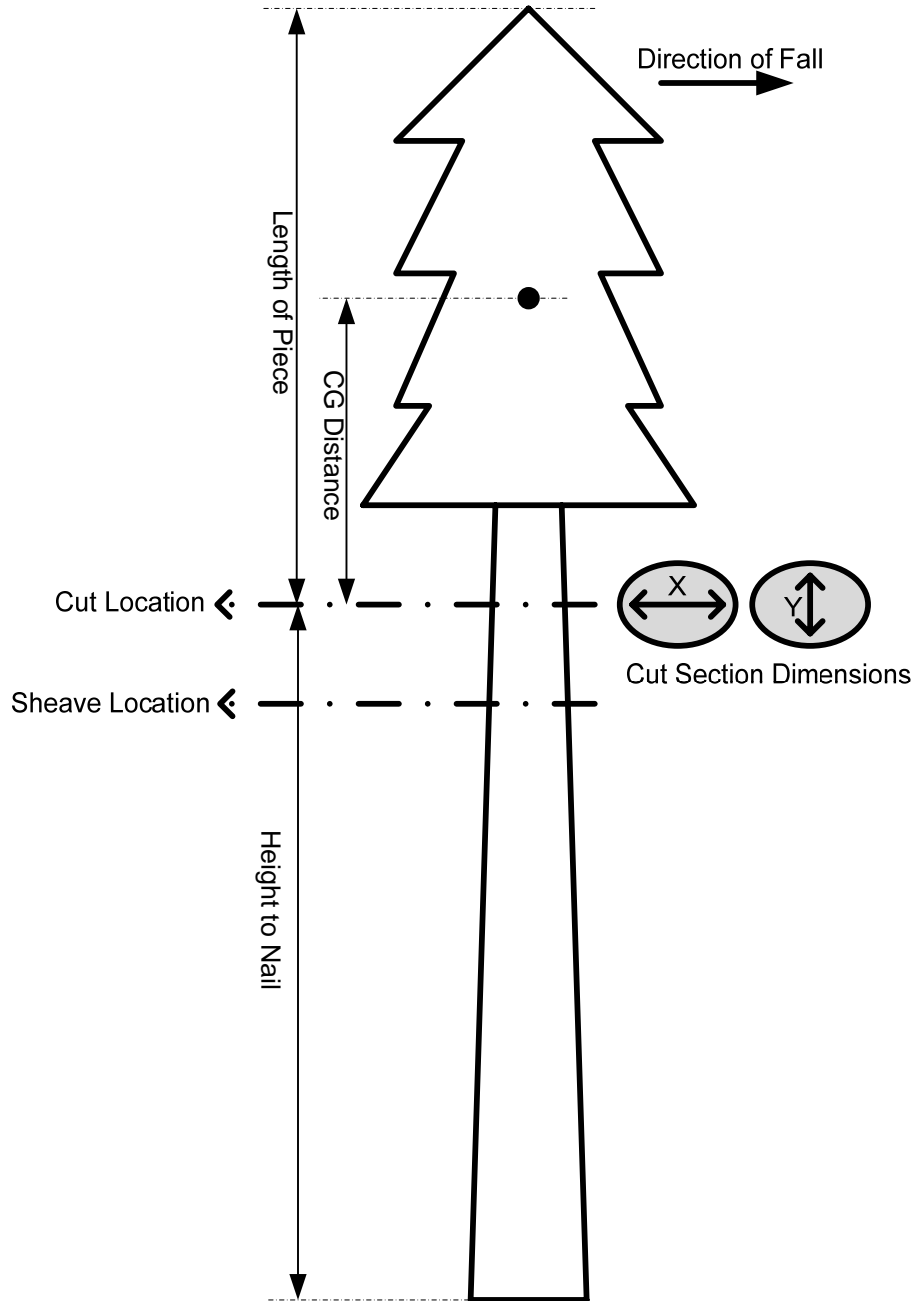


Figure 1.3 - Measurements - tree dimensions

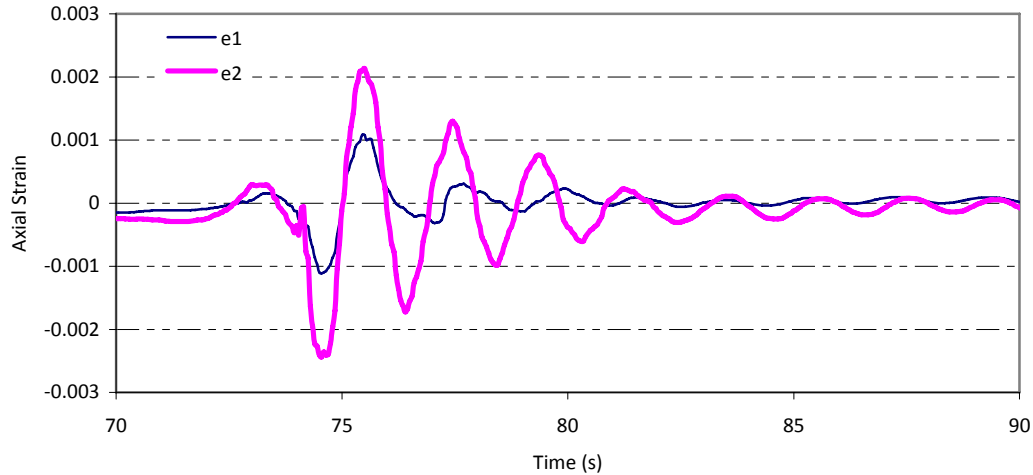
Referring to Figure 1.3, sheave location indicates the point where rigging tools connect the cut piece to the tree trunk, which is the point where apical loads (cutting process loads) are applied to the tree trunk. The dimensions, X and Y represent the trunk major and minor axes at the cut section in the direction of fall and normal to the direction of fall, respectively. Available data collected from these field measurements are listed in Table 1.1.

Table 1.1 - Typical data collected during field cutting

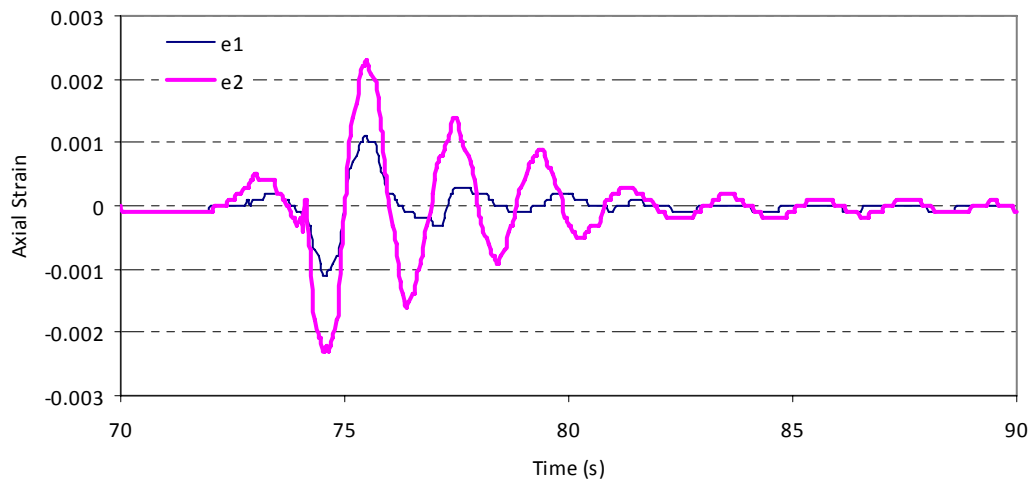
Parameter	Data available
Cut piece	Length Mass Height of center of gravity
Tree trunk	Height
Rigging tools	Sheave to cut distance
Probe	Height of probes
Force	Maximum tension in rope
Deformation	Maximum horizontal deflection at the top of the tree during each piece removal
Strain	Axial strain at the location of probes Figure 1.4

The field data used in this research is based on field measurement on a tree labeled as tree No.7 (Appendix G - Tree No7 Measurements and Data). In Figure 1.4, axial strain recorded during the first piece removal from tree No.7 is shown. Instrument e1 represents

axial strain in the location of probe 1 which is situated normal to the direction of fall and e2 represents axial strain in the direction of fall.



(a)



(b)

Figure 1.4- Variation of axial strain with time (Probe 2 is in the direction of fall)
 (a) Before baseline correction (b) After baseline correction

The horizontal axis in Figure 1.4 shows time and it can be seen that cutting started approximately 72 seconds after recording was started, and significant tree vibrations lasted approximately 15 seconds after cutting process started. Figure 1.4 indicates that axial strain in the direction of fall is larger than the axial strain in the normal direction.

Significant axial strain in the gauge normal to the direction of fall (probe 1) indicates that motion of the cut piece is not completely a 2D motion in the direction of fall and cutting forces are applied to the tree trunk not exactly in the direction of fall of the piece.

The first 3 seconds the recorded axial strain (from 72 sec to 75 sec) gives us valuable information about cutting process forces because the cutting operation occurs during this period. After that the tree vibrates freely therefore the recorded axial strain (after 75 sec) can be used to obtain dynamic properties of tree (such as E and ξ).

To use the recorded axial strain precisely, base line correction was done on the signals² in order to remove some errors produced by instruments and other environmental sources.

As discussed in Section 1.4.2.1, the damping coefficient can be determined from experimental data with the logarithmic decrement method. With this method, the damping is evaluated in the time-domain and calculated between two adjacent amplitude peaks, or averaged over several peaks in the measured signal by using equation (1.1).

$$\xi = \frac{1}{\sqrt{1 + \left(\frac{2\pi}{\frac{1}{n} \ln(x_0/x_n)}\right)^2}} \quad (1.1)$$

The method has been deployed on the axial strains in Figure 1.4 to obtain the damping ratio of tree trunk. The equation (1.1) has been written for several peak values and the results for ξ are listed in Table 1.2.

² The base line correction is done by SeismoSignal software.

Table 1.2 - Calculation of damping ratio (Refer to equation 1.1)

x_0	x_n	ξ
0.002132	0.001300	0.078
0.002132	0.000764	0.081
0.002132	0.000226	0.118
Average		0.093

Thus, damping ratio of 9% was obtained by applying the logarithmic decrement method on recorded axial strain near the bottom of tree during field measurements. The calculated damping ratio is within the range of values 5-10% acceptable for wood. The obtained value for damping ratio is rounded up to 10% and will be used later to model the tree trunk.

1.6. Scope of Thesis

This thesis presents some analytical tools and models to simulate the motion of the cut piece and calculate induced forces to the tree top during cutting process. In Chapter 2 of the thesis, the 'piece by piece' cutting procedure and trunk-piece motions are divided into 6 stages and each stage is simulated using simpler dynamic models. Then the motion function for the cut piece and induced apical loads due to the cutting process are formulated in a general case and calculated for a sample tree (Tree No.7). The outputs of the model are force function and displacement of tree top during cutting process. MATLAB and C++ are used frequently in Chapter 2 to numerically solve the equations of motion. The dynamic models presented in Chapter 2 are among the first attempts to use analytical tools to find the forces induced to the tree during cutting process.

In Chapter 3, finite element model of tree is created in SAP200 and ANSYS. The finite element model is validated and adjusted by comparing the modal analysis results with field measurements. Then the adjusted finite element model is excited by the force function obtained from Chapter 2. Axial strain near the bottom of the tree is the main output of the FE model and is compared with axial strain recorded during the field measurements. In addition, a simpler FE model with beam elements and an analytical procedure are proposed in Chapter 3 to skip the FE model with solid elements and simplify the calculations. Furthermore, tree defects are placed into tree trunk in some FE models to study the effect of tree defects on dynamic behavior of tree.

Since some calculations in Chapter 2 are based on assumed values for the parameters which were not measured in field experiments, the sensitivity of the calculations and

results to these parameters is studied in Chapter 4. The outputs of this study can be used to determine which parameters have to be measured more precisely.

In each step of modeling in this thesis, simplified models and methods are suggested that capture the important characteristics of the real tree and process. Finally, in Chapter 5, some future researches on the topic are suggested.

CHAPTER 2

MOTION FUNCTION OF CUT PIECE AND INDUCED APICAL LOADS DUE TO CUTTING PROCESS

The 'piece by piece' cutting process can be simulated using simple dynamic models. To cut the tree piece by piece, a worker cuts the edges of a predefined location on the trunk then pushes the top of the tree until the cut section breaks. Thus the cut piece falls after the worker pushes it and, while it is connected to the tree by rigging tools, may hit the trunk abruptly or after some swinging. In this research the cutting procedure and trunk-piece motions are categorized in 6 stages (Figure 2.1):

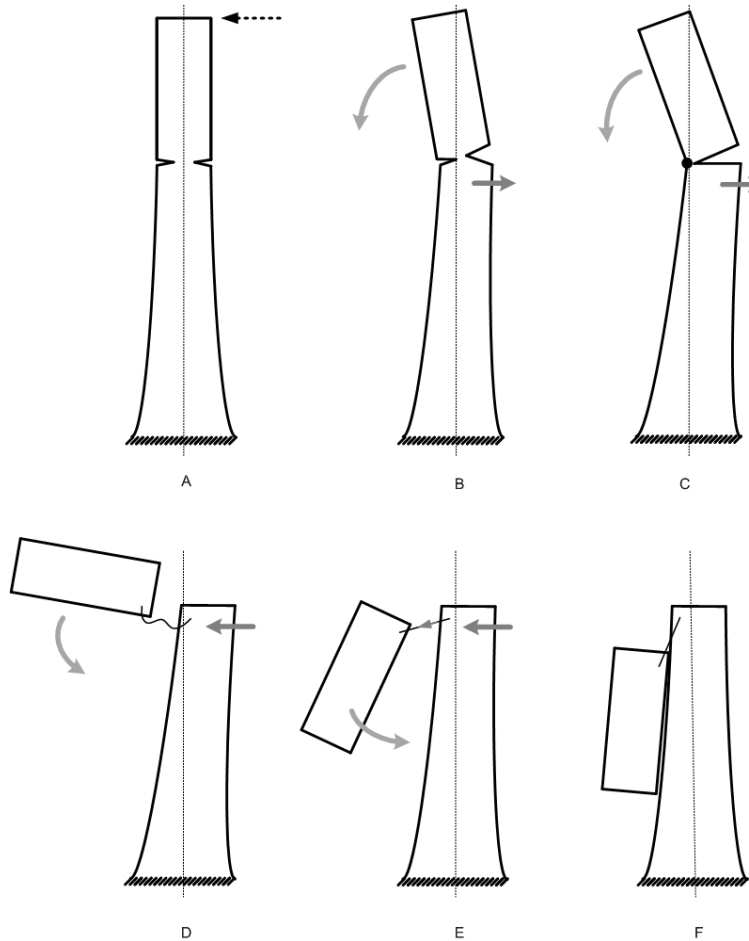


Figure 2.1- Cutting process modeling

The Cutting process can be divided for modeling into the following stages:

- A) Worker cuts tree trunk in predefined locations and pushes top of the tree.
- B) Fractures in piece-trunk connection start propagating until breakage after an initial push of worker and weight of piece.
- C) Partially released piece rotates around the outmost part of trunk until it is completely released. During this movement, piece pushes the trunk backward.
- D) The fallen piece moves under gravity force and trunk vibrates freely.
- E) Rope is tightened and cut piece will start a pendulum like motion under gravity and rope tension. Meanwhile, trunk oscillates under tension in rope.
- F) Cut piece hits the trunk either after some swinging or abruptly.

Note that trunk and piece positions at the end of each stage are the initial conditions for the subsequent stage.

2.1. Modeling of Stages A, B and C

Trunk and piece motions during cutting process have been modeled in each stage. To obtain the trunk backward motion function during stages A, B and C, the cut piece was modeled as a rigid bar and the trunk was modeled as a dynamic model consisting of a concentrated mass, linear spring and viscous damper³. It has to be mentioned that after the piece is released from the trunk (stage D), the motion consists of free fall motion so it is modeled separately:

During stage C, the piece rotating around the outmost part of trunk has been modeled like rotating of a rigid bar around pin roller. Indeed, the piece rotates under gravity force and induces horizontal forces to the top of the trunk and, consequently, this horizontal force moves trunk backward.

The angle (θ) and the displacement (u) are the two degrees of freedom of the model (Figure 2.2). The first one represents the rotation angle of the falling piece, and the second one is horizontal displacement of the top of the tree.

The motion can be formulated using the coordinates of the center of gravity of the cut piece during motion (x and y); θ , u , x , and y are four geometric variables which are related using the two coordinate transformation equations (2.1) and (2.2).

$$x = u + d_{cg} \cdot \sin(\theta) \quad (2.1)$$

$$y = d_{cg} \cdot \cos(\theta) \quad (2.2)$$

where d_{CG} is the distance from the roller to the CG of the cut piece.

³ Refer to Appendix. A for calculation of M, C, K

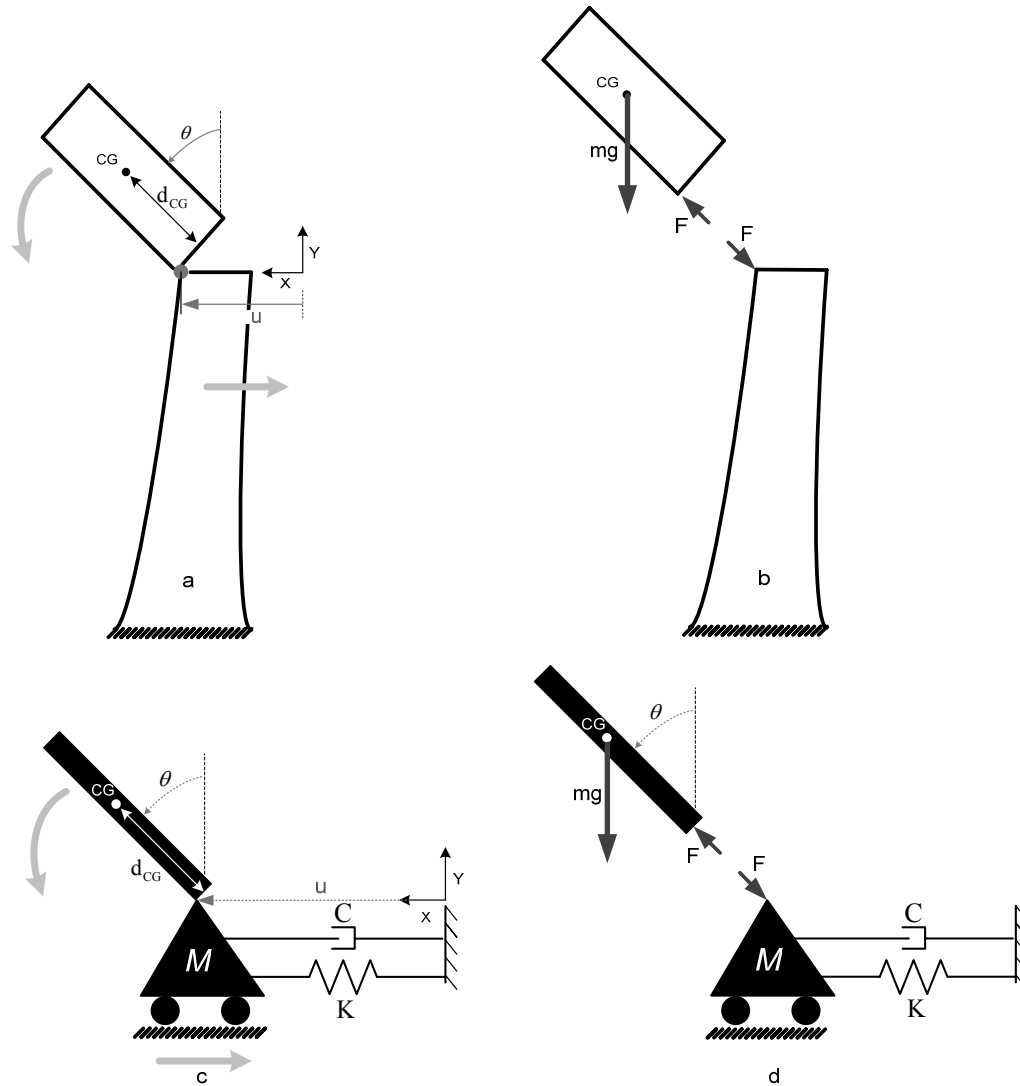


Figure 2.2- Stages A, B and C model sketch⁴: (a, c) Geometry (b, d) Forces

Mechanics equations are used to complete the set of necessary equations to determine the motion function and finally find the force applied to the top of tree. Following the Newtonian approach, the equations of motion for center of gravity of the cut piece can be written as⁵:

$$m \cdot \ddot{x} = F \cdot \sin(\theta) \quad (2.3)$$

⁴ Width of cut piece is neglected in models c and d of Figure 2.2 to simplify the geometry of the system.

⁵ θ , x and y are function of time.

$$m \cdot \ddot{y} = -m \cdot g + F \cdot \cos(\theta) \quad (2.4)$$

where m is the mass of the falling piece and F is the force applied to the piece from pin roller. The other equation is dynamic equilibrium of the tree trunk (M):

$$-F \cdot \sin(\theta) = M \cdot \ddot{u} + C \cdot \dot{u} + K \cdot u \quad (2.5)$$

After combining the geometric equations (2.1 and 2.2) with dynamic equations (2.3, 2.4 and 2.5), a system of ordinary differential equations is obtained. The system of equations can be simplified to the two equations below:

$$\ddot{\theta} \cdot d_{CG} + \ddot{u} \cdot \cos(\theta) - g \cdot \sin(\theta) = 0 \quad (2.6)$$

$$\ddot{\theta} \cdot d_{CG} \cdot \cos(\theta) - \dot{\theta}^2 \cdot d_{CG} \cdot \sin(\theta) + \ddot{u} \cdot \left(\frac{M}{m} + 1\right) + \dot{u} \cdot \frac{C}{M} + u \cdot \frac{K}{M} = 0 \quad (2.7)$$

This system of equations (2.6 & 2.7) can also be derived from a Lagrangian approach as described in Appendix E.

Equation (2.6) can also be derived by writing torque equilibrium around roller-piece contact point (O') after using relative motion rule. In other words, roller can be assumed fixed and then a virtual force of $-m \cdot \ddot{u}$ being applied to the CG of the falling piece.

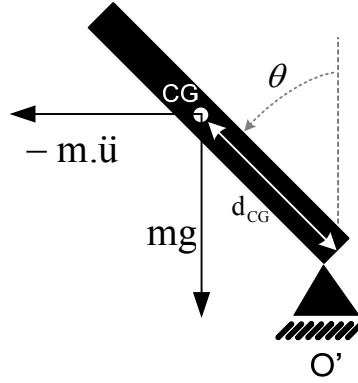


Figure 2.3- Free diagram of cut piece

$$\ddot{\theta} \cdot I + m \cdot \ddot{u} \cdot d_{CG} \cdot \cos(\theta) - m \cdot g \cdot d_{CG} \cdot \sin(\theta) = 0 \quad (2.8)$$

Assuming $I = m \cdot d_{CG}^2$ ⁶, equation (2.8) will be simplified to equation (2.6).

To solve the system of ordinary differential equations (2.6 & 2.7), 4 initial conditions are needed. Two of these conditions are values of $u(0), \dot{u}(0)$ which have to be set to zero and remaining are values of $\theta(0), \dot{\theta}(0)$.

Solving the system of ordinary differential equations (2.6 and 2.7) numerically is done by using the Runge Kutta method of order four which is a very popular and commonly used method for the approximation of the solutions of ordinary differential equations. To make these equations solvable by the Runge Kutta method, they must be written in the form of $\ddot{\theta} = \text{function}(\theta, u, \dot{u})$ and $\ddot{u} = \text{function}(\theta, \dot{\theta}, u)$. Thus, these equations were rewritten in a way that there would be only $\ddot{\theta}$ or \ddot{u} in each equation.

⁶ This simplification means that we neglected the rotational momentum of rod and assumed it as a concentrated mass located at the CG.

$$\ddot{\theta} = \frac{g \cdot \sin(\theta) \cdot \left(\frac{M}{m} + 1\right) + \cos(\theta) \cdot \left\{ \dot{u} \cdot \frac{C}{M} + u \cdot \frac{K}{M} - \dot{\theta}^2 \cdot d_{CG} \cdot \sin(\theta) \right\}}{d_{CG} \cdot \left(\frac{M}{m} + 1\right) - d_{CG} \cdot \cos^2(\theta)} \quad (2.9)$$

$$\ddot{u} = \frac{-g \cdot d_{CG} \cdot \sin(\theta) \cdot \cos(\theta) - d_{CG} \cdot \left\{ \dot{u} \cdot \frac{C}{M} + u \cdot \frac{K}{M} - \dot{\theta}^2 \cdot d_{CG} \cdot \sin(\theta) \right\}}{d_{CG} \cdot \left(\frac{M}{m} + 1\right) - d_{CG} \cdot \cos^2(\theta)} \quad (2.10)$$

Due to the large volume of calculations, a C++ program was written to perform the Runge Kutta calculations for this system of ordinary differential equations (Refer to Appendix I- Codes Written in C++). Outputs of the program are motion angle and deflection of top of the trunk. It has to be mentioned that, with this method, the falling piece angle (θ) and top of tree deflection (u) are calculated during the time the piece is in connection with edge of trunk and after that moment the trunk undergoes free vibration which can be described by:

$$M \cdot \ddot{u} + C \cdot \dot{u} + K \cdot u = 0 \quad (2.11)$$

The release point is assumed to occur when the force applied to the trunk by the falling piece starts changing its direction which means that the piece is not in connection with trunk anymore. This equation can be written like the discussed format to be solved with the Runge Kutta method.

$$\ddot{u} = -\frac{(C \cdot \dot{u} + K \cdot u)}{M} \quad (2.12)$$

2.1.1. Simplified Method (Modeling of Stages A, B and C)

It can be observed that the mentioned calculations are time consuming and, in most cases, an approximation is sufficient. Therefore, a simplified, but sufficiently accurate method is proposed here to model the initial stages of the falling of the piece. In this method, the system is divided into two separate models, the piece and the trunk. The piece is modeled as a rigid bar with a pinned restraint on its end and the trunk is modeled as a dynamic model consisting of a concentrated mass, viscous damper and linear spring as before. In other words, piece rotating around outmost part of trunk has been modeled like a rigid bar rotating around a fixed pin. Indeed, piece rotates under gravity force and induces horizontal forces to the top of the trunk. In addition, this horizontal force moves trunk backward.

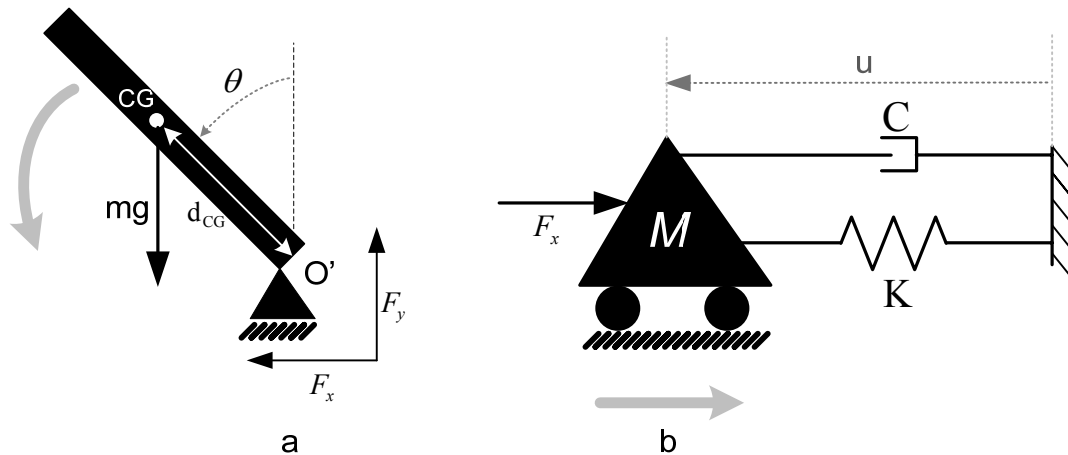


Figure 2.4- Sketch of stages A, B and C simplified model

Dynamic equations corresponding to this model are provided below:

Rotation moment around pinned restraint (O') is

$$\tau = m \cdot g \cdot d_{CG} \cdot \sin(\theta) \quad (2.13)$$

In which m is cut piece mass and θ is rotation angle along vertical axis, and the moment of inertia of rigid bar with concentrated mass at its center of gravity (CG) is:

$$I = m \cdot d_{CG}^2 \quad (2.14)$$

In addition, relation between moment of inertia and rotation moment is:

$$\tau = I \cdot \ddot{\theta} \quad (2.15)$$

Thus, after rewriting equations (2.13), (2.14) and (2.15), differential equation of cut piece will be obtained:

$$\ddot{\theta} \cdot d_{CG} - g \cdot \sin(\theta) = 0 \quad (2.16)$$

Initial conditions to solve the differential equation of motion are $\theta(0)$ and $\dot{\theta}(0) = 0$. Thus, θ can be solved by using mathematical software or analytically. Having $\theta(t)$, radial and angular accelerations of the center of mass of the cut piece can be obtained:

$$a_{\theta} = d_{CG} \cdot \ddot{\theta} \quad (2.17)$$

$$a_r = d_{CG} \cdot \dot{\theta}^2 \quad (2.18)$$

Acceleration of the center of mass along x-direction can be obtained by substituting a_r and a_{θ} from equations (2.17) and (2.18) into equation (2.19):

$$a_x = a_{\theta} \cdot \cos(\theta) - a_r \cdot \sin(\theta) \quad (2.19)$$

$$a_x = d_{CG} \cdot \ddot{\theta} \cdot \cos(\theta) - d_{CG} \cdot \dot{\theta}^2 \cdot \sin(\theta) \quad (2.20)$$

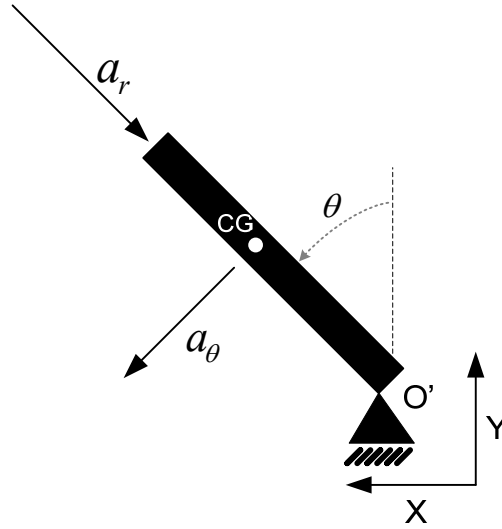


Figure 2.5- Accelerations - simplified model of stages A, B and C

Now, using force equilibrium in horizontal direction, pinned constraint reactions F_x and F_y can be calculated. However, F_y is not an important factor in the trunk lateral deflection since it works axially. Thus, F_x is calculated using equation (2.20) and force equilibrium along X-axis.

$$F_x = m \cdot a_x \quad (2.21)$$

F_x will cease after the falling piece releases from the tree top and this event is assumed to be when F_x changes direction (when the piece get close to horizontal position). Thus, the release instant is defined to be when the applied force starts changing direction.

On the other hand, F_x acts simultaneously on top of trunk which has been modeled as a dynamic model consisting of a concentrated mass, linear spring and viscous damper (Figure 2.4). Therefore, dynamic force equilibrium is written for spring-mass-damper system as:

$$M \cdot \ddot{u} + C \cdot \dot{u} + K \cdot u = -F_x \quad (2.22)$$

In which, u is deflection of top of trunk with respect to its initial position, M is concentrated mass representing dynamic mass of trunk, K is spring constant representing tree stiffness, and C is damper constant. These factors are calculated in Appendix A. In addition, Initial conditions for solving differential equations of motion of tree top are $u(0) = 0$ and $\dot{u}(0) = 0$.

After solving differential equations (2.16) and (2.22), cut piece angle (θ) and trunk motion (u) can be found. It should be noticed again that the cut piece angle (θ) is calculated by the time the piece is in connection with edge of trunk, while calculated u is showing the trunk oscillatory motion even after the piece loses its contact with trunk. A program has been written in MATLAB to perform mentioned calculations.

2.1.2. Results (Modeling of Stages A, B and C)

2.1.2.1. Simplified Method

Now these methods can be applied to a real set of data. Starting with initial condition of the motion, it can be assumed correctly that initial piece angular velocity, trunk horizontal deflection and trunk horizontal velocity are zero and, only, piece initial angle is set to a non zero value which makes sense since the worker pushes the top of the piece and do not give significant initial velocity to the piece or the trunk. The initial conditions of the motion are listed in Table 2.1.

Table 2.1- Motion initial condition: Stage A, B and C

Piece angle (rad)	θ	0.1 ⁷
Angular velocity of piece (rad/s)	θ'	0
Horizontal deflection of trunk (m)	u	0
Horizontal velocity of trunk (m/s)	u'	0

Table 2.1 shows rest position before starting cutting process. Now, by using stages A, B and C model, piece angle and trunk horizontal deflection is calculated. Angle (θ) is obtained with Table 2.1 initial conditions. The cut piece loses its contact with the trunk at $t=1.5s$ when the applied force equals zero. Thus, stage C is estimated to be finished at $t=1.5$ sec.

⁷ This value is used because a small angle is needed initially to start the piece motion. Sensitivity of results to this assumed parameter is studied in next chapter.

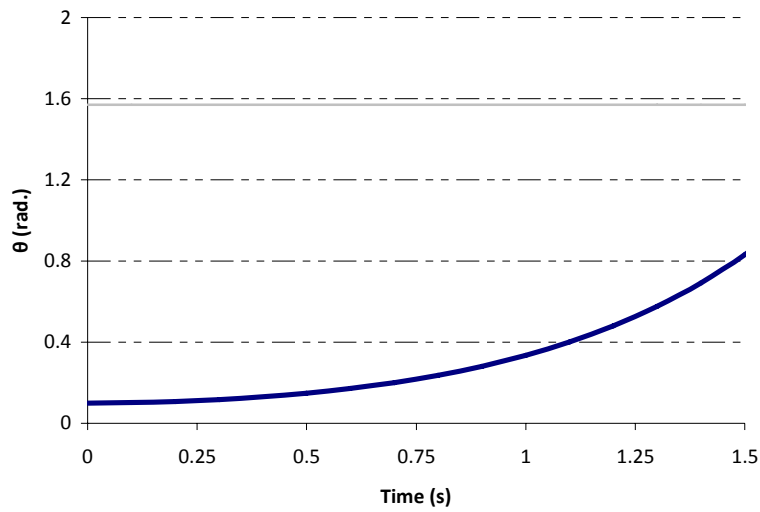


Figure 2.6- Variation of piece angle (θ) with time⁸

Horizontal acceleration of the CG of the piece (a_x) obtained from equation (2.20) is showed in Figure 2.7.

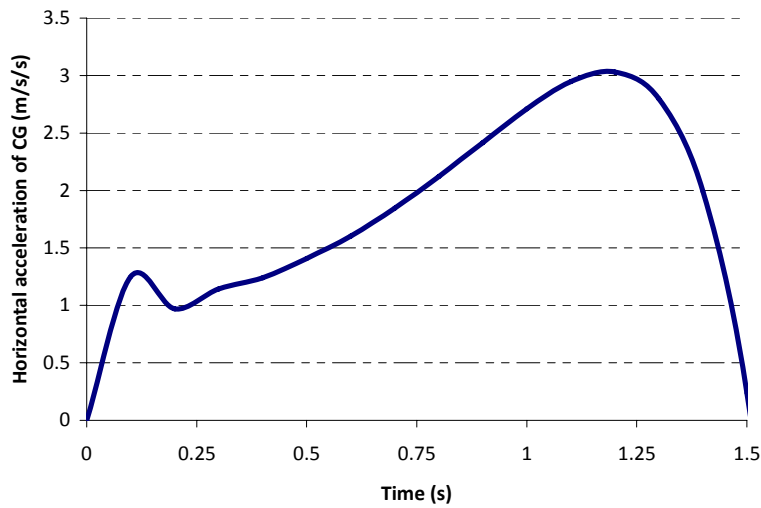


Figure 2.7- Variation of horizontal acceleration of the CG of the piece with time

⁸ Gray line shows $\theta=90^\circ$.

Then, horizontal reaction force (force applied to the top of the tree) can be estimated from equation (2.21) and imported into equation (2.22). It should be noted that for the mentioned stages representing the cutting process, a force is applied on the top of trunk only while the piece is connected to it ($t < 1.5$ sec.).

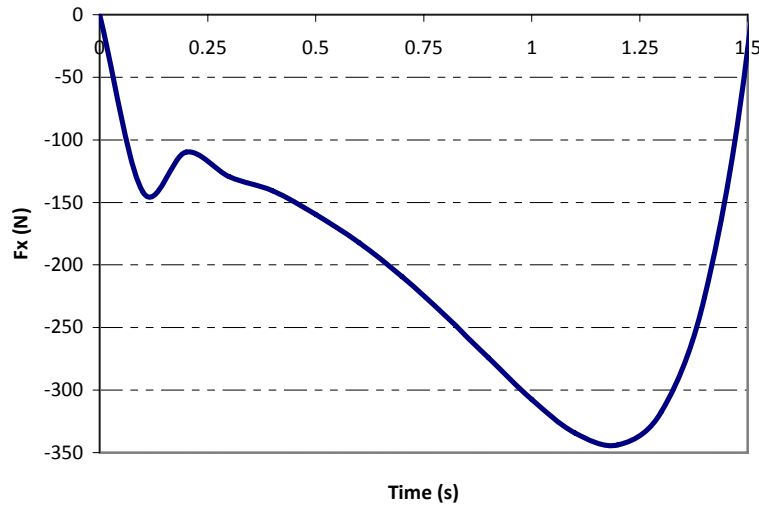


Figure 2.8- Variation of horizontal force with time

Deflection of tree top is graphed in Figure 2.9. It should be noticed that trunk vibrates with apical force during stages A, B and C and vibrates freely after $t = 1.5$ sec. and before stage E getting started (in stage D).

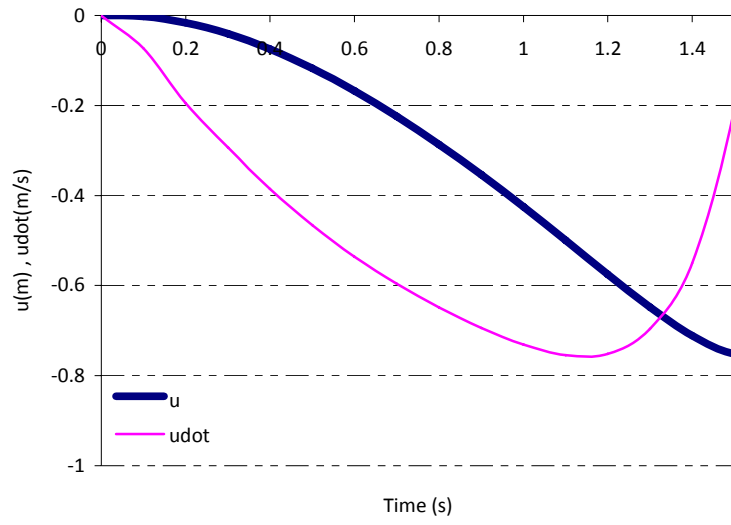


Figure 2.9- Variation of deflection and velocity of tree top with time during stages A, B, C

2.1.2.2. Detailed Method

As discussed before, it can be assumed correctly that initial piece angular velocity, trunk horizontal deflection and trunk horizontal velocity are zero and, only, piece initial angle is set to a non zero value which makes sense since the worker pushes the top of the piece and do not give significant initial velocity to the piece or the trunk. The initial conditions of the motion are listed in Table 2.2.

Table 2.2- Motion initial condition: Stage A, B and C

Piece angle (rad)	θ	0.1
Angular velocity of piece (rad/s)	θ'	0
Horizontal deflection of trunk (m)	u	0
Horizontal velocity of trunk (m/s)	u'	0

Now, by using stages A, B and C main model, cut piece angle and trunk horizontal deflection is calculated. Then, horizontal reaction force (force applied to the top of the tree) can be estimated from equation (2.5).

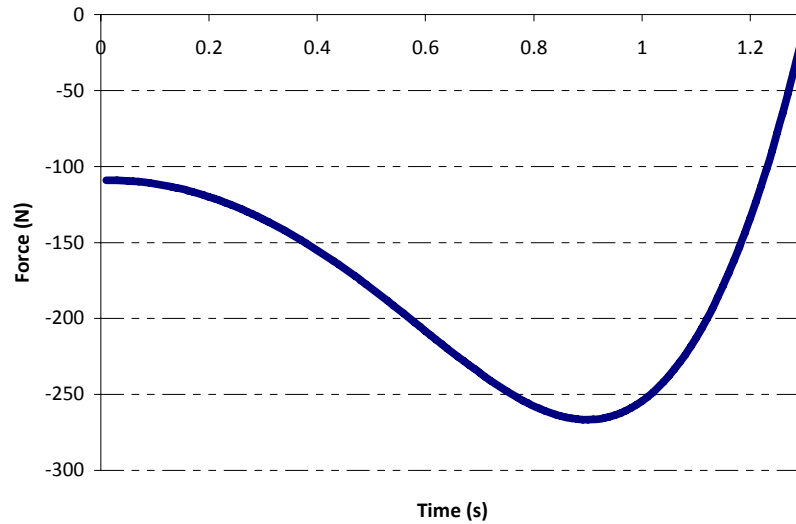


Figure 2.10- Variation of horizontal force applied to the tree top with time

By calculating the applied force to the top of tree, the approximate release point is calculated to be 1.31 sec. Then the piece angle of rotation can be calculated to the release time by the stages A, B, C model discussed.

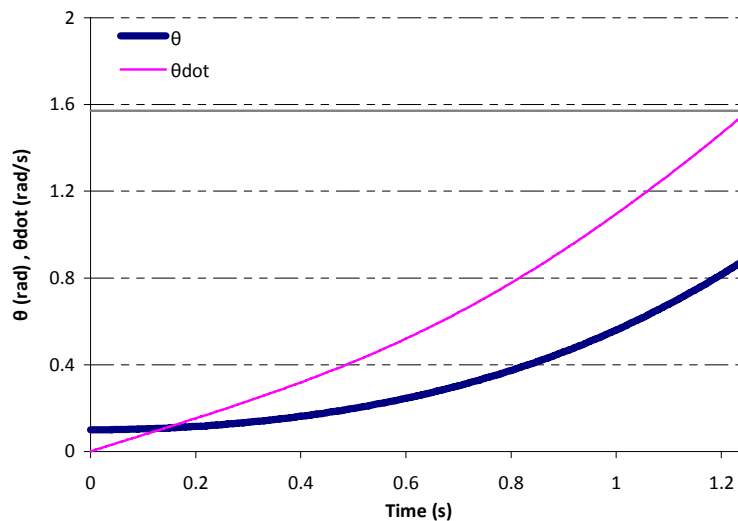


Figure 2.11- Variation of angle and angular velocity of piece (θ , θ -dot) with time⁹

⁹ Gray line shows $\theta=90^\circ$.

Deflection of tree top is graphed in Figure 2.12. It should be noted that the trunk vibrates with apical force during stages A, B and C and vibrates freely after release time ($t=1.31$ sec. in this case) and before stage E initiates. Stage D ends, in most cases, at the end of the first half cycle.

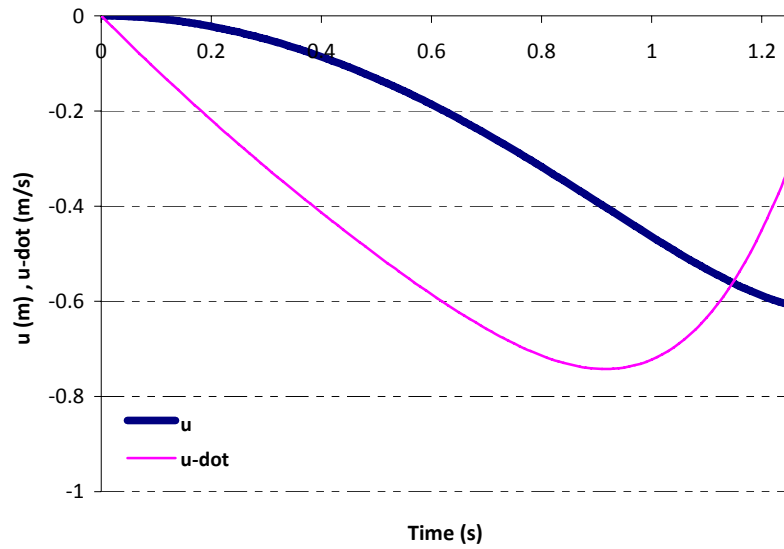


Figure 2.12- Variation of deflection and velocity of tree top with time during stages A, B, C

Results can be summarized in the following table:

Table 2.3- Summary of results: Stage A, B and C

PARAMETER \ STAGE		Initial condition	Release point
		Beginning of stage A	End of stage C
Time (s)	t	0	1.31
Piece angle (rad)	θ	0.10	$\theta_C = 0.99$
Angular velocity of piece (rad/s)	θ'	0	$\omega_C = 1.69$
Horizontal deflection of trunk (m)	u	0	$u_C = -0.62$
Horizontal velocity of trunk (m/s)	u'	0	$u'_C = -0.11$

2.1.2.3. Comparison of Results from Simplified and Detailed Method

A detailed and a simplified method were proposed to model the motion of falling piece and deflection of tree top during stages A, B and C. In this section, results from these two methods are compared.

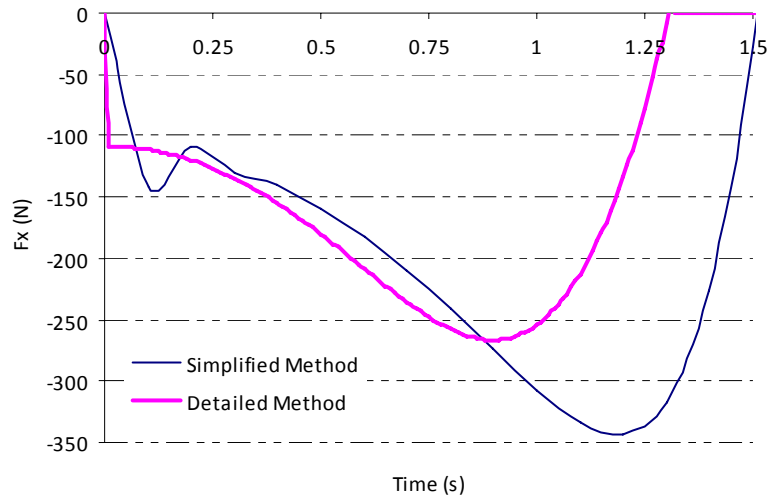


Figure 2.13- Variation of horizontal force with time during stage A, B, C

The calculated horizontal forces are compared in Figure 2.13 and it is clear that the force calculated using the detailed method has the lower peak and ends at an earlier time than simplified method. The probable explanation for this behavior is that in the detailed method a portion of energy of the system is dissipated in the dynamic mass, spring and damper so the horizontal force gets to the lower peak and ends sooner than simplified method. The same behavior is observed in the variation of deflection and velocity of tree top with time as shown in Figure 2.14 and Figure 2.15, respectively.

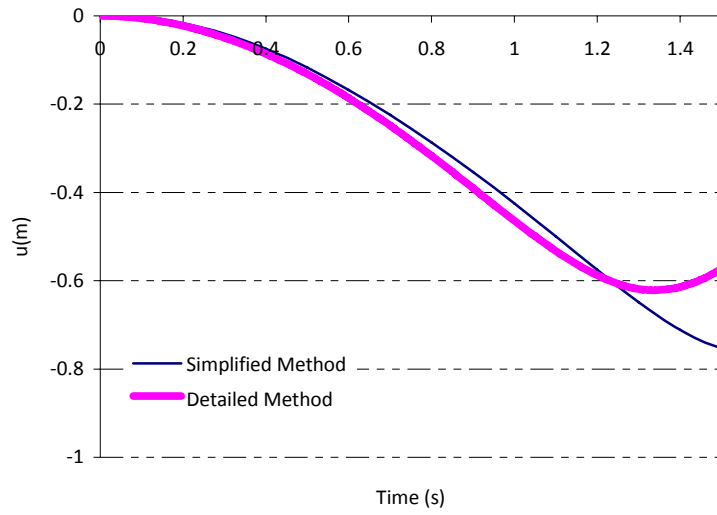


Figure 2.14- Variation of deflection of tree top with time during stages A, B, C

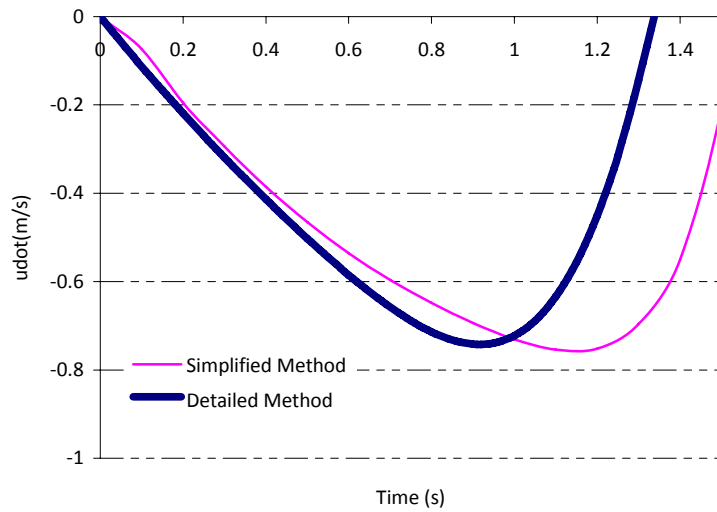


Figure 2.15- Variation of velocity of tree top with time during stages A, B, C

2.1.3. Verification of Results by the Energy Method

In this section the results of main model of stages A, B, C is validated by using the energy method. According to Conservation of Energy Rule, during a phenomenon the total energy must remain constant. In this case the energy term is:

$$E = \frac{1}{2}M.\dot{u}^2 + \frac{1}{2}m.(\dot{u}^2 + d^2.\dot{\theta}^2 + 2.d.\dot{u}.\dot{\theta}.\cos(\theta)) + \frac{1}{2}K.u^2 + m.g.d.\cos(\theta) + \int C.\dot{u}.du$$

Where

$$\text{Kinetic energy} = \frac{1}{2}M.\dot{u}^2 + \frac{1}{2}m.(\dot{u}^2 + d^2.\dot{\theta}^2 + 2.d.\dot{u}.\dot{\theta}.\cos(\theta))$$

$$\text{Potential energy} = \frac{1}{2}K.u^2 + m.g.d.\cos(\theta)$$

and

$$\text{Friction work due to material damping} = \int C.\dot{u}.du$$

The energy term variation and total energy term is plotted in the graph below.

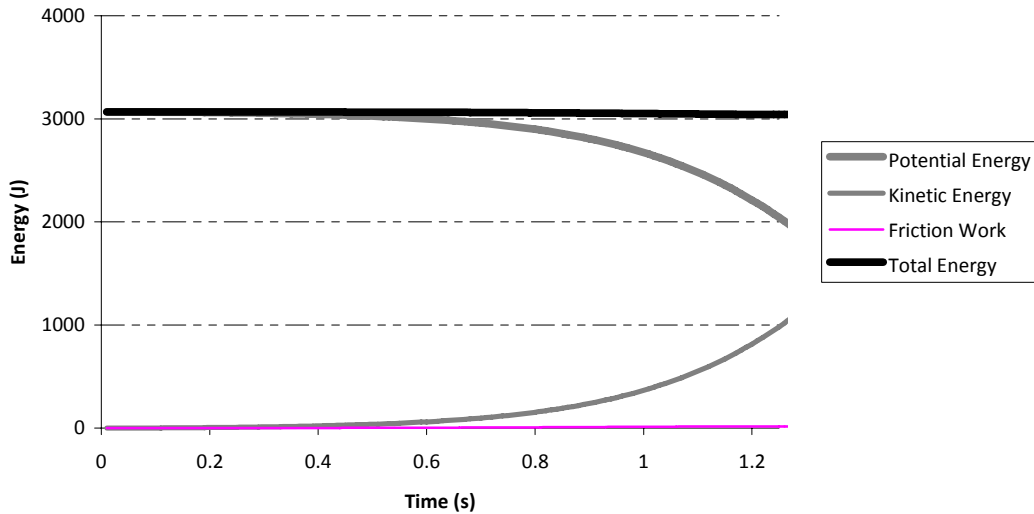


Figure 2.16- Variation of energy terms with time in stages A, B, C

It is obvious from Figure 2.16 that total energy (the top most line) remains constant during the motion but the potential energy decreases and kinetic energy increases. The lowest line is related to friction work (damper energy dissipation). To better understand the energy variation another graph is plotted in semi log.

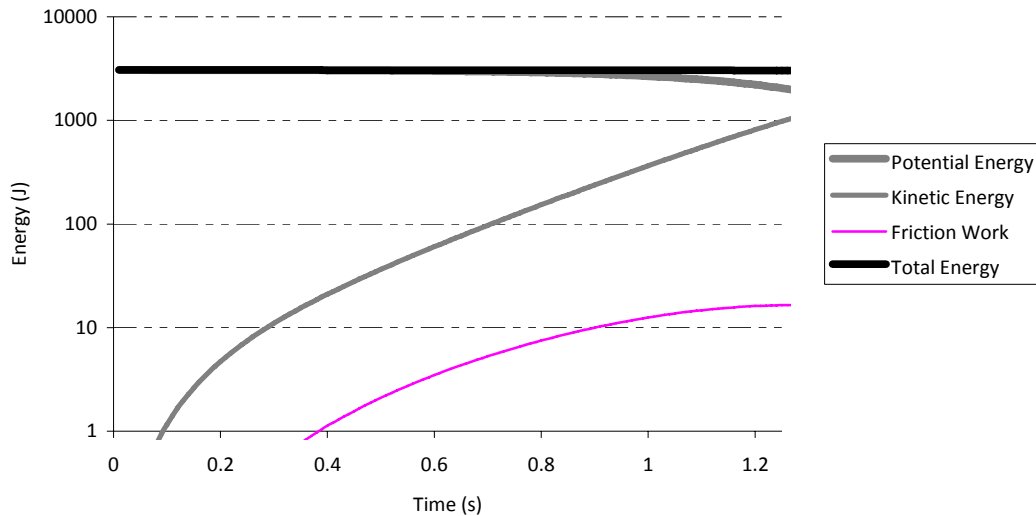


Figure 2.17- Variation of energy terms with time in stages A, B, C

Again it can be observed from Figure 2.17 that total energy (the top most line) remains constant while the potential energy decreases and kinetic energy increases. The friction work (energy dissipation due to material damping) is the lowest line and logically increases during the motion.

2.2. Modeling of Stage D

After the cut piece releases from the tree trunk, it falls freely while trunk keeps oscillating due to initial cutting forces that were mentioned before (stages A, B and C). Piece keeps falling until the rope is tightened and a pendulum motion of the cut piece starts while trunk keeps moving freely according to equation (2.11). As mentioned before, trunk and piece motion variables at the end of each stage are the initial conditions for the subsequent stage.

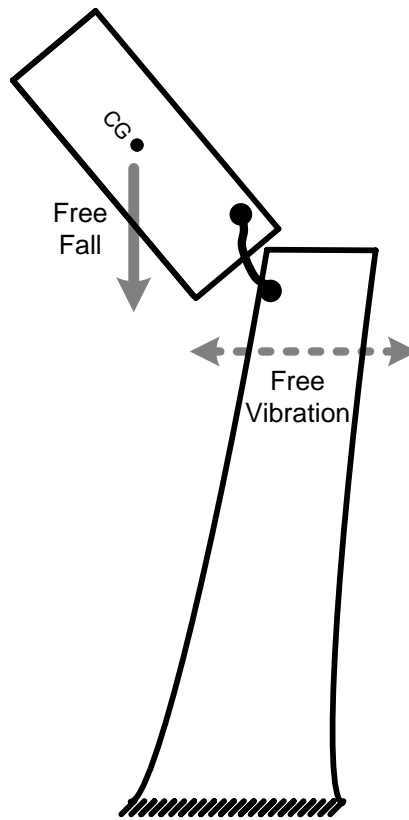


Figure 2.18- Release moment (end of stage C)

Obtaining top of tree deflection during stage D is straight forward using free vibration model discussed before (equation 2.11). It is assumed that after the moment piece reaches release point, the cut piece does not apply any force to the tree until rope becomes taught.

Thus, if the first method is used, top of tree deflection (u) and velocity (\dot{u}) have to be calculated at release point (u_c and \dot{u}_c in Table 2.3) and then being imported as initial conditions into free vibration equation (2.11) to model tree movement during stage D motion. In the mentioned methods, the current equations are enough to obtain top of tree deflection (u) even after release point.

At the start of stage D, piece is initially in known orientation (θ_c) with calculated rotational velocity (ω_c) from previous stage model¹⁰. A phenomenon observed from the cutting process after the release point was a sliding motion of piece on the top of trunk edge causing it to develop a linear velocity of V_Δ which is the reason of forward moving of the cut piece while no horizontal force is being applied to the piece. Also, the angular velocity (ω_c) of the piece may change due to this sliding motion and bottom end releasing from the trunk. Thus, a moment after the release instant, linear velocity is V_Δ at one end and $V_\Delta + \varpi_c \cdot L_p$ at farther end (when L_p is piece total length and ϖ_c is angular velocity a moment after release point).

¹⁰ $\omega_c = \left. \frac{d\theta}{dt} \right|_{\theta=\theta_c}$ in stage C model.

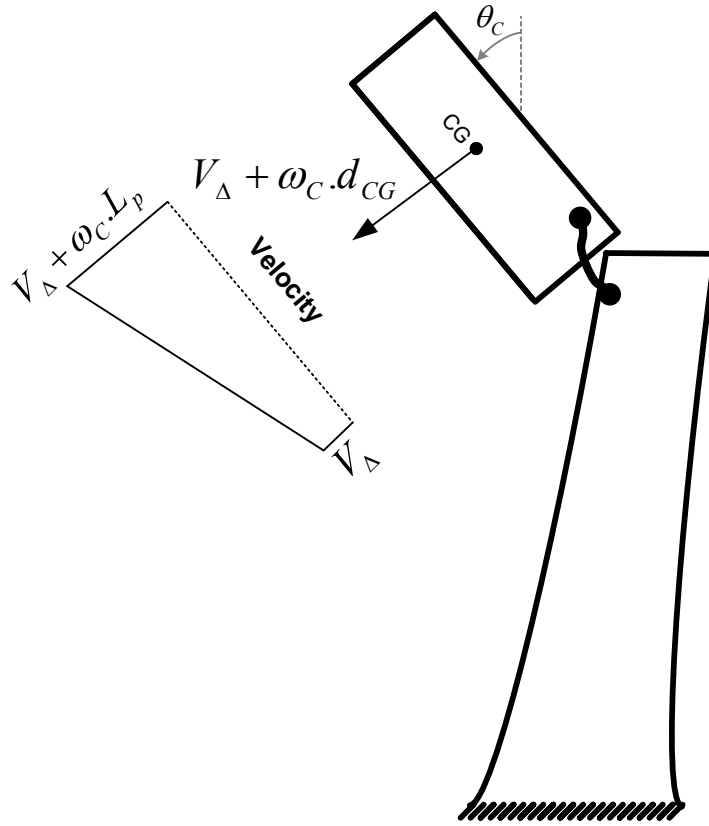


Figure 2.19- Velocity of falling piece a moment after release instant

During free-fall the only force considered is gravity. Drag forces were assumed to be negligible because this stage lasts only a fraction of second. During free-fall motion, gravity will not produce any moment around CG therefore piece keeps its initial angular velocity of ω_c .

$$\omega_D = \omega_c \quad (2.23)$$

$$\theta_D = \theta_c + \omega_c \cdot t \quad (2.24)$$

And consequently

$$\beta = 180 - \theta_D = 180 - (\theta_c + \omega_c \cdot t) \quad (2.25)$$

Where t is the duration of stage D.

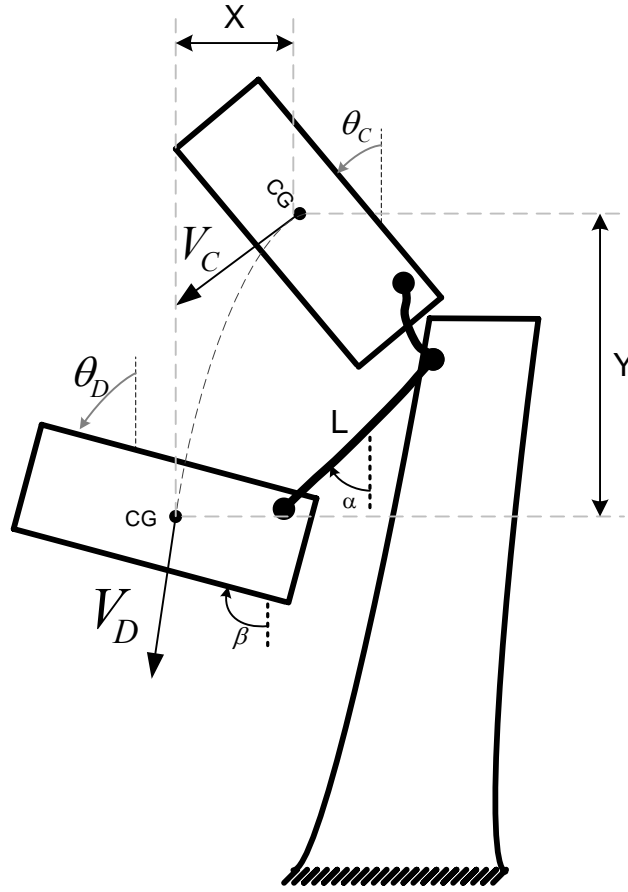


Figure 2.20- Modeling of stage D–Movement of CG of the piece

Also, the distance the CG of the piece travels can be computed using the coordinates $y = \frac{g.t^2}{2} + V_{CY}.t$ and $x = V_{CX}.t$ and reaches a final linear velocity equal to V_D , at the end of stage D. The velocity components are:

$$V_{DX} = V_{CX} = V_C \cdot \cos(\theta_C) \quad (2.26)$$

$$V_{DY} = V_{CY} + g.t = V_C \cdot \sin(\theta_C) + g.t \quad (2.27)$$

Now, most necessary parameters to track tree and piece after stag D are calculated. Also α and β values can be determined using simple geometric relations:

$$L \cdot \sin(\alpha) = x + d \cdot \sin(\theta_C) - d \cdot \sin(\theta_D) - \{u(t_D) - u(t_C)\} \quad (2.28)$$

Where t_D and t_C are times at the beginning of stages D and C.

$$L \cdot \cos(\alpha) = y - d \cdot \cos(\theta_C) + d \cdot \cos(\theta_D) \quad (2.29)$$

$$L = \sqrt{[x + d \cdot \sin(\theta_C) - d \cdot \sin(\theta_D) - \{u(t_D) - u(t_C)\}]^2 + \{y - d \cdot \cos(\theta_C) + d \cdot \cos(\theta_D)\}^2} \quad (2.30)$$

$$\alpha = \tan^{-1} \left(\frac{x + d \cdot \sin(\theta_C) - d \cdot \sin(\theta_D) - \{u(t_D) - u(t_C)\}}{y - d \cdot \cos(\theta_C) + d \cdot \cos(\theta_D)} \right) \quad (2.31)$$

$$\beta = 180^\circ - \theta_D = 180^\circ - (\theta_C + \varpi_C \cdot t) \quad (2.32)$$

$$\dot{\alpha} \approx 0 \text{ and } \dot{\beta} \approx -\varpi_C \quad (2.33)$$

α and β angles and velocities values will be used later as initial condition for modeling of stage E.

The solving strategy for stage D is to:

- ✓ Obtain θ_C and from modeling of stage C.
- ✓ Assume a value for V_Δ and ϖ_C that would be tricky

ϖ_C can be simply assumed to be equal to ω_C

- ✓ Calculate $V_C = V_\Delta + d_{CG} \cdot \varpi_C$
- ✓ Find V_C components $V_{CX} = V_C \cdot \cos(\theta_C)$ and $V_{CY} = V_C \cdot \sin(\theta_C)$
- ✓ Find V_D components as functions of time:

$$V_{DX} = V_{CX} = V_C \cdot \cos(\theta_C) \text{ And } V_{DY} = V_{CY} + g \cdot t = V_C \cdot \sin(\theta_C) + g \cdot t$$

- ✓ Calculate movement of the CG of the piece as function of time:

$$y = g \cdot t^2 / 2 + V_{CY} \cdot t \text{ and } x = V_{CX} \cdot t$$

- ✓ Solve geometric equation to find time:

$$L = \sqrt{[x + d \cdot \sin(\theta_C) - d \cdot \sin(\theta_D) - \{u(t_D) - u(t_C)\}]^2 + \{y - d \cdot \cos(\theta_C) + d \cdot \cos(\theta_D)\}^2}$$

✓ Finally, obtain initial conditions for modeling of subsequent stage:

$$\alpha = \tan^{-1}\left(\frac{x + d \cdot \sin(\theta_C) - d \cdot \sin(\theta_D) - \{u(t_D) - u(t_C)\}}{y - d \cdot \cos(\theta_C) + d \cdot \cos(\theta_D)}\right)$$

$$\beta = 180^\circ - \theta_D = 180^\circ - (\theta_C + \varpi_C \cdot t)$$

$$\dot{\alpha} \approx 0 \text{ and } \dot{\beta} \approx -\varpi_C$$

2.2.1. Results (Modeling of Stage D)

As discussed before, it can be assumed that the initial angular velocity of the piece, the trunk horizontal deflection, and trunk horizontal velocity at the beginning of stage D are related to their values at the end of stage C. The initial conditions considered for the motion in stage D are listed in Table 2.4.

Table 2.4- Motion initial condition: Stage D

Parameter		At the end of stage C	At the beginning of stage D
Piece Angle (rad)	θ	$\theta_C = 0.99$	0.99
Angular velocity of piece (rad/s)	θ'	$\omega_C = 1.69$	$\varpi_C = 1.69$
Linear velocity of the CG of the piece (m/s)	V_C	4.69	$V_\Delta + d_{CG} \cdot \varpi_C$
Horizontal deflection of trunk (m)	u	$u_C = -0.62$	-0.62
Horizontal velocity of trunk (m/s)	u'	$u'_C = -0.11$	-0.11

Using the stage D model described in Section 2.2, the cut piece motion and trunk horizontal deflection are calculated and plotted in Figure 2.21, Figure 2.22, Figure 2.23, Figure 2.24. Deflection of tree top is graphed in Figure 2.21. It should be noticed that trunk vibrates with apical force during stages A, B and C and vibrates freely after release time ($t=1.31$ sec. in this case) during stage D. V_Δ was assumed to be approximately 2 m/s and ϖ_C was assumed to be equal to the angular velocity of piece at the end of stage C (1.69 rad/s).

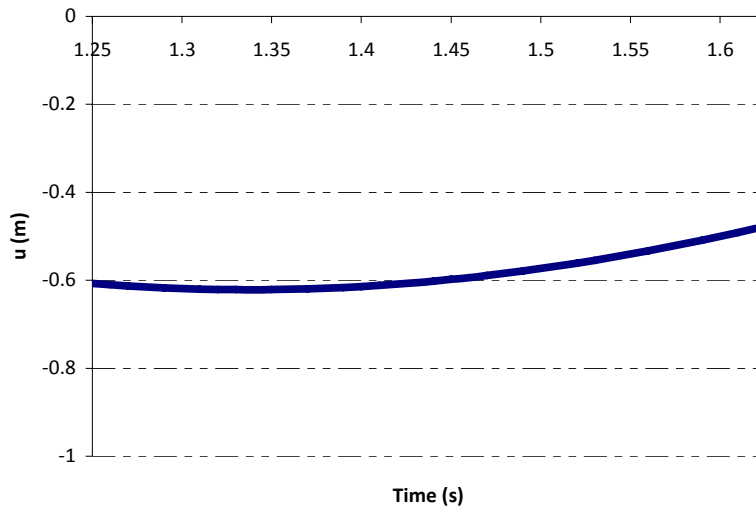


Figure 2.21- Variation of displacement of tree top with time during stage D

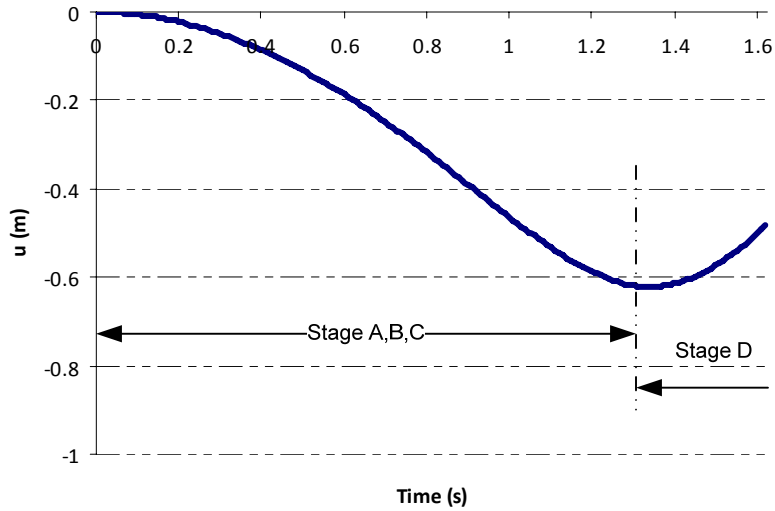


Figure 2.22- Variation of displacement of tree top with time during stages A, B, C and D

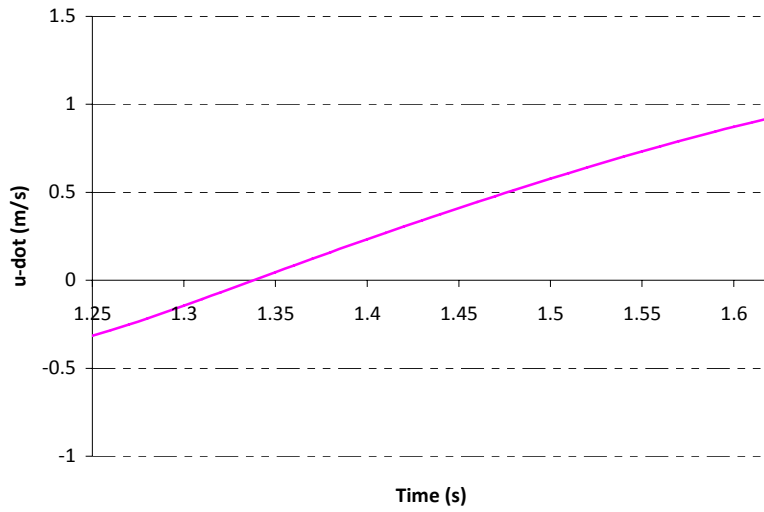


Figure 2.23- Variation of velocity of tree top with time during stage D

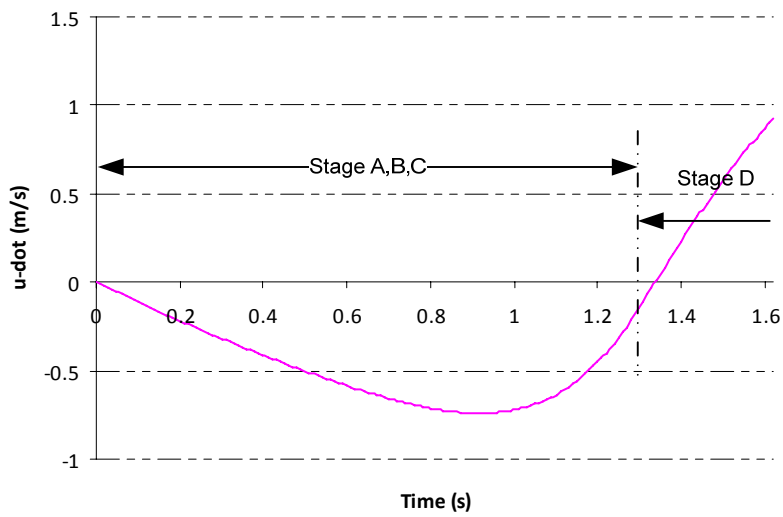


Figure 2.24- Variation of deflection and velocity of tree top with time during stages A, B, C and D

An interesting output of this stage is the motion trajectory of the CG of the piece which is plotted in Figure 2.25.

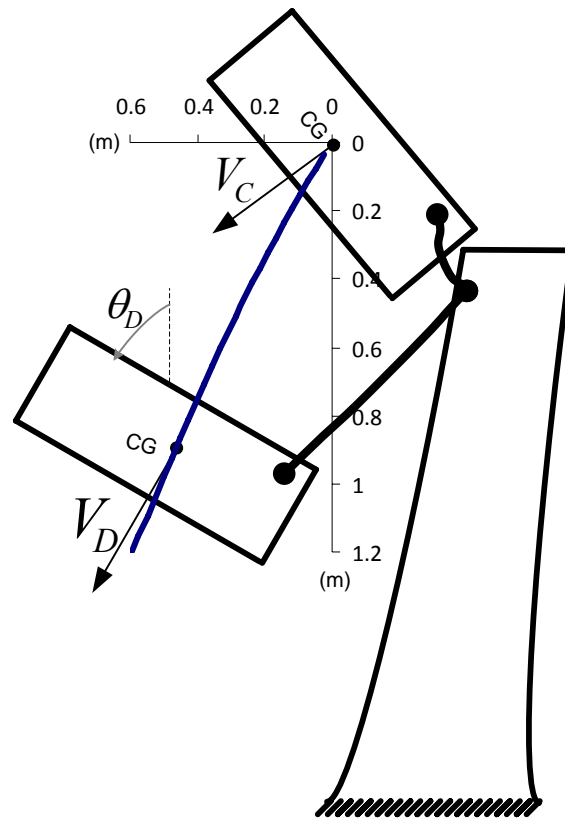


Figure 2.25- Stage D results– Motion trajectory of the CG of the piece

The results in stage D can be summarized as in Table 2.5:

Table 2.5- Summary of results: Stage D

STAGE		End of stage C	End of stage D
PARAMETER			
Time (s)	t	1.31	1.62
Piece angle (rad)	θ	$\theta_C = 0.99$	$\theta_D = 1.51$
Angular velocity of piece (rad/s)	θ'	$\omega_C = 1.69$	$\omega_D = 1.69$
Horizontal deflection of trunk (m)	u	$u_C = -0.62$	$u_D = -0.48$
Horizontal velocity of trunk (m/s)	u'	$u'_C = -0.11$	$u'_D = 0.92$

By using equations (2.31) to (2.33) initial conditions of stage E can be calculated:

$$\alpha = \tan^{-1} \left(\frac{x + d \cdot \sin(\theta_C) - d \cdot \sin(\theta_D) - \{u(t_D) - u(t_C)\}}{y - d \cdot \cos(\theta_C) + d \cdot \cos(\theta_D)} \right) \quad (2.31)$$

$$\beta = 180^\circ - \theta_D = 180^\circ - (\theta_C + \omega_C \cdot t) \quad (2.32)$$

$$\dot{\alpha} \approx 0 \text{ and } \dot{\beta} \approx -\omega_C \quad (2.33)$$

Table 2.6- Final condition of motion at end of stage D

Time (s)	t	1.62
Rope angle (rad)	α	0.58
Piece angle (rad)	β	1.62
Horizontal deflection of trunk (m)	u	-0.48
Angular velocity of rope (rad/s)	α'	0
Angular velocity of piece (rad/s)	β'	-1.69
Horizontal velocity of trunk (m/s)	u'	0.92

2.2.2. Verification of Results by the Energy Method

In this section the results of the model in stage D is validated like in Section 2.1.3 by using the energy method. In this case we have two separate systems: (1) the falling piece and (2) oscillating trunk. The oscillating trunk equation is similar to what we had in stages A,B,C and is not verified here again. The energy term for falling piece is now:

$$E = \frac{1}{2}.m.V^2 - m.g.Y$$

Where

Kinetic energy = $\frac{1}{2}.m.V^2$ and V can be calculated from equations (2.26 and 2.27)

And

Potential energy = $-m.g.Y$ where Y is derived in section 2.2.1.

The energy term variation and total energy term is plotted in the graph below.

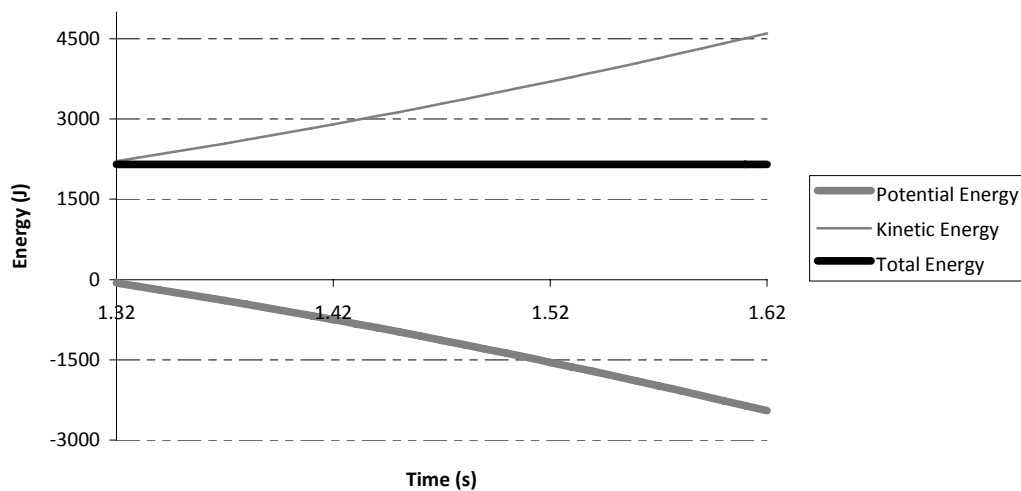


Figure 2.26- Variation of energy terms with time in stage D

It is clear from the graph that total energy remains constant during the motion while the potential energy and kinetic energy changes.

2.3. Modeling of Stage E

The falling piece starts swinging after the rope becomes taut (E in Figure 2.1) and will stop either gradually after swinging or abruptly after hitting the trunk. The motion can be formulized like a three degree of freedom motion which is a combination of a double pendulum and a mass-spring-damper system.

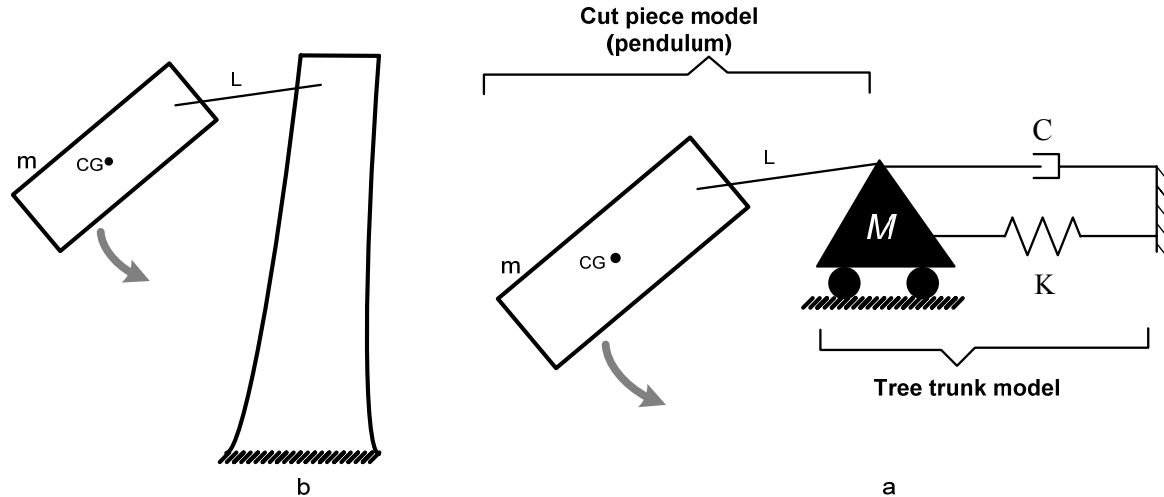


Figure 2.27- Stage E model
a) Simplified model, b) Real model

The geometry of the model can be seen in Figure 2.28, in which trunk is modeled as a dynamic model consisting of a concentrated mass, linear spring and damper. A roller is placed below the concentrated mass to assume an axially rigid trunk. This representation is to simplify the actual dynamic system which consists of distributed mass, stiffness and damping (Refer to Appendix A to see derivation of M, K and C).

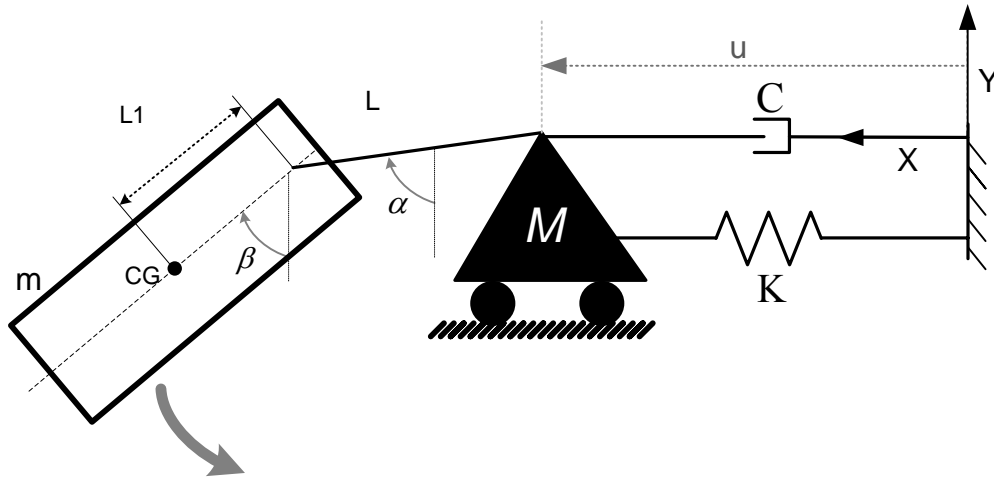


Figure 2.28- Stage E model - Geometry

The angle α , β and u are three degrees of freedom of the model. The first one is the rotation angle of the taut rope, the second one is the rotation angle of the cut piece, and the third one is horizontal displacement of the top of the tree.

The motion can be formulated using the coordinates of the center of gravity of the cut piece during motion (x and y); α , β , u , x , and y are five geometric variables which are related with two coordinate transformation equations(2.34) and (2.35).

$$x = u + L \cdot \sin(\alpha) + L1 \cdot \sin(\beta) \quad (2.34)$$

$$y = L \cdot \cos(\alpha) + L1 \cdot \cos(\beta) \quad (2.35)$$

L and $L1$ are the length of the rope and the distance from the attachment point to the CG of the cut piece, respectively. Mechanics equations are used to complete the set of necessary equations to determine the motion function and finally find the rope force.

Following the Newtonian approach, the equations of motion for center of gravity of the cut piece can be written as¹¹:

$$m.\ddot{x} = -T.\sin(\alpha) \quad (2.36)$$

$$m.\ddot{y} = m.g - T.\cos(\alpha) \quad (2.37)$$

Where m is the falling piece mass and T is tension force of the rope. The other dynamic equation of cut piece (2.38) relates its rotation torque to moment of inertia.

$$I_c.\ddot{\beta} = T.\sin(\alpha - \beta).L_1 \quad (2.38)$$

I_c is the rotational moment of inertia of the cut piece about the center of gravity. J_c can also be defined for simplification in more complex equations as $J_c = \frac{I_c}{m}$.

T is tension in the rope connecting the piece to the trunk. In fact, one end of rope is connected to the cut piece directly and the other end is connected to a pulley which is attached to the trunk. In other words, the rope is not directly connected to the trunk so the reaction force of rope tension on the tree trunk is a function of T (actual tension in rope) which relates to the pulley and rope characteristics. Thus, the total force acting on the top of tree can be estimated as:

$$R = p \cdot T + q \quad (2.39)$$

In which p and q are factors determined by pulley and rope characteristics. (Refer to Appendix C for details about pulley and rope forces)

¹¹ α, β, u, x, y are functions of time.

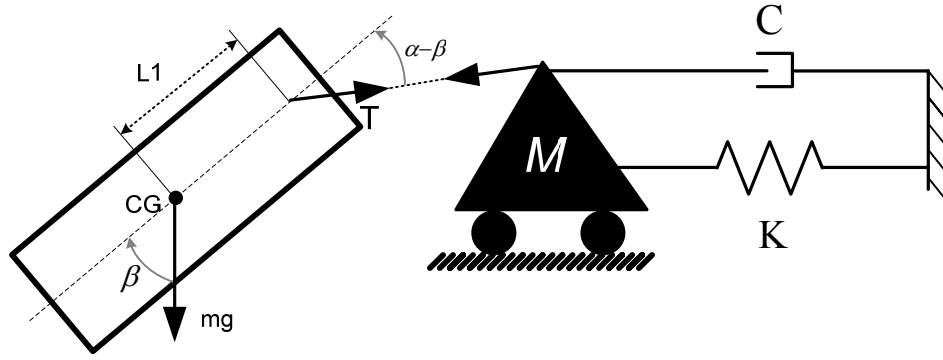


Figure 2.29- Stage E model - Forces

Now, equilibrium of dynamic forces is written for concentrated mass (M) as:

$$T \cdot \sin(\alpha) = M \cdot \ddot{u} + C \cdot \dot{u} + K \cdot u \quad (2.40)$$

After combining the geometric equations (2.34 and 2.35) with dynamic equations (2.36), (2.37), (2.38) and (2.40), a system of ordinary differential equations is obtained.

$$\ddot{\alpha} \cdot L \cdot \cos(\alpha) - \dot{\alpha}^2 \cdot L \cdot \sin(\alpha) + \ddot{\beta} \cdot L_1 \cdot \cos(\beta) - \dot{\beta}^2 \cdot L_1 \cdot \sin(\beta) + \quad (2.41)$$

$$\ddot{u} \cdot \left(\frac{M}{m} + 1\right) + \dot{u} \cdot \left(\frac{C}{m}\right) + u \cdot \left(\frac{K}{m}\right) = 0$$

$$\ddot{\alpha} \cdot L \cdot \sin(\alpha) + \dot{\alpha}^2 \cdot L \cdot \cos(\alpha) + \ddot{\beta} \cdot L_1 \cdot \sin(\beta) + \dot{\beta}^2 \cdot L_1 \cdot \cos(\beta) \quad (2.42)$$

$$- \ddot{u} \cdot \left(\frac{M \cdot \cos(\alpha)}{m \cdot \sin(\alpha)}\right) - \dot{u} \cdot \left(\frac{C \cdot \cos(\alpha)}{m \cdot \sin(\alpha)}\right) - u \cdot \left(\frac{K \cdot \cos(\alpha)}{m \cdot \sin(\alpha)}\right) + g = 0$$

$$\ddot{\beta} \cdot \frac{J_c}{L_1} - \ddot{u} \cdot \left(\frac{M \cdot \sin(\alpha - \beta)}{m \cdot \sin(\alpha)}\right) - \dot{u} \cdot \left(\frac{C \cdot \sin(\alpha - \beta)}{m \cdot \sin(\alpha)}\right) - u \cdot \left(\frac{K \cdot \sin(\alpha - \beta)}{m \cdot \sin(\alpha)}\right) = 0 \quad (2.43)$$

Six initial conditions are needed to solve this system of ordinary differential equations. Solving the system of differential equations (2.41, 2.42 and 2.43) numerically is done by using the Runge Kutta method of order four which is a very popular and commonly used method for the approximation of the solutions of ordinary differential equations. To make these equations solvable by the Runge Kutta method, they must be written in the forms

of $\ddot{\alpha} = \text{function}(\alpha, \dot{\alpha}, \beta, \dot{\beta}, u, \dot{u})$, $\ddot{\beta} = \text{function}(\alpha, \dot{\alpha}, \beta, \dot{\beta}, u, \dot{u})$, $\ddot{u} = \text{function}(\alpha, \dot{\alpha}, \beta, \dot{\beta}, u, \dot{u})$.

Thus, these equations were rewritten in a way that there would only be a function of $\ddot{\alpha}$, $\ddot{\beta}$ or \ddot{u} in each equation. To perform this, equations (2.41, 2.42 and 2.43) were rewritten in the format below:

$$\ddot{\alpha}.A_1 + \dot{\alpha}^2.A_2 + \ddot{\beta}.B_1 + \dot{\beta}^2.B_2 + \ddot{u}.C_1 + \dot{u}.C_2 + u.C_3 + E_1 = 0 \quad (2.44)$$

$$\ddot{\alpha}.A_3 + \dot{\alpha}^2.A_4 + \ddot{\beta}.B_3 + \dot{\beta}^2.B_4 + \ddot{u}.C_4 + \dot{u}.C_5 + u.C_6 + E_2 = 0 \quad (2.45)$$

$$\ddot{\beta}.B_5 + \ddot{u}.C_7 + \dot{u}.C_8 + u.C_9 + E_3 = 0 \quad (2.46)$$

Now, all three equations can be written in one matrix-formatted equation and variables F_1, F_2 and F_3 will be defined to simplify the equation:

$$\begin{bmatrix} A_1 & B_1 & C_1 \\ A_3 & B_3 & C_4 \\ 0 & B_5 & C_7 \end{bmatrix} \begin{bmatrix} \ddot{\alpha} \\ \ddot{\beta} \\ \ddot{u} \end{bmatrix} = \begin{bmatrix} -\dot{\alpha}^2.A_2 - \dot{\beta}^2.B_2 - \dot{u}.C_2 - u.C_3 - E_1 \\ -\dot{\alpha}^2.A_4 - \dot{\beta}^2.B_4 - \dot{u}.C_5 - u.C_6 - E_2 \\ -\dot{u}.C_8 - u.C_9 - E_3 \end{bmatrix} = \begin{bmatrix} F_1 \\ F_2 \\ F_3 \end{bmatrix} \quad (2.47)$$

The left-side 3x3 matrix is inverted and multiplied by right-side matrix to solve for values of $\ddot{\alpha}$, $\ddot{\beta}$, and \ddot{u} .

$$\begin{bmatrix} \ddot{\alpha} \\ \ddot{\beta} \\ \ddot{u} \end{bmatrix} = \frac{1}{(\Delta)} \begin{bmatrix} -F_1 \cdot B_3 \cdot C_7 + F_1 \cdot B_5 \cdot C_4 + F_2 \cdot B_1 \cdot C_7 - F_2 \cdot B_5 \cdot C_1 - F_3 \cdot B_1 \cdot C_4 + F_3 \cdot B_3 \cdot C_1 \\ A_3 \cdot C_7 \cdot F_1 - A_1 \cdot C_7 \cdot F_2 + A_1 \cdot C_4 \cdot F_3 - A_3 \cdot C_1 \cdot F_3 \\ -A_3 \cdot B_5 \cdot F_1 + A_1 \cdot B_5 \cdot F_2 - A_1 \cdot B_3 \cdot F_3 + A_3 \cdot B_1 \cdot F_3 \end{bmatrix}$$

$$\Delta = -A_1 \cdot B_3 \cdot C_7 + A_1 \cdot B_5 \cdot C_4 + A_3 \cdot B_1 \cdot C_7 - A_3 \cdot B_5 \cdot C_1$$

(2.48)

Now we have proper equations to run the Runge Kutta method. Due to the large volume of calculations, a C++ program was written to perform the Runge Kutta calculations for this system of ordinary differential equations (Refer to Appendix I – Codes Written in C++). Outputs of the program are motion angles and angular velocities of cut piece, and deformation of top of the trunk which can be plugged into any of equations (2.49, 2.59 and 2.51) to calculate tension in rope.

$$T = -\frac{m}{\sin(\alpha)} \{ \ddot{u} + \ddot{\alpha} \cdot L \cdot \cos(\alpha) - \dot{\alpha}^2 \cdot L \cdot \sin(\alpha) + \ddot{\beta} \cdot L_1 \cdot \cos(\beta) - \dot{\beta}^2 \cdot L_1 \cdot \sin(\beta) \} \quad (2.49)$$

$$T = -\frac{m}{\cos(\alpha)} \{ g + \ddot{\alpha} \cdot L \cdot \sin(\alpha) + \dot{\alpha}^2 \cdot L \cdot \cos(\alpha) + \ddot{\beta} \cdot L_1 \cdot \sin(\beta) + \dot{\beta}^2 \cdot L_1 \cdot \cos(\beta) \} \quad (2.50)$$

$$T = \frac{1}{\sin(\alpha_i)} \{ M \cdot \ddot{u} + C \cdot \dot{u} + K \cdot u \} \quad (2.51)$$

Energy of system includes of kinetic, potential and friction work (due to material damping):

$$\begin{aligned} \text{Kinetic energy} &= \frac{1}{2}.m.(\dot{x}^2 + \dot{y}^2) + \frac{1}{2}.I_c.\dot{\beta}^2 + \frac{1}{2}.M.\dot{u}^2 \\ &= \frac{1}{2}.m.\{(\dot{u} + L.\dot{\alpha}.\cos(\alpha))^2 + (L.\dot{\alpha}.\sin(\alpha) + L_1.\dot{\beta}.\sin(\beta))^2 + J_c.\dot{\beta}^2\} + \frac{1}{2}.M.\dot{u}^2 \end{aligned} \quad (2.52)$$

$$\begin{aligned} \text{Potential energy} &= -m.g.y + \frac{1}{2}.K.u^2 \\ &= \frac{1}{2}.m.\{-2.g.(L.\cos(\alpha) + L_1.\cos(\beta))\} + \frac{1}{2}.K.u^2 \end{aligned} \quad (2.53)$$

$$\text{Friction work (Damper energy dissipation)} = \int C\dot{u}.du \quad (2.54)$$

2.3.1. Simplified Method (Modeling of Stage E)

Due to large calculations in this section, a simplified model with 2 degree of freedom (DOF) is suggested and has been verified by 3 DOF model discussed before. Thus, the motion can be formulized like a two degree of freedom pendulum which is a familiar physics problem. In other words, the top of tree motion has been neglected in this method. So, angles α and β are the two degrees of freedom of the problem. The first one is the rotation angle of the taut rope and the second is the rotation angle of the cut piece.

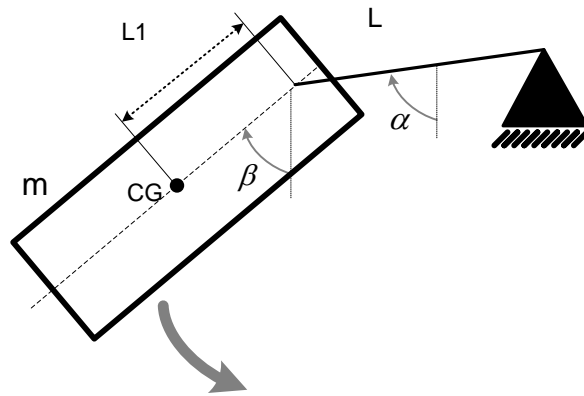


Figure 2.30- Simplified model of stage E - Parameters

The motion can be formulated using the coordinates of the center of gravity of the cut piece during motion (x and y); the combination of these four variables (α , β , x , y) is the easiest approach although two coordinate transformation equations have to be written to relate these variables.

$$x = L \cdot \sin(\alpha) + L1 \cdot \sin(\beta) \quad (2.55)$$

$$y = L \cdot \cos(\alpha) + L1 \cdot \cos(\beta) \quad (2.56)$$

L and L1 are the length of the rope and the distance from the attachment point to the CG of the cut piece, respectively (Figure 2.30). Mechanics equations are used to complete the set of equations necessary to determine the motion function and finally find the rope force. For this research two classical mechanics approaches (Newtonian and Lagrangian) are used separately and results are compared to minimize the undesired errors. Only the Newtonian approach is described here and the Lagrangian approach is described in Appendix E. Following the Newtonian approach, the equations of motion for the center of gravity of the cut piece can be written as¹²:

$$m \cdot \ddot{x} - T \cdot \sin(\alpha) = 0 \quad (2.57)$$

$$m \cdot \ddot{y} = m \cdot g - T \cdot \cos(\alpha) \quad (2.58)$$

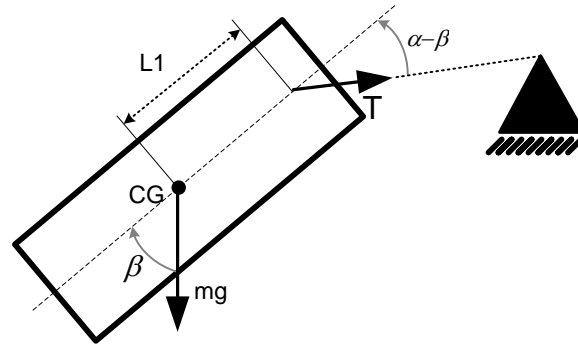


Figure 2.31- Simplified model of stage E - Forces

¹² α, β, x, y are functions of time.

The last equation is related to the cut piece rotation.

$$I_c \ddot{\beta} = T \sin(\alpha - \beta) L_1 \quad (2.59)$$

Where T is tension force of the rope; and I_c is the rotational moment of inertia of the cut piece about the center of gravity. J_c can also be defined for simplification in more complex equations as

$$J_c = \frac{I_c}{m}$$

Where m is the falling piece mass. After combining the two geometric equations (2.55 and 2.56) with three Newtonian equations (2.57, 2.58 and 2.59), a system of ordinary differential equations is obtained. These equations are in exact compatibility with Lagrangian results. However the Lagrangian results are neater. (Refer to Appendix E)

$$\ddot{\alpha} L + \ddot{\beta} L_1 \cos(\alpha - \beta) + \dot{\beta}^2 L_1 \sin(\alpha - \beta) + g \sin(\alpha) = 0 \quad (2.60)$$

$$\begin{aligned} & \ddot{\alpha} \{L L_1 \sin(\alpha - \beta) \cos(\alpha)\} + \ddot{\beta} \{L_1^2 \sin(\alpha - \beta) \cos(\beta) + J_c \sin(\alpha)\} \\ & - \dot{\alpha}^2 \{L L_1 \sin(\alpha - \beta) \sin(\alpha)\} + \dot{\beta}^2 \{L_1^2 \sin(\alpha - \beta) \sin(\beta)\} = 0 \end{aligned} \quad (2.61)$$

Rope tension (T) is also obtained from:

$$T = \frac{m}{\sin(\alpha)} \{\dot{\alpha}^2 L \sin(\alpha) + \dot{\beta}^2 L_1 \sin(\beta)\} - \frac{m}{\sin(\alpha)} \{\ddot{\alpha} L \cos(\alpha) + \ddot{\beta} L_1 \cos(\beta)\} \quad (2.62)$$

Solving the system of ordinary differential equations numerically (2.60 and 2.61) was done by using the Runge Kutta Method of order four as before. Outputs of the program are motion angles and angular velocities which can be plugged into the equation (2.62) to calculate tension in the rope.

Energy term in this case is:

$$= \frac{1}{2}.m.\{(L.\dot{\alpha}.\cos(\alpha))^2 + (L.\dot{\alpha}.\sin(\alpha) + L_1.\dot{\beta}.\sin(\beta))^2 + J_c.\dot{\beta}^2 - 2.g.(L.\cos(\alpha) + L_1.\cos(\beta))\}$$

(2.63)

Energy of system consists of kinetic, potential energies:

$$\text{Kinetic energy} = \frac{1}{2}.m.(\dot{x}^2 + \dot{y}^2) + \frac{1}{2}.I_c.\dot{\beta}^2$$

$$= \frac{1}{2}.m.\{(L.\dot{\alpha}.\cos(\alpha))^2 + (L.\dot{\alpha}.\sin(\alpha) + L_1.\dot{\beta}.\sin(\beta))^2 + J_c.\dot{\beta}^2\}$$

$$\text{Potential energy} = -m.g.y^2$$

$$= \frac{1}{2}.m.\{-2.g.(L.\cos(\alpha) + L_1.\cos(\beta))\}$$

There are two ways to check the results for the problem. First way is by substituting results into differential equations and second way is to check if energy term remains constant during time. The second method is used in Section 2.3.3 to check the results.

2.3.2. Results (Detailed modeling of Stage E)

These findings for modeling of stage E can be applied to tree.No.7 to check their validity.

The detailed method is used here. The initial conditions for stage E were obtained from modeling of stage D.

Table 2.7- Motion initial condition: Stage E

Time (s)	t	1.62
Rope angle (rad)	α	0.58
Piece angle (rad)	β	1.62
Horizontal deflection of trunk (m)	u	-0.48
Angular velocity of rope (rad/s)	α'	0
Angular velocity of piece (rad/s)	β'	-1.69
Horizontal velocity of trunk (m/s)	u'	0.92

Table 2.8- Analysis results: Stage E

Rope angle (rad)	α	Figure 2.32
Piece angle (rad)	β	Figure 2.33
Horizontal deflection of trunk (m)	α'	Figure 2.34
Angular velocity of rope (rad/s)	β'	Figure 2.35
Angular velocity of piece (rad/s)	u	Figure 2.36
Horizontal velocity of trunk (m/s)	u'	Figure 2.37

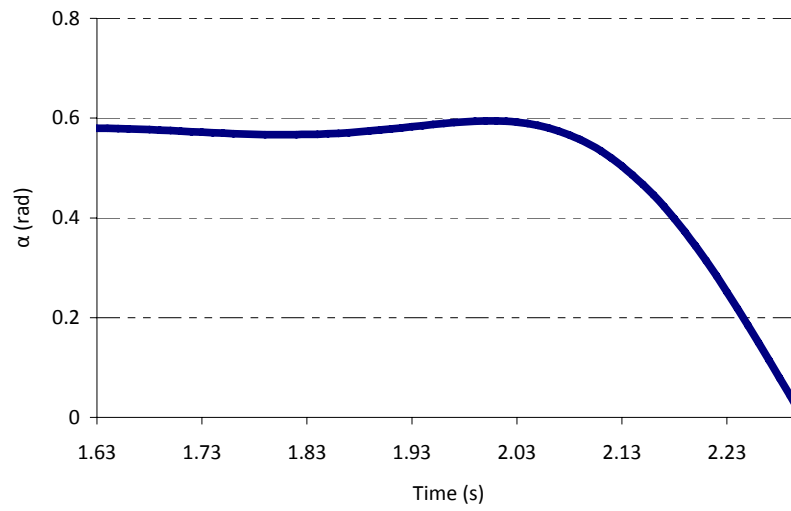


Figure 2.32- Variation of α (in radian) with time -as described before

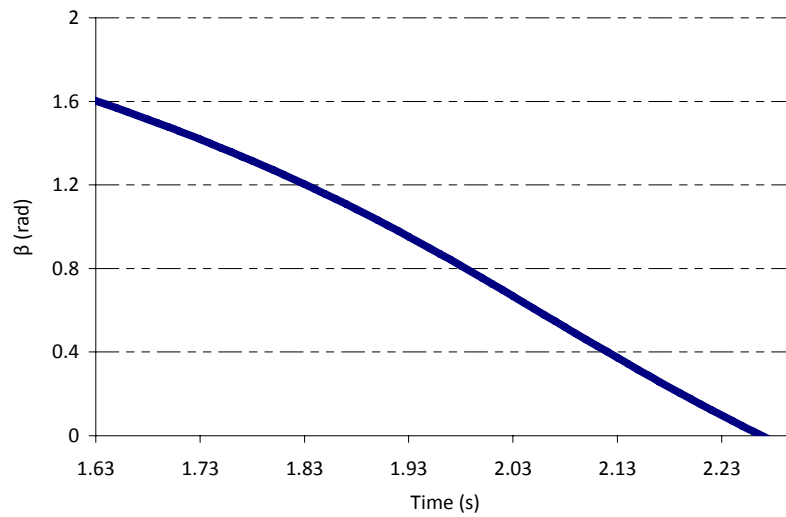


Figure 2.33- Variation of β (in radian) with time -as described before

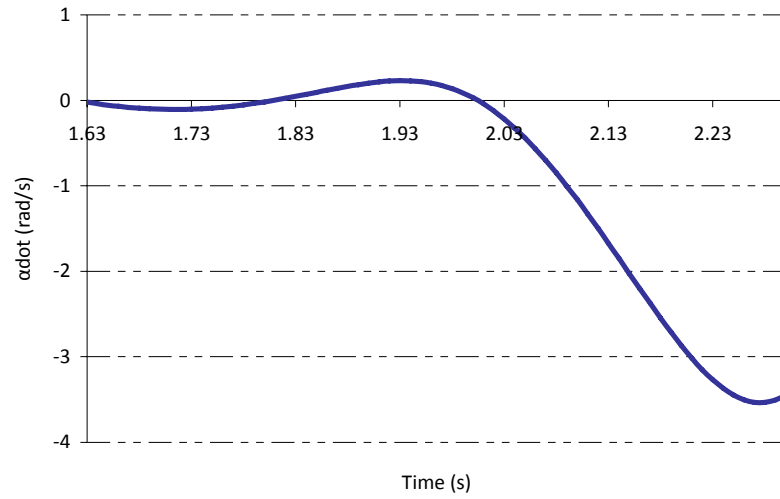


Figure 2.34- Variation of α angular velocity (in radian/s) with time - as described before

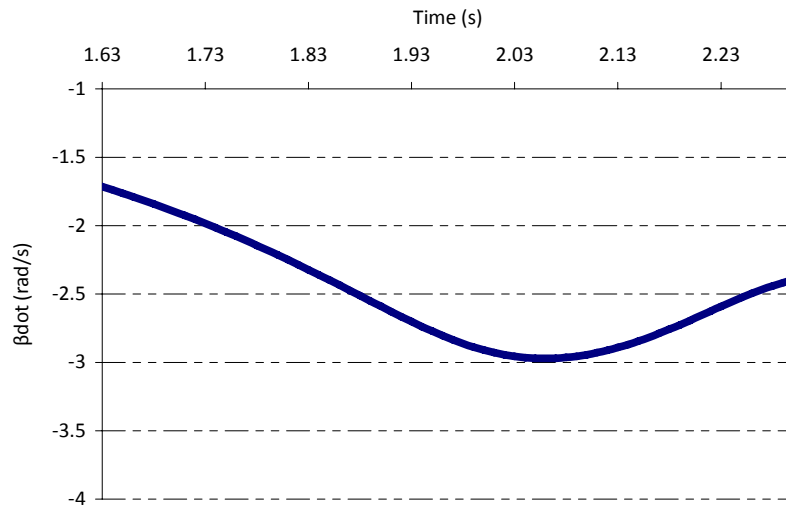


Figure 2.35-Variation of β angular velocity (in radian/s) with time - as described before

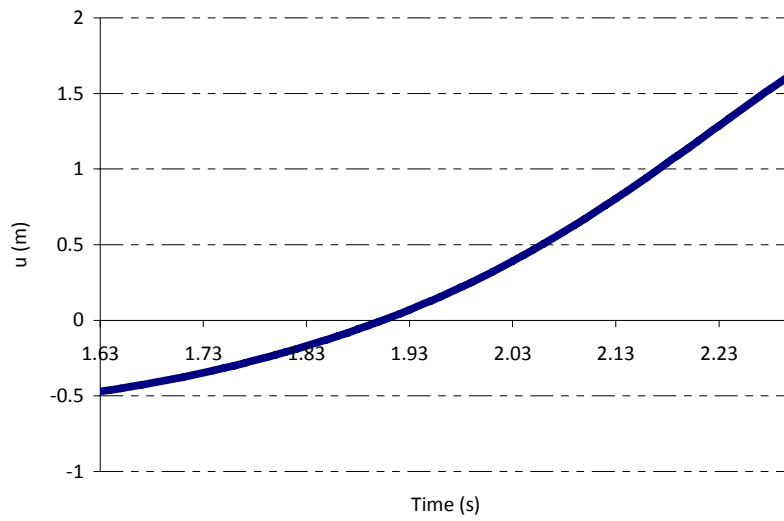


Figure 2.36- Variation of deflection of tree top (m) with time

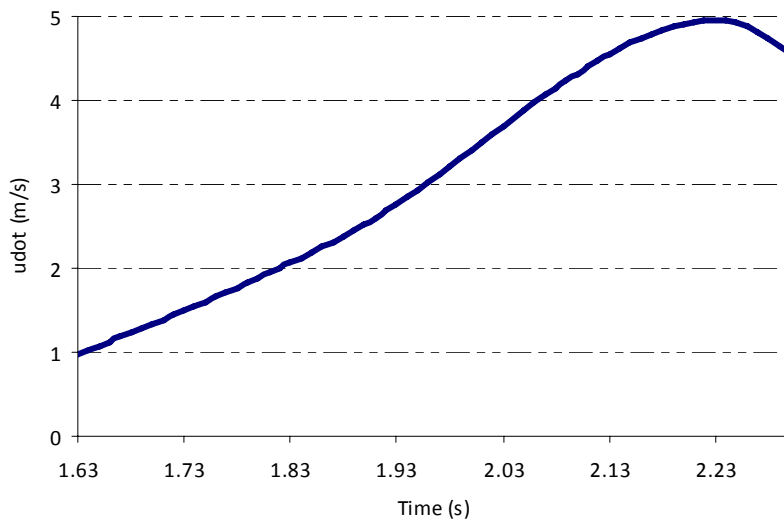


Figure 2.37- Variation of velocity of tree top (m/s) with time

Table 2.9- Motion final condition: Stage E

Time (s)	t	2.31
Rope angle (rad)	α	0
Piece angle (rad)	β	-0.1
Horizontal deflection of trunk (m)	u	1.67
Angular velocity of rope (rad/s)	α'	-3.37
Angular velocity of piece (rad/s)	β'	-2.38
Velocity of the CG of the piece (m/s)	V_p	3.87

2.3.3. Verification of Results by the Energy Method

In this section the results of the main model of stage E is validated like Sections 2.1.3 and 2.2.2 by using the energy method. According to Conservation of Energy Rule, during a phenomenon the total energy must remain constant. In this case the energy term consists of:

$$\begin{aligned} \text{Kinetic energy} &= \frac{1}{2}.m.(\dot{x}^2 + \dot{y}^2) + \frac{1}{2}.I_c.\dot{\beta}^2 + \frac{1}{2}.M.\dot{u}^2 \\ &= \frac{1}{2}.m.\{(\dot{u} + L.\dot{\alpha}.\cos(\alpha))^2 + (L.\dot{\alpha}.\sin(\alpha) + L_1.\dot{\beta}.\sin(\beta))^2 + J_c.\dot{\beta}^2\} + \frac{1}{2}.M.\dot{u}^2 \end{aligned}$$

$$\begin{aligned} \text{Potential energy} &= -m.g.y + \frac{1}{2}.K.u^2 \\ &= \frac{1}{2}.m.\{-2.g.(L.\cos(\alpha) + L_1.\cos(\beta))\} + \frac{1}{2}.K.u^2 \end{aligned}$$

$$\text{Friction work (Damper energy dissipation)} = \int C.\dot{u}.du$$

The energy term variation and total energy term is plotted in the graph below.

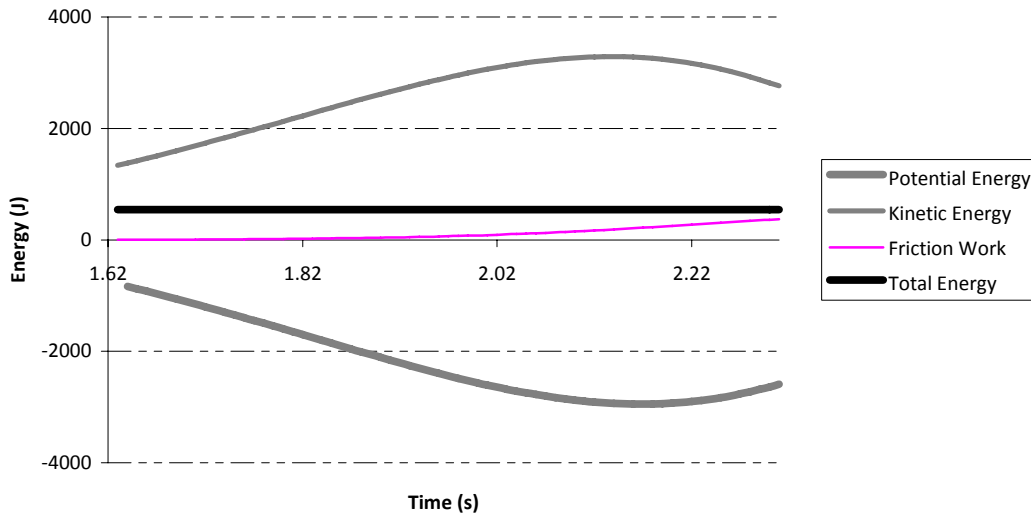


Figure 2.38- Variation of energy terms with time in stage E

It is obvious from the graph that total energy remains constant during the motion while the potential energy decreases and kinetic energy increases. The smallest magnitude is

related to friction work (damper energy dissipation). To better understand the energy variation another graph is plotted in semi log format where the potential energy term is not plotted because it is negative.

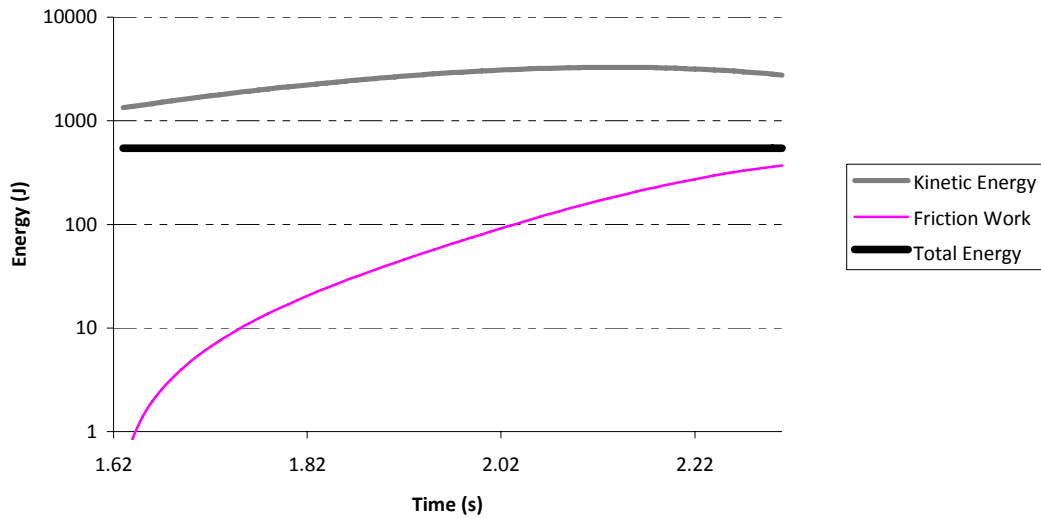


Figure 2.39- Variation of energy terms with time in stage E

Also it can be observed from the graph that total energy remains constant while the kinetic energy increases. The friction work (energy dissipation due to material damping) logically increases during the motion.

2.4. Modeling of Stage F

During tree cutting, a cut segment that is tied to the trunk falls until the rope become taut and the piece starts following a motion similar to a pendulum. Usually the top piece (which has crown and more branches) will start swinging without hitting the trunk until its motion ends because of damping generated by friction forces (effect of dissipating energy via branch motion). In another phenomenon, lower segments that have no branches will likely hit the tree trunk without any significant swinging. In this case, impact forces are generated from collision of the cut piece and the trunk.

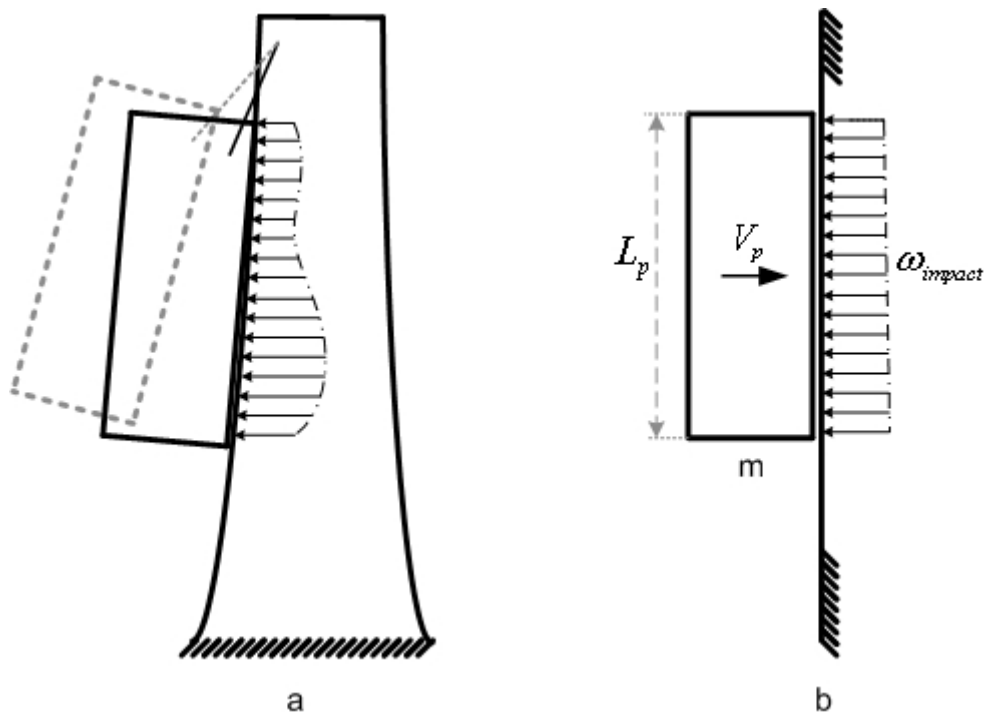


Figure 2.40- Stage F model - Impact
a) Real model, b) Simplified model

The impact phenomenon can be modeled by assuming a simplified 2D face to face contact of a rigid bar with a wall and assuming that a uniformly distributed impact force

is created. Rewriting simple collision equations results in equation (2.64) which defines ω_{impact} , the impact load per unit length.

$$\omega_{impact} = \frac{m}{L_p} \cdot \frac{\partial V_p}{\partial t} \approx \frac{m}{L_p} \cdot \frac{V_p}{\Delta t} \quad (2.64)$$

In which V_p is the piece velocity at the moment it hits the trunk. V_p can be calculated from results obtained during the stage E model. The components of velocity of the CG of the piece are calculated (equations 2.65 and 2.66) by differentiating equations (2.34) and 2.35.

$$\dot{x} = \dot{u} + L \cdot \dot{\alpha} \cdot \cos(\alpha) + L_1 \cdot \dot{\beta} \cdot \cos(\beta) \quad (2.65)$$

$$\dot{y} = -L \cdot \dot{\alpha} \cdot \sin(\alpha) - L_1 \cdot \dot{\beta} \cdot \sin(\beta) \quad (2.66)$$

$$V_p = \sqrt{\dot{x}^2 + \dot{y}^2} \quad (2.67)$$

Thus, the essential variables needed to solve the simplified impact problem are defined and can be substituted in equation (2.64). The impact time, Δt , needs to be estimated.

It has to be noted that the impact modeled in this section does not occur during removal of the top piece from the tree because the crown of the tree prevents the direct impact of the piece with the trunk. Thus, the impact force is not significant during removal of the top (first) piece from the tree.

2.4.1. Results (Modeling of Stage F)

The impact condition can be obtained from the final result of modeling of stage E and being imported into equations (2.65), (2.66) and (2.67) to find the impact velocity. Then the impact velocity can be used to calculate the distributed impact load.

Table 2.10- Impact condition (Stage F)¹³

Time (s)	t	2.31
Rope angle (rad)	α	0
Piece angle (rad)	β	-0.1
Horizontal deflection of trunk (m)	u	1.67
Angular velocity of rope (rad/s)	α'	-3.37
Angular velocity of piece (rad/s)	β'	-2.38
Velocity of the CG of the piece (m/s)	V_p	3.87
Impact time (s)	Δt	Variable

Finding impact force needs the impact duration (Δt) which can not be calculated precisely. Thus, the impact distributed load, w_{impact} , is calculated for different values of impact duration (Δt) in Figure 2.41, plotted in log-log scale. Figure 2.41 shows that impact distributed load increases linearly with time in log-log scale. A reasonable value for impact duration (Δt) is about 0.01 s which relates to distributed impact load of 7000 N/m.

¹³ Refer to Figure 2.20, **Figure 2.28** and **Figure 2.40** where these parameters are illustrated.

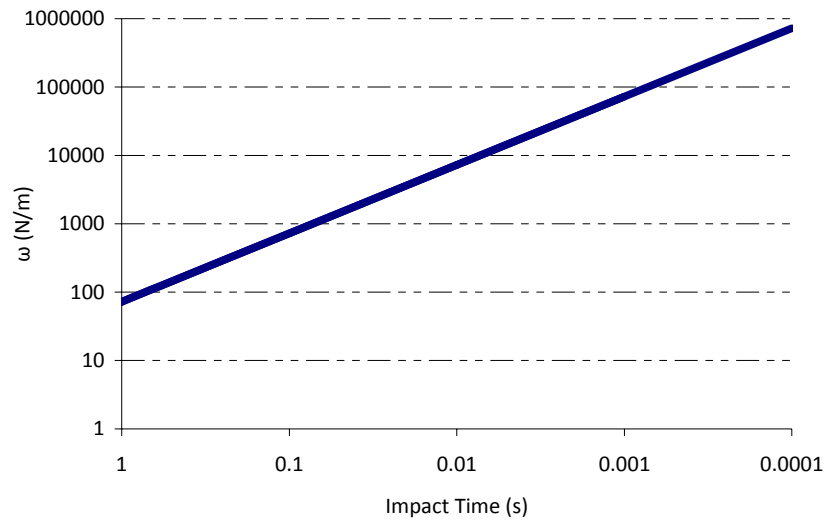
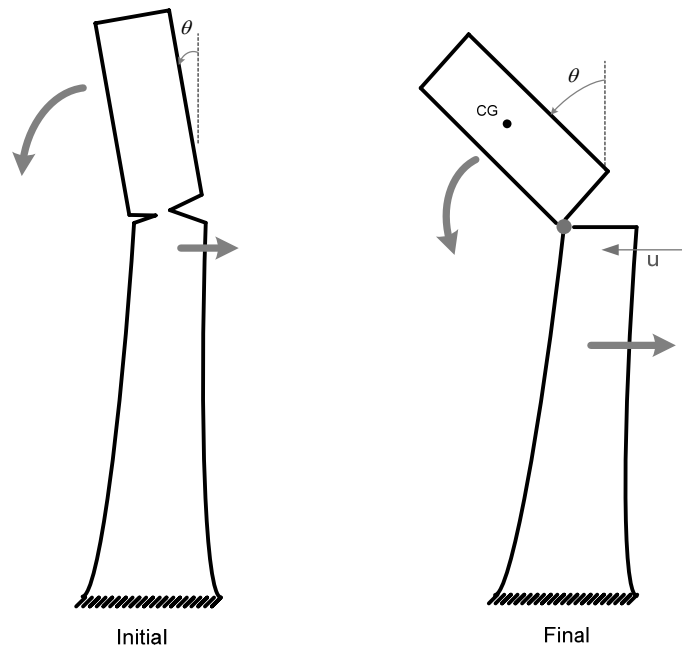


Figure 2.41- Variation of uniformly distributed impact force, ω_{impact} , as a function of impact time (Δt)

2.5. Summary of Results

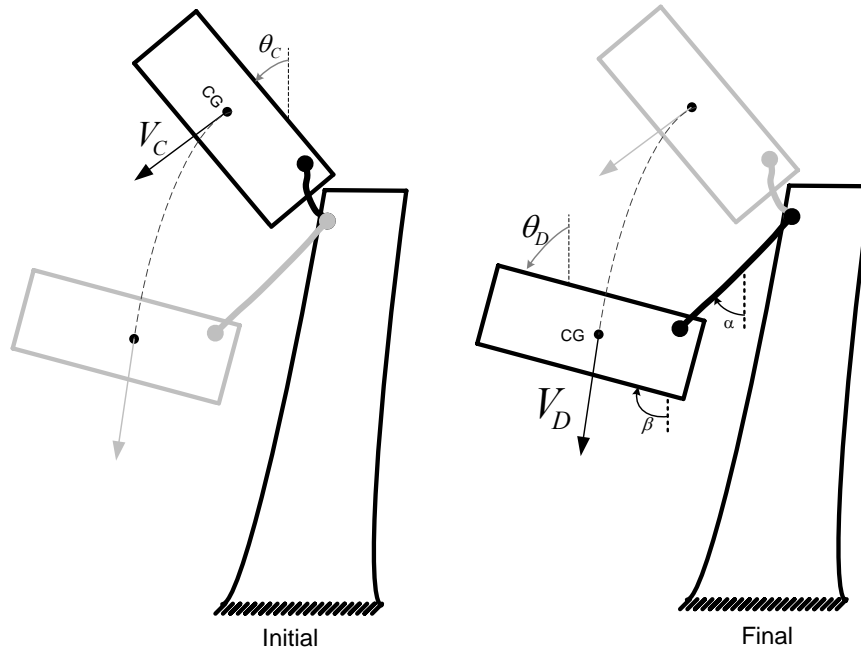
Tree No.7 top piece removal forces: In this section, the results from all sub models presented in this chapter are put together.

Stages A, B, C model:



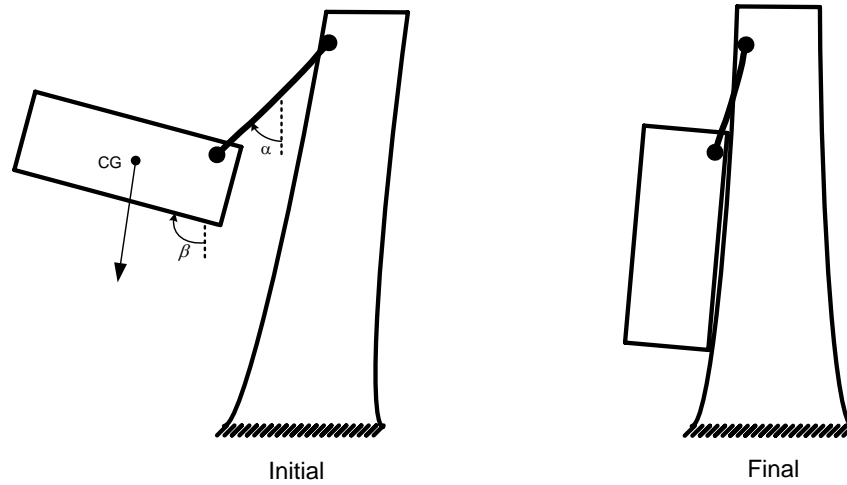
Stages A, B, C			
PARAMETER		STAGE	
		Initial condition	Release point
		Beginning of stage A	End of stage C
Time (s)	t	0	1.31
Piece angle (rad)	θ	0.10	$\theta_C = 0.99$
Angular velocity of piece (rad/s)	θ'	0	$\omega_C = 1.69$
Horizontal deflection of trunk (m)	u	0	$u_C = -0.62$
Horizontal velocity of trunk (m/s)	u'	0	$u'_C = -0.11$

Stage D model:



Stage D - Motion final condition		
Time (s)	t	1.62
Rope angle (rad)	α	0.58
Piece angle (rad)	β	1.62
Horizontal deflection of trunk (m)	u	-0.48
Angular velocity of rope (rad/s)	α'	0
Angular velocity of piece (rad/s)	β'	-1.69
Horizontal velocity of trunk (m/s)	u'	0.92

Stages E and F model:



Stage E - Motion final condition		
Time (s)	t	2.31
Rope angle (rad)	α	0
Piece angle (rad)	β	-0.1
Horizontal deflection of trunk (m)	u	1.67
Angular velocity of rope (rad/s)	α'	-3.37
Angular velocity of piece (rad/s)	β'	-2.38
Velocity of the CG of the piece(m/s)	V_p	3.87

Impact distributed load is not significant in the removal of the first piece because the crown of the tree prevents the direct impact of the piece with the tree. Displacement of tree top and force function calculated in each stage during cutting process are put together and plotted in Figures Figure 2.42 Figure 2.43.

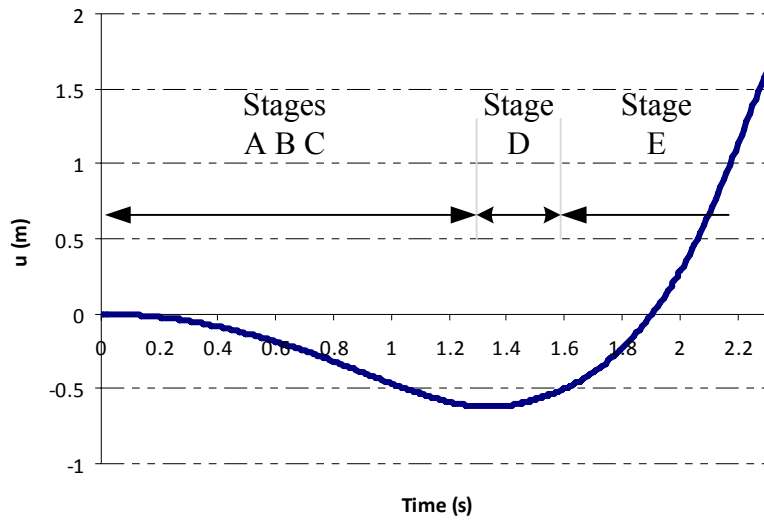


Figure 2.42 - Variation of displacement of tree top with time during

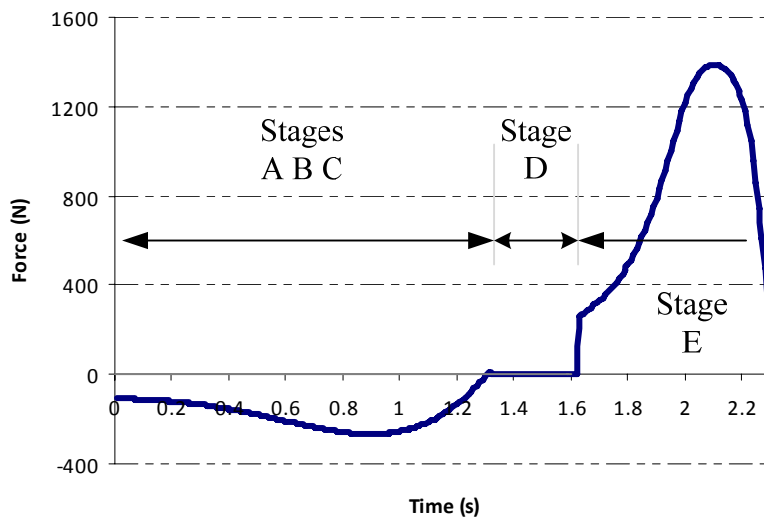


Figure 2.43 – Cutting process loads

The maximum force applied to the tree top is found to be 1383N from Figure 2.43 while the maximum horizontal force measured in the field tests is 2985N. The 53% difference in the calculated and measured value is due to the phenomenon that happens at the beginning of stage E. The rope is tightened abruptly and this impulse creates large force in the rope which is not considered in the model proposed in this research.

CHAPTER 3

VERIFICATION OF CALCULATED APICAL LOAD FUNCTION WITH EXPERIMENTAL DATA

3.1. Finite Element Modeling

Mechanical modeling of natural systems is a difficult issue because: (1) Biological systems have variable material properties such as modulus of elasticity and density within their body; (2) imperfections in their body are hard to notice and model exactly; and (3) their dimensions can rarely fit exactly in a simple geometric shape. In spite of these complexities having relevant experimental data is useful to create a more accurate finite element model. In this chapter, the FE model of tree No.7¹⁴ has been created and its dynamic response is studied.

¹⁴ Refer to Section 1.5 – field measurement and Appendix G.

3.1.1. Modal Analysis and Verification of Finite Element Model

The material and geometry properties obtained from field measurements of tree No.7 are listed in Table 3.1.

Table 3.1 – Tree No.7 field parameters

Material properties	
Modulus of elasticity (MPa)	5065
Damping ratio (%) ¹⁵	10
Density (Kg/m ³)	942.466
Geometry	
Shape	Truncated cone
Height (m)	15.519
Bottom diameter (cm)	25.2
Top diameter (cm)	17.6

To acquire natural frequencies, a finite element model (FEM) of tree No.7 was built in ANSYS¹⁶ using properties shown in Table 3.1. Material properties were assumed constant along the tree trunk. Tree trunk was modeled like a truncated cone. It can be seen that the truncated trunk results converge better than the cylindrical trunk model. Yung (1975) found that use of truncated conical beam elements better reflects actual tree properties than cylindrical beam elements.

¹⁵ Refer to Section 1.5 for calculation of damping ratio.

¹⁶ ANSYS is used because it is easy and quick to analyze numerous models with different dimensions.

Model was meshed using fine tetrahedral elements with a maximum element size of 0.5m. The actual size of most elements is about 0.1m and there are 1152 elements (Figure 3.1)

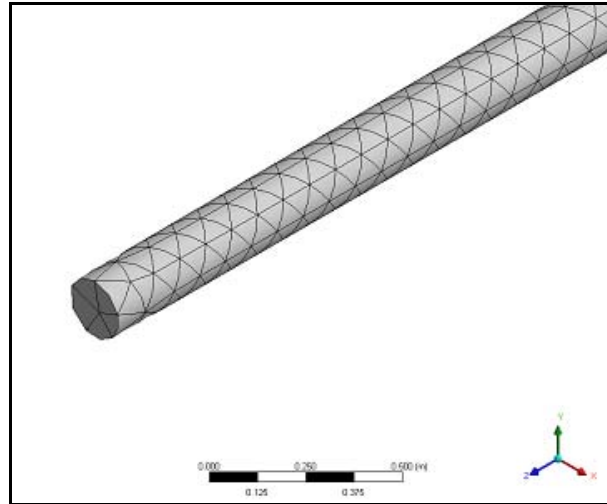


Figure 3.1 – FEM meshing of tree trunk

Modal analysis with at-rest initial conditions was conducted on the FE model of tree No.7 and modes between 0-25 Hz were extracted (Table 3.2). It is observed that the obtained frequencies related to bending mode are coupled because of identical cross section bending characteristics of structure in both horizontal directions. Modal analyses results are listed in Table 3.2. The frequencies of mode numbers of 1 to 6 are related to the bending deformation mode shapes¹⁷.

¹⁷ Natural frequencies of tree are important parameters for dynamic modeling. A tree, as a distributed mass system, absorbs energy at all its natural frequencies; however, most energy is absorbed at the tree's first natural frequency (Peltola, 1996).

Table 3.2 – FEM modal analysis result for tree No.7

Mode Number	Frequency (Hz)	Period (s)	Description
1	0.3920	2.5508	Bending
2	1.9770	0.5058	Bending
3	5.1975	0.1924	Bending
4	10.0401	0.0996	Bending
5	16.5562	0.0604	Bending
6	24.8139	0.0403	Bending
7	28.4900	0.0351	Axial

Table 3.2 indicates that the fundamental mode of vibration of the FE model has a frequency of 0.3920 Hz. If the value corresponds to the natural frequency of real tree, then the validity of the FE model used for the tree would be verified. A way to obtain the actual natural frequency of the tree is to further study the dynamic response of the tree during cutting process.

The axial strain recorded during cutting process at probe 2 (in the direction of fall) is plotted in Figure 3.2. It can be guessed from Figure 3.2 that the fundamental period of vibration of tree is about 2 second and consequently the natural frequency of tree is approximately 0.5 Hz. Because the frequency content of vibrations is not precisely obtainable from time domain plots, a Fourier transform is performed on the time history function to get the frequency domain function. The Fourier transform can be done by performing the Fourier integration numerically or using suitable software.

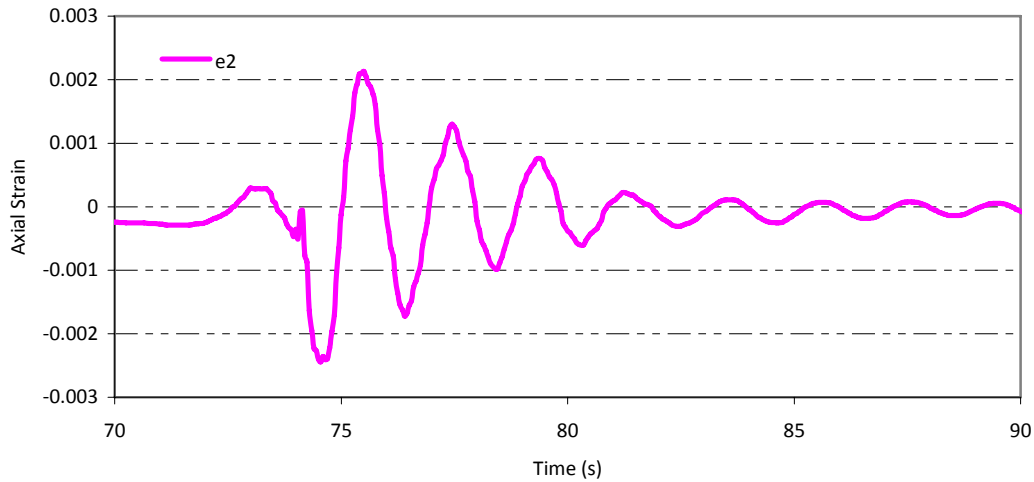


Figure 3.2 - Variation of axial strain with time (time domain graph)¹⁸

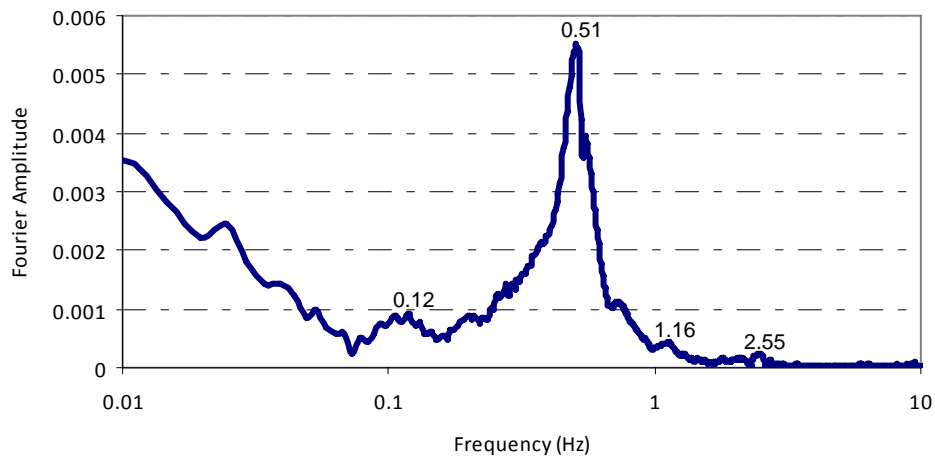


Figure 3.3 – Fourier amplitudes for axial strains as a function of frequency¹⁹

The peaks on Figure 3.3 indicate the governing frequencies of vibration of tree during cutting process. The first local peak is related to frequency 0.0097Hz and does not reflect

¹⁸ Refer to Section 1.5 and Figure 1.4.

¹⁹ Numbers written on peaks indicate the frequency value.

the dynamic characteristics of the tree but the highest peak (frequency = 0.5078Hz) is close to the frequency of natural vibration of the tree (frequency = 0.3920Hz related to first vibration mode of finite element model).

It is obvious that the FEM used does not properly represent the dynamic properties of the tree and there is a 30% difference in the calculated and measured frequencies of the fundamental modes of vibration.

The parameters affecting the dynamic properties of the tree are height, density and modulus of elasticity. Error in calculating height and density is negligible but error in calculating modulus of elasticity can be a source of difference in dynamic parameters of model and real tree. In addition, modeling tree-ground connection as a fixed connection may be a significant cause of error.

To evaluate the effects of different tree properties in modal frequencies of FE model, various modal analyses have been carried out with $\pm 30\%$ variation in height, $\pm 40\%$ variation in modulus of elasticity and $\pm 50\%$ change in average diameter. Results of this parametric analysis are discussed in Section 3.1.2.

3.1.2. Effect of Dimension and Material Parameters on Dynamic Properties of Tree²⁰

In this section, various modal analyses have been carried using finite element models with variations in height, modulus of elasticity and average diameter. Also, an analytical approach is presented to verify the results. In addition, more analyses have been performed to study the effect of trunk decay on the frequencies of vibration of the tree. These analyses have been done to study the effect of each parameter on the frequency of modes of vibration.

The study can be strengthened with a proper analytical calculation of natural frequency of the tree trunk. The analytical study presented here was modified from assumptions used in the model presented in Appendix A equations. To analytically study the effect of tree height, diameter and modulus of elasticity on its natural frequency, the tree is assumed to be a simple cylindrical shape cantilever beam. Hence, Appendix A equations, written for a truncated shaped tree, are modified for the cylinder shape beam.

The assumed shape function $\psi(z)$ for cantilever beam which satisfies the boundary conditions is:

$$\psi(z) = 1 - \cos\left(\frac{\pi \cdot z}{2 \cdot H}\right) \quad (3.1)$$

In this case, $m(z)$, $EI(z)$ are calculated by assuming that geometric shape of trunk is a cylinder and radius of the trunk in each section remains constant. Thus $m(z)$ and $EI(z)$ remain constant as well, and are calculated using

$$m = \rho \cdot \pi \cdot r^2 \quad (3.2)$$

²⁰ Truncated conical shape is used for FEM and cylindrical shape is used for analytical calculations in this section.

$$EI = \frac{\pi}{4} . r^4 . E \quad (3.3)$$

After substituting m , EI and $\psi(z)$ functions into Appendix A equations (3.4, 3.5 and 3.6), M , K and ω are obtained.

$$M = \int_0^H m(z) . \psi(z)^2 . dz \quad (3.4)$$

$$K = \int_0^H EI(z) . \psi''(z)^2 . dz \quad (3.5)$$

$$M = H . \rho . r^2 \left(\frac{3}{2} . \pi - 4 \right) \quad (3.6)$$

$$K = \frac{\pi^5}{128} . \frac{E . r^4}{H^3} \quad (3.7)$$

$$\omega = \sqrt{K/M} \quad (3.8)$$

$$\omega = \frac{r}{H^2} \sqrt{\frac{E}{\rho}} \cdot \sqrt{\frac{\pi^5}{128 . \left(\frac{3}{2} . \pi - 4 \right)}} \quad (3.9)$$

It can be seen that natural frequency of the tree is related to the average radius, height, density and modulus of elasticity.

$$\omega \propto \frac{r}{H^2} \sqrt{\frac{E}{\rho}} \quad (3.10)$$

$$f \propto \frac{r}{H^2} \sqrt{\frac{E}{\rho}} \quad (3.11)$$

To study the effect of tree height on natural frequency of tree, various modal analyses were carried out on a model for tree No.7 with a $\pm 30\%$ variation in height and results are shown in Figure 3.4 and Figure 3.5.

It is obvious from Figure 3.4 that frequencies of vibration decrease when the tree height increases that means the tree is stiffer when it is shorter.

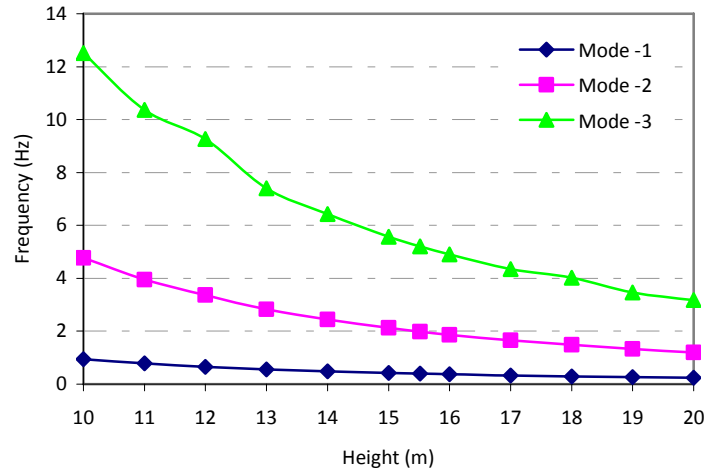


Figure 3.4 - Variation of frequency of the first three modes of vibration with height

Variation of natural frequency of the tree with height is plotted in Figure 3.5. The trend line is also plotted on the same figure. R squared value of 1 indicates that the trend line equation $f = \frac{94.667}{H^2}$ precisely fits the curve. The trend line equation is consistent with

equation (3.11) showing $f \propto \frac{1}{H^2}$.

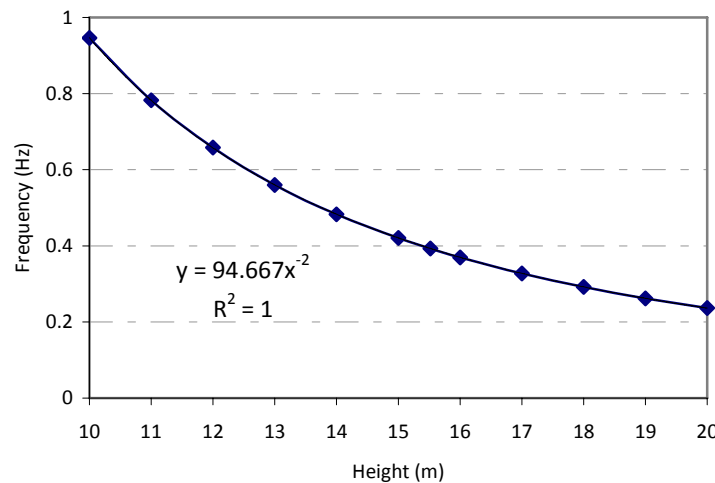


Figure 3.5 - Variation of natural frequency with height and the trend line

To study the effect of average tree diameter on natural frequency of the tree, various modal analyses were carried out on the model for tree No.7 with $\pm 50\%$ variation in average diameter (while tapering slope was constant) and results are shown in Figure 3.6 and Figure 3.7. It is obvious from Figure 3.6 that frequencies of vibration increase when the tree diameter increases, that means the tree is stiffer when it is thicker.

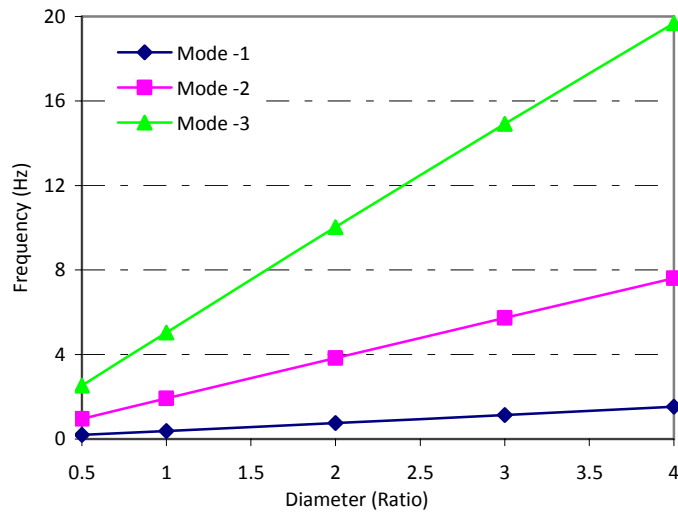


Figure 3.6 - Variation of frequency of the first three modes of vibration with average diameter

It is also observed from the results of average diameter variation analysis that frequency of the axial mode shape remains constant. Variation of natural frequency of the tree (modes 1 and 2) is plotted in Figure 3.7. The trend line is also plotted on the same figure. R squared value of 1 indicates that the trend line equation precisely fits the curve. The trend line equation is consistent with equation (3.11) showing $f \propto r$ where r is the average radius of cross section of the tree.

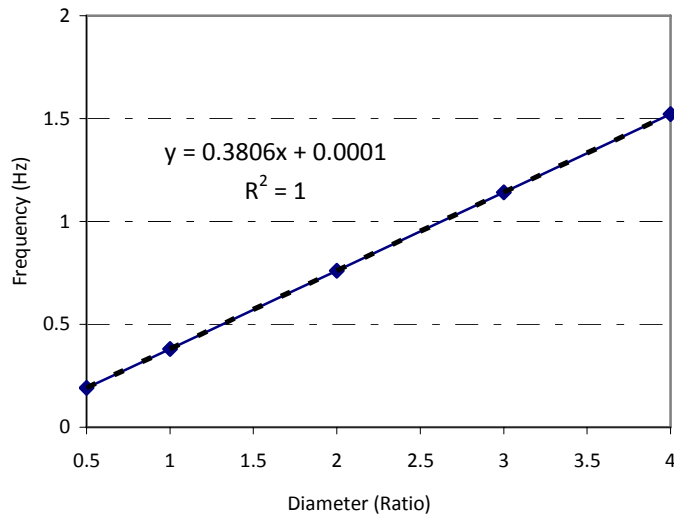


Figure 3.7 - Variation of natural frequency with average diameter and its trend line

To study the effect of modulus of elasticity of wood on natural frequency of the tree, various modal analysis were carried out on the tree No.7 model with $\pm 40\%$ variation in modulus of elasticity of wood and results are shown in Figure 3.8 and Figure 3.9.

It is obvious from Figure 3.8 that frequencies of vibration increase when modulus of elasticity increases, that means the tree is stiffer when the modulus of elasticity of wood is higher.

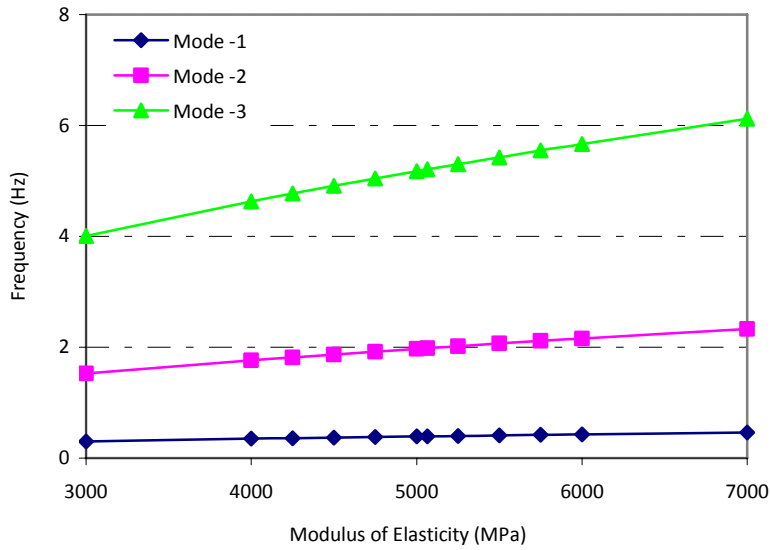


Figure 3.8 - Variation of frequency of the first three modes of vibration with modulus of elasticity

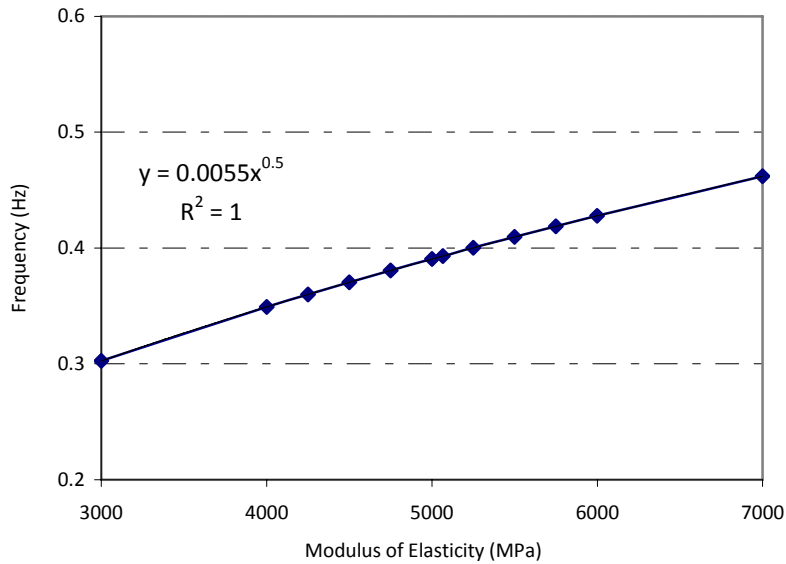


Figure 3.9 - Variation of natural frequency with modulus of elasticity and its trend line

Variation of natural frequency of the tree with modulus of elasticity is plotted in Figure 3.9. The trend line is also plotted on the same figure. R squared value of 1 indicates that

the trend line equation precisely fits the curve. The trend line equation is consistent with equation (3.11) showing $f \propto \sqrt{E}$.

Tree defects such as trunk decays are very common (Figure 3.10). Considering these defects in the FE model causes stress concentrations in the trunk during dynamic loading and also changes natural frequencies of the tree. This phenomenon is studied by applying trunk decay to the finite element model. All model properties are identical with previous models except a hole with variable dimension was introduced inside the trunk starting at the height of 0.5m above the ground. A simplification of modeling decay in the trunk as a simple hole inside the body has been done. Various analyses with different defect height have been carried out, as listed in Table 3.3.



Figure 3.10 - Common type of decay in tree trunk
 From left to right: Longitudinal sketch of tree defect, Real cross section of decayed trunk, Modeled cross section of decayed trunk

Table 3.3 - Defect Dimensions

Model	Length (m)	Diameter (cm)
I	1	17.6
II	2	17.6
III	3	17.6
IV	4	17.6
V	5	17.6

Defect in all of these models starts at the height of 0.5m with given dimensions. Meshing detail is the same as previous models (fine meshed tetrahedral elements with maximum size of 0.5m) but the meshing will be much finer in the decay area (Figure 3.11)

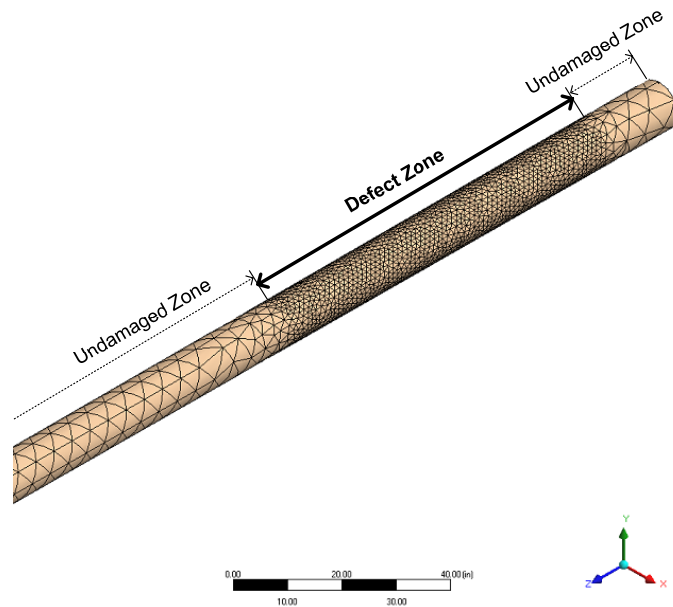


Figure 3.11 - Meshing around decay zone

For models I to IV, the modal analysis results are shown in Figure 3.12 to Figure 3.15. It is clear that the major bending and axial modes should have higher frequency with larger

trunk defects but it is not really clear, in the term of equations, why this does not happen in other modes.

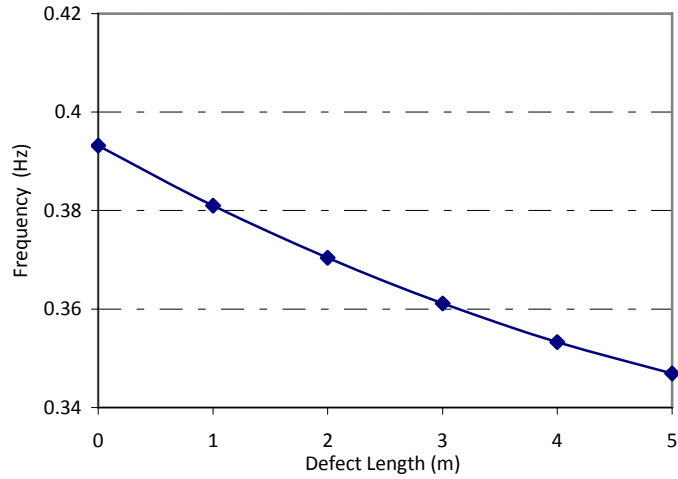


Figure 3.12 - Variation of frequency of the 1st mode with defect length

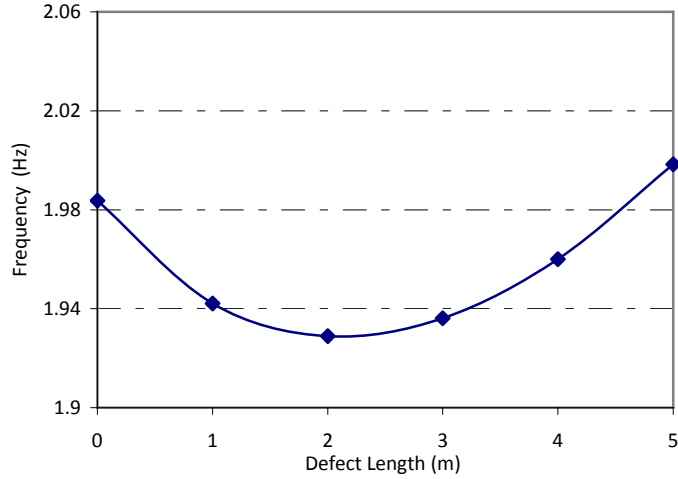


Figure 3.13 - Variation of frequency of the 2nd mode with defect length

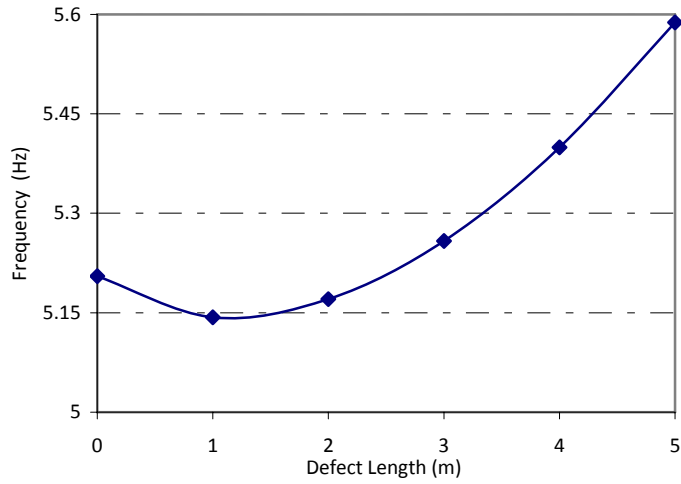


Figure 3.14 - Variation of frequency of the 3rd mode with defect length

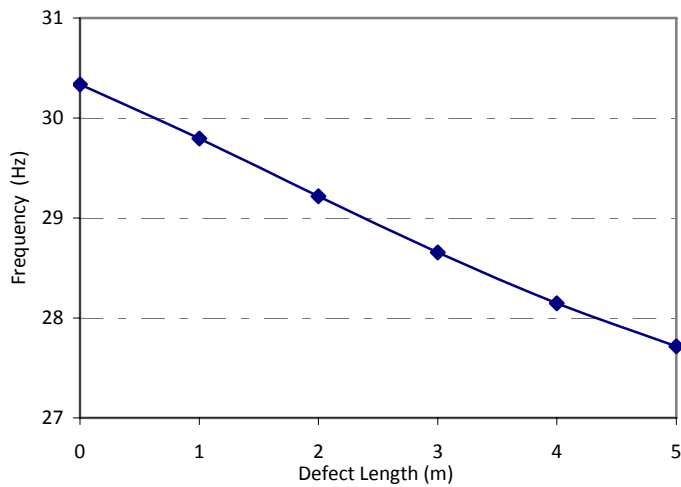


Figure 3.15 - Variation of frequency of axial mode (mode 7) with defect length

The frequency axis in Figure 3.12 to Figure 3.15 is not scaled similarly so it makes the comparison of the plots difficult. Thus the ratio of frequency of models with defect to the frequency of the model without defect²¹ has been calculated for each mode and plotted in

$$^{21} \frac{f_{FEM \text{ without defect}}}{f_{FEM \text{ with defect}}} \cdot (100\%)$$

Figure 3.16 in order to easily compare the variation of modal frequencies of models with different defect length.

Figure 3.16 shows that frequencies of the first bending and the axial modes of vibration decrease with increasing defect length. But frequencies of the second and third modes of vibration behave differently. This phenomenon may be originated from the difference in mode shapes of vibration of cantilever beam. In Figure 3.17 shapes of the first three modes of vibration of tree No.7 which assumed to behave like a cantilever beam are illustrated. It can be seen that the modeled defects inside the tree trunk are placed close to the location of peak of the second and third mode shapes and caused the strange behavior observed in Figure 3.16.

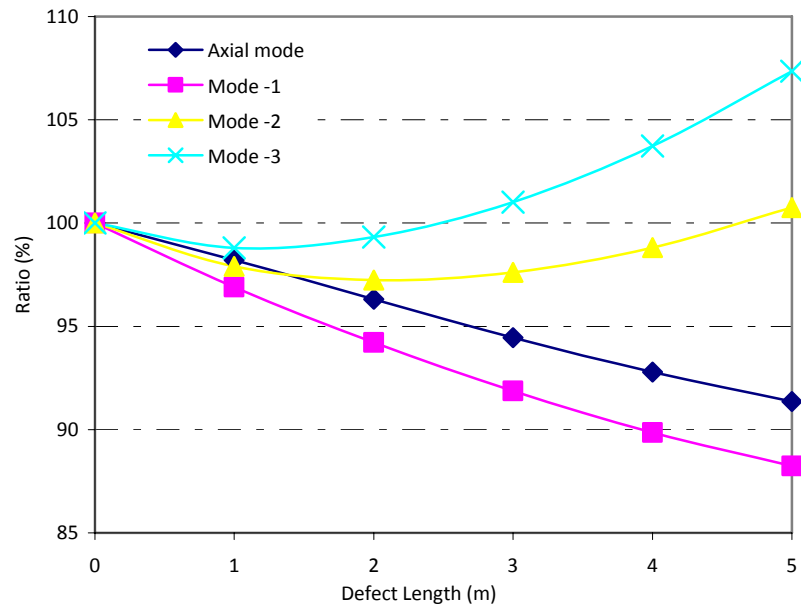


Figure 3.16 - Variation of frequency of different modes (mode 1, 2, 3 and 7) with defect length

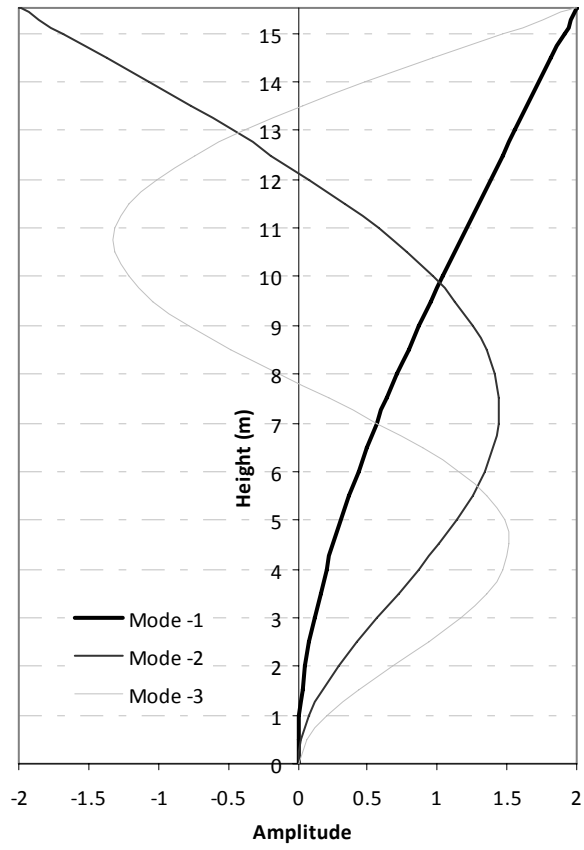


Figure 3.17 - Mode shapes of vibration of tree No.7 (height=15.52m)

3.1.3. Modification of Finite Element Model

In Section 3.1.1, it was concluded that the dynamic properties of finite element model are different from real tree. The natural frequency of real tree (0.5078Hz) is 30% higher than the frequency of vibration of the model (0.3920Hz related to the natural mode of vibration of finite element model).

The parameters affecting dynamic properties of the tree are dimensions, density, modulus of elasticity, trunk-ground connection, and defects in the trunk. Table 3.4 summarizes the amount of error in measuring each parameter required to cause the mentioned difference in natural frequency (31%).

Table 3.4 – Amount of error required to cause 31% error in natural frequency

Parameter	Model	Required	Percent Error
Natural frequency (Hz)	0.39 Hz	0.51 Hz	31
Height (m)	15.52	13.57	11
Average diameter (cm)	21.40	27.98	31
Density (Kg/m ³)	942.47	551.133	41
Modulus of elasticity (MPa)	5065	8661	71
Defect height (m) with diameter of 17.6 cm	N/A		N/A

From Table 3.4, it is clear that only 11 percent error in measuring the height of the tree can cause the 31% difference between natural frequencies of model and real tree. On the other hand, it has to be noted that 11% error in measuring the height of the tree is a large error which, most of times, does not happen experimentally. Also, the theoretical height of tree should be measured from where the trunk ground connection ends which would be

hard to determine in a real tree-ground connection and it can be a source of error in calculating height of tree.

A 31 percent error in measuring the trunk diameter and 41 percent error in measuring density would explain the difference in dynamic properties of model and real tree. These high errors are not believed to happen in measurements. Also, 71 percent error in approximating modulus of elasticity is not commonly accepted for a field measurement. However, different method for calculating modulus of elasticity may produce very different values.

It is concluded from finite element modeling of tree defects in Section 3.2.2 and Figure 3.12 that increasing the defect size in tree trunk does not increase the natural frequency and is not the reason for higher natural frequency of real tree.

In addition, assuming tree-ground connection as a fixed connection is not flawless and can be a source of error but assuming the connection as semi-fixed will not fix the problem because it would decrease the natural frequency of the tree (more flexible tree).

3.1.4. Dynamic Analysis of FE Model under Apical Forces during Cutting Process

Tree was also modeled using the finite element software/package SAP 2000 with material properties and dimensions obtained from field measurements (Table 3.1 and Appendix G). SAP2000 is used for finite element modeling because it allows for easier meshing the model with mapped elements (Figure 3.18).

Tree trunk was modeled as a truncated conical shape and trunk-ground connection was assumed to be fixed. Loads created during cutting process are applied to the sheave location, approximately less than one meter below the top of the tree. Model is meshed with the radial solid elements as shown in Figure 3.18. Tree is meshed with 1800 elements and actual element size is shown in Figure 3.18.

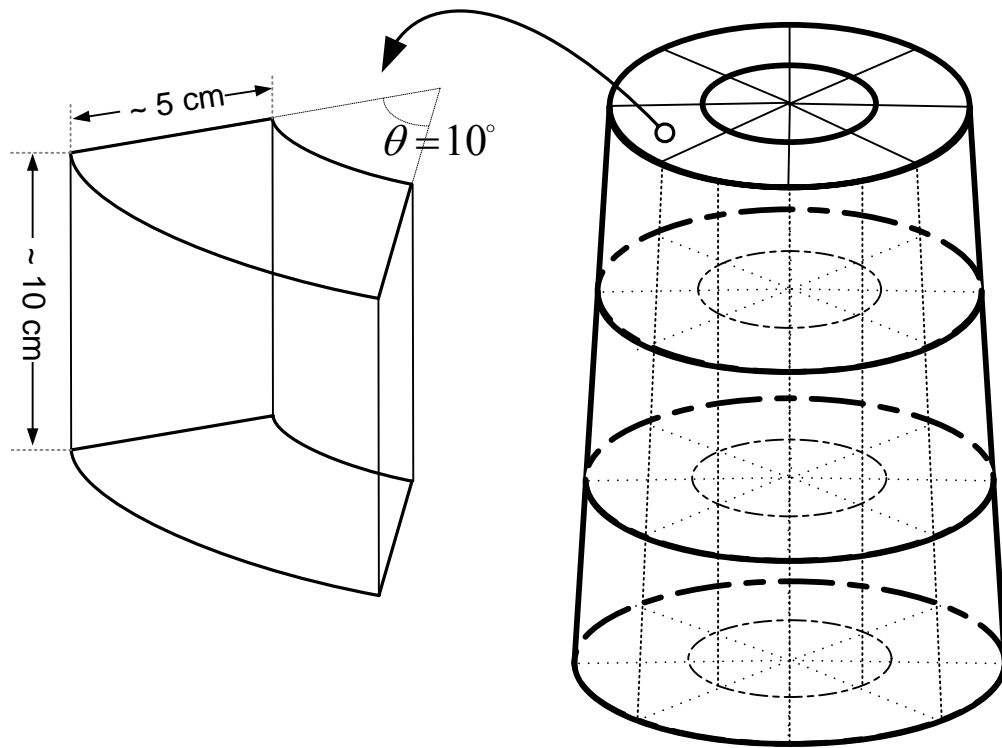


Figure 3.18- Radial meshing and actual dimension of an element

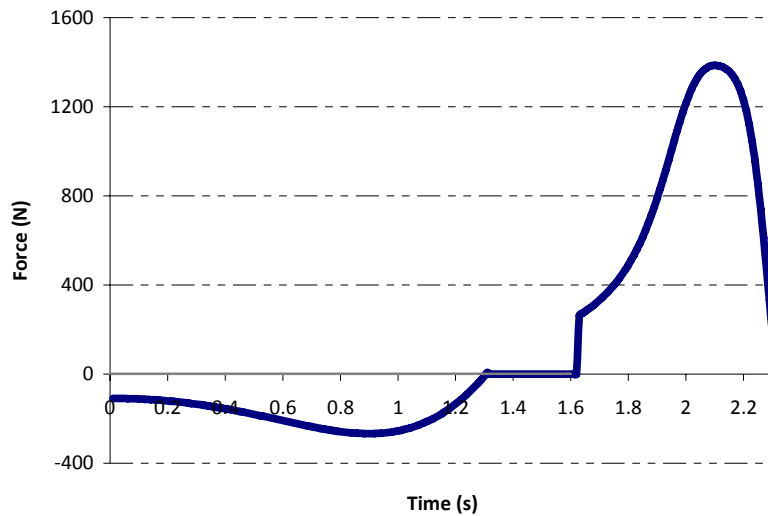


Figure 3.19 - Cutting process loads

Figure 3.19 indicates the load function applied to the top of tree No.7 (Sheave location) during cutting process. This force function was calculated directly from the results in Chapter 2. Axial strain near the bottom of the trunk (at the location of probe 2) and horizontal displacement of top of the tree are the outputs of finite element analysis that were monitored. Axial strain obtained from SAP2000 is compared with field measurements in Figure 3.20. It has to be noted that the first 2.3 s of the vibration of tree is forced and the remaining is free vibration. The accuracy of force function plotted in Figure 3.19 can be studied by comparing the first three peaks of curves in Figure 3.20 and the accuracy of FEM in modeling dynamic characteristics of tree can be studied by comparing the frequency of vibrations and free vibration part of the graphs.

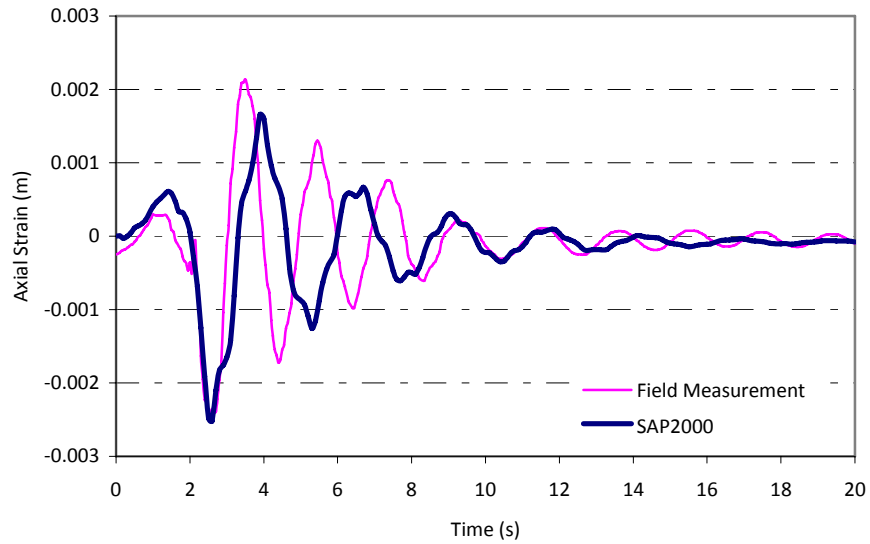


Figure 3.20 – Axial strain time history at the location of probe 2 in FE model

Table 3.5 - Comparison of axial strain from FEM and field measurements (Refer to Figure 3.20)

Peak No.	FEM	Field measurements	Error (%)
1	0.00058	0.00028	51
2	-0.00252	-0.00239	5
3	0.00160	0.00204	27
4	-0.00126	-0.00167	32

It is clear from Figure 3.20 and Table 3.5 that the finite element model behaves well in predicting maximum axial strain near the bottom of the tree. But it is also obvious from the figure that natural frequency of vibrations of model does not match well with the real tree. This phenomenon is consistent with findings from the modal analyses in Section 3.1.1, and is clearly observable in Figure 3.21 that shows the axial strain in frequency domain.

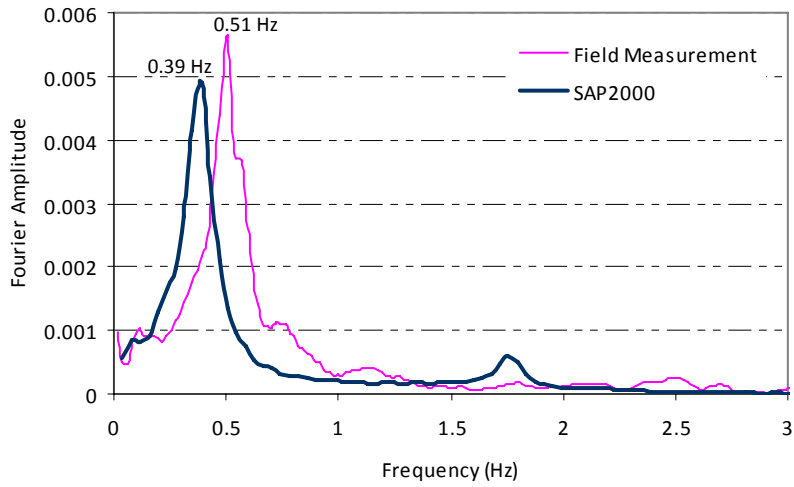


Figure 3.21 - Axial strain in frequency domain at the location of probe 2 in FE model²²

Horizontal displacement of tree top is plotted in Figure 3.22. Maximum value of displacement is 2.03m which is in good agreement with reported value of 2.60m from field measurements (30% error).

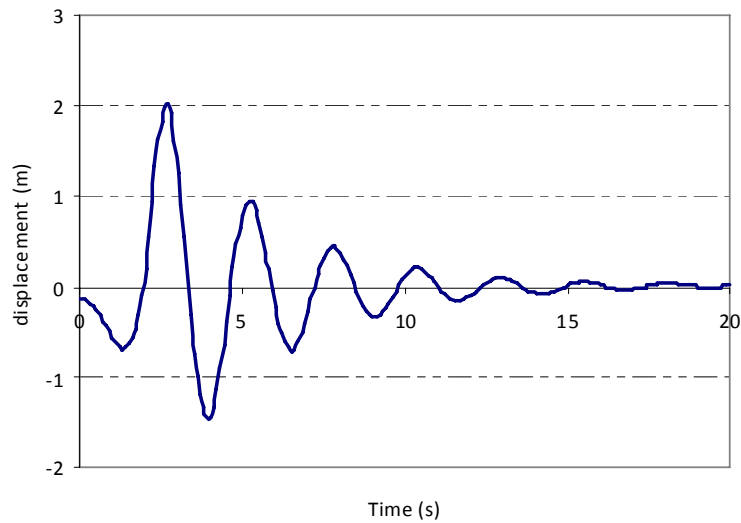


Figure 3.22 - Variation of displacement with time of tree top in FE model

²² Natural frequencies obtained from FEM and field measurements are discussed in Section 3.1.1.

Comparison of results from finite element model with field measurements indicates that the calculated force function works reasonable and predicts the maximum axial and horizontal displacements. But the finite element model has to be adjusted to represent the dynamic behavior of real tree.

The finite element model was therefore modified to be consistent with findings from Section 3.1.3. The easiest way to modify the model to obtain the actual natural frequency of the real tree was to change the modulus of elasticity from 5065MPa to 8661MPa. It is not meant to represent an actual change in modulus of elasticity but it is intended to get the desired frequency. Axial strain near the bottom of tree is plotted again in Figure 3.23.

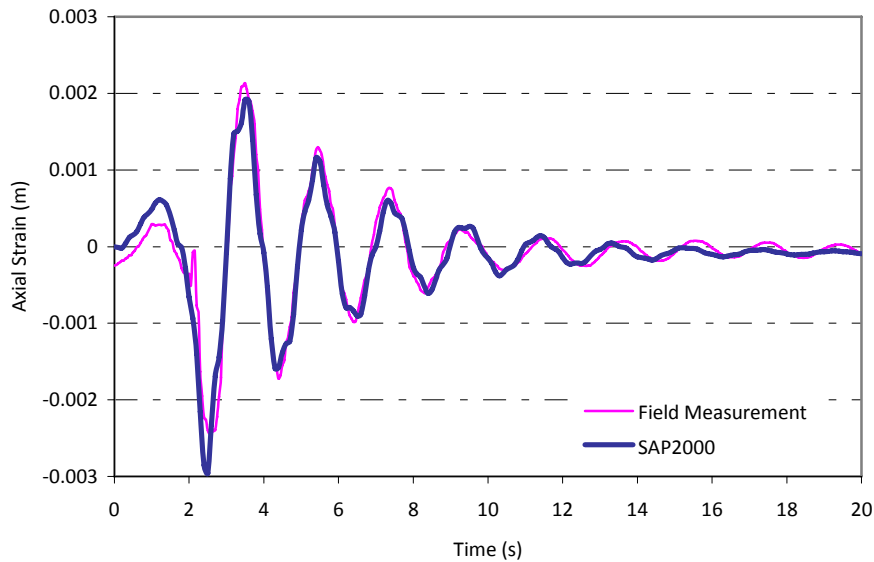


Figure 3.23 - Variation of axial strain at the location of probe 2 in modified FE model with time

Table 3.6 - Comparison of axial strain from FEM and field measurements (Refer to Figure 3.23)

Peak No.	FEM	Field measurements	Error (%)
1	0.00061	0.00028	54
2	-0.00295	-0.00239	19
3	0.00189	0.00204	8
4	-0.00157	-0.00167	6

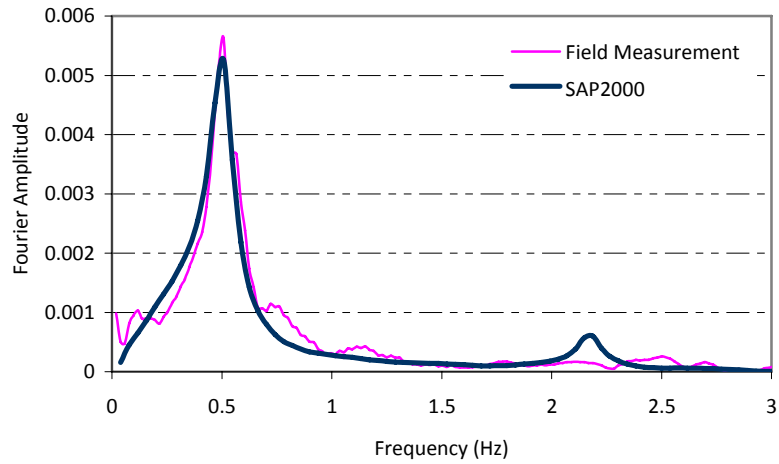


Figure 3.24 - Axial strain in frequency domain at the location of probe 2 in modified FE model

It is obvious from Table 3.6 and Figure 3.24 that this simple modification precisely matched the field measurements with finite element model outputs. Displacement of tree top with modified finite element model is plotted in Figure 3.25.

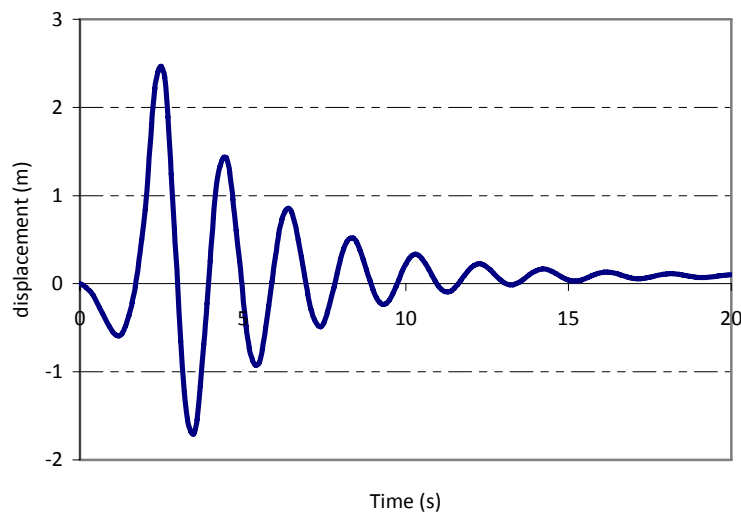


Figure 3.25 - Variation of displacement of tree top with time in modified FE model

3.2. Simplification of FE model

Modeling with solid elements is costly and time consuming. In this section, simpler element (like beam elements) is used in finite element model and its effect on the results and running time is studied.

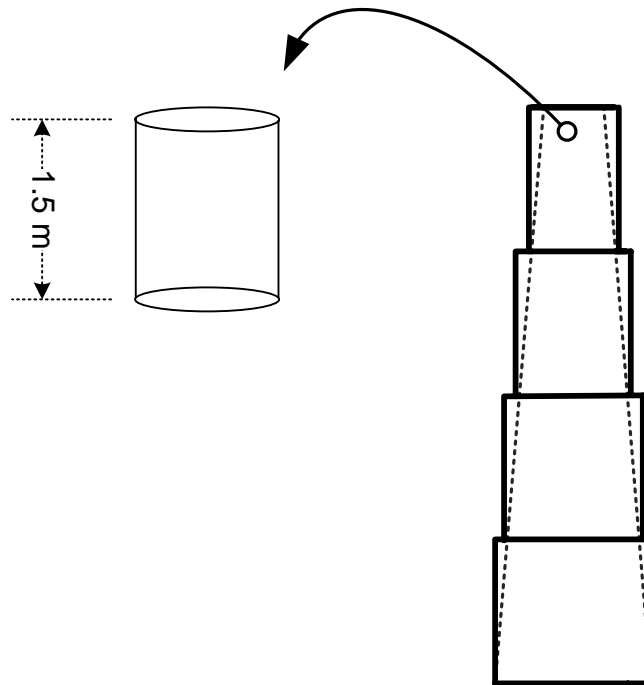


Figure 3.26 – Sample of meshing tree trunk with beam element

Table 3.7 – Modeling with beam element

Number of elements	10^{23}
Shape of element	Cylindrical

²³ This optimum number of elements was chosen by running the model for fewer and more elements and comparing their results (convergence method).

After running the dynamic analysis, moment in a beam element at the location of probe 2 is obtained:

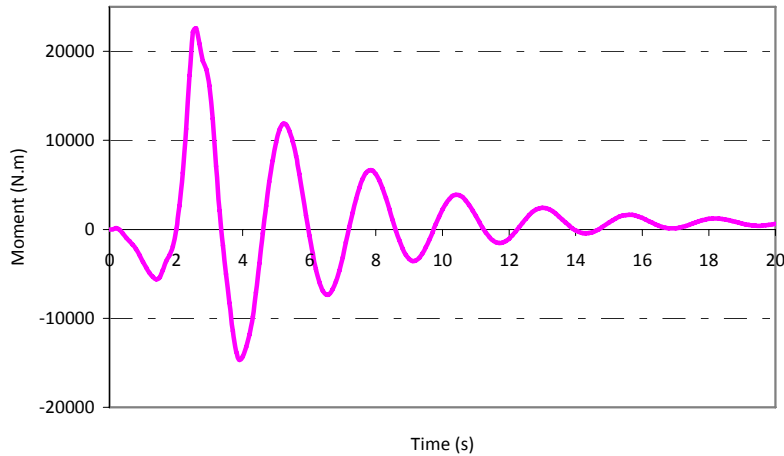


Figure 3.27 - Variation of moment with time in a frame at the location of probe 2

Then by using the equation $\varepsilon = \frac{M.c}{E.I}$ axial strain is calculated and compared with results

from previous finite element model meshed with solid elements:

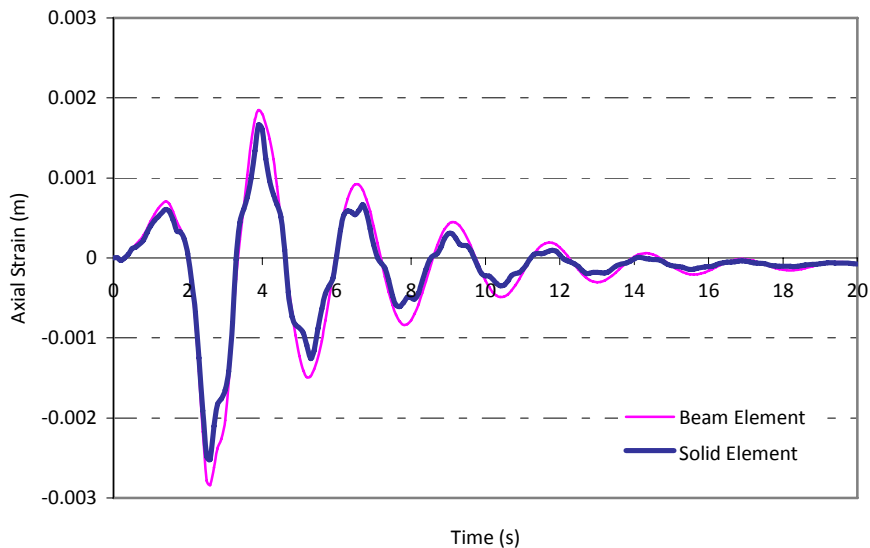


Figure 3.28 - Variation of axial strain with time at the location of probe 2 in FE model meshed with beam and solid elements

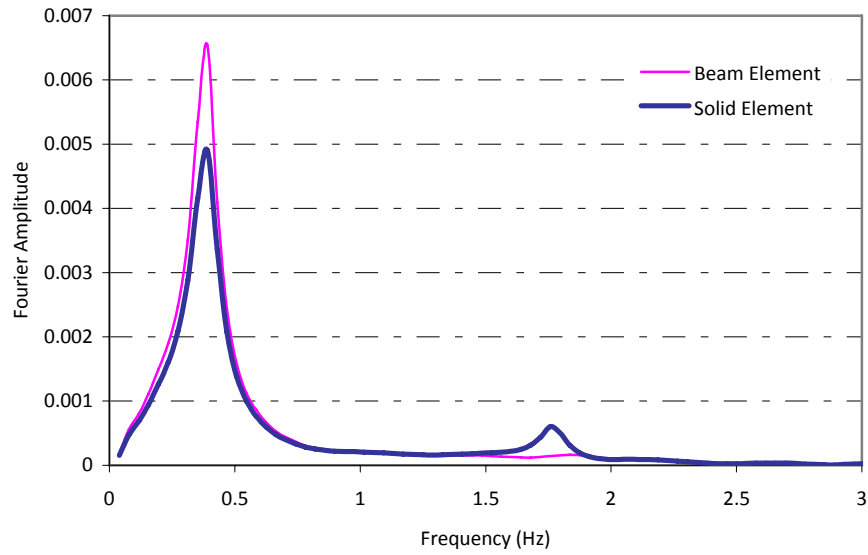


Figure 3.29 - Axial strain (in frequency domain) at the location of probe 2 in FE model meshed with beam and solid elements

It is concluded that modeling the real tree with only 10 beam elements has similar accuracy with the model meshed with hundreds of solid elements. Also, in some cases, using beam elements is more compatible with real tree. For example, from Figure 3.29, Figure 3.24 and Figure 3.21, it is clear that the solid-element model has a second peak in the frequency range of 1.5-2.0 which does not appear in field measurements and beam-element model. The second peak in solid element curve is not related to higher modes of vibration of model since the second mode of vibration has frequency of 1.97 Hz and the third mode of vibration has frequency of 5.19 Hz.

3.3. Analytical Method to Obtain Axial Strain near the Bottom of the Tree from Displacement of Tree Top

In Chapter 2, the cut piece motion and induced force at the top of tree were calculated. Then In Chapter 3, the force function calculated in the second chapter was applied to FE model to obtain the axial strain near the bottom of the tree (where probe 2 was located in field tests) and to calculate the displacement time history of tree top.

In addition, the displacement of tree top was obtained in Chapter 2 by modeling the tree trunk as a dynamic model consisting of a concentrated mass, linear spring and viscous damper. (Refer to Appendix A – Calculating M, K and C of the trunk simplified model)

In this section, an analytical method is proposed to calculate the axial strain near the bottom of the tree from the displacement of tree top. This method is proposed to obtain the axial strain near the bottom of the tree from the displacement of tree top calculated in Chapter 2 without the need to use a FE model of the tree.

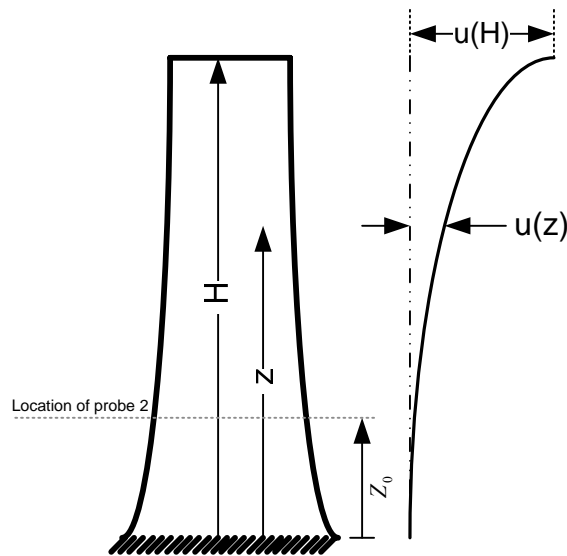


Figure 3.30 - Tree horizontal displacement and shape function

The tree horizontal displacement function, $u(z)$, is assumed to be:

$$u(z) = u(H) \cdot [1 - \cos(\frac{\pi \cdot z}{2 \cdot H})] \quad (3.14)$$

The assumed shape function for tree satisfies the boundary conditions $u(0)=0$ and $u'(0) = 0$ (Figure 3.30). Moment at a section at the location of probe 2 (height z_0) is:

$$M(z_0) = E I u''(z_0) \quad (3.15)$$

And axial strain at the location of probe 2 near the bottom of the tree is:

$$\varepsilon(z_0) = \frac{M(z_0) \cdot c}{E I} \quad (3.16)$$

Where c is the perpendicular distance to neutral axis of cross section of tree trunk.

$$\varepsilon(z_0) = c u''(z_0) \quad (3.17)$$

Equation (3.17) is a familiar equation in solid mechanics. Second derivative of $u(z)$ is calculated (equation 3.18) and is substituted into equation (3.17) to find the axial strain (equation 3.19):

$$u''(z) = u(H) \cdot (\frac{\pi}{2 \cdot H})^2 \cos(\frac{\pi \cdot z}{2 \cdot H}) \quad (3.18)$$

$$\varepsilon(z_0) = c u(H) \cdot (\frac{\pi}{2 \cdot H})^2 \cos(\frac{\pi \cdot z_0}{2 \cdot H}) \quad (3.19)$$

Where $u(H)$ is the displacement at the top of tree and $\varepsilon(z_0)$ is the strain near the bottom of the tree. Axial strains near the bottom of the tree can be calculated by substituting displacement of tree top obtained from Chapter 2 into equation (3.19) instead of using a FE model. The proposed method is verified in Figure 3.31 with the FEM results from Section 3.1.4. The cutting force is applied to FE model then the displacement of tree top is obtained and axial strain near the bottom of tree trunk is plotted in Figure 3.31. Also,

the plot from the proposed analytical method is obtained by substituting the displacement of tree top from FE model into equation (3.19). The axial strain near the bottom of the tree obtained from FEM and analytical method are compared in Figure 3.31. It is obvious from the figure that the equation (3.19) works accurately.

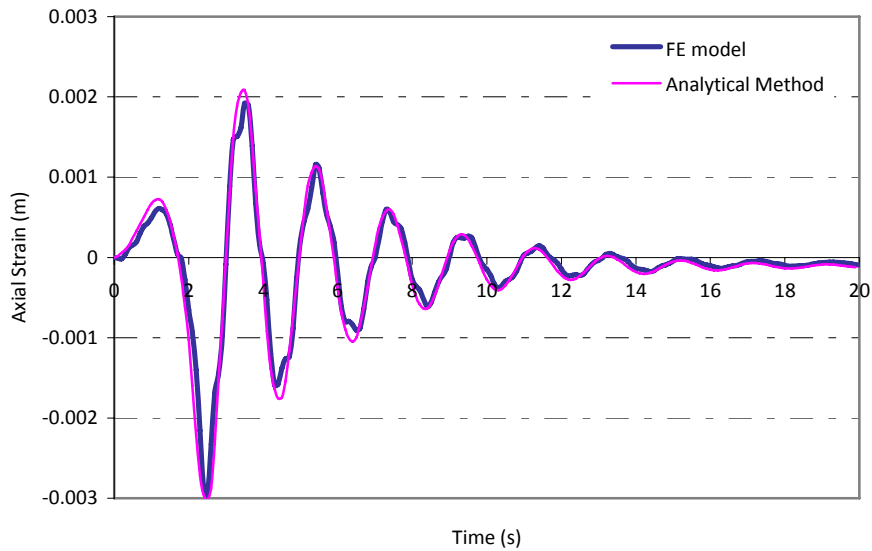


Figure 3.31 - Verification of axial strain at the location of probe 2

To implement the proposed method, the displacement at the top of tree is calculated using the techniques in Chapter 2 and substituted into equation (3.19) to get axial strain at z_0 . These are compared with strain obtained from the FE model of Section 3.1.4. It is clear that the proposed method is consistent with FE model. In Figure 3.32, only the response of tree during forced vibration is plotted (first 2.3 sec) and it can be observed that the proposed method has good agreement with FEM.

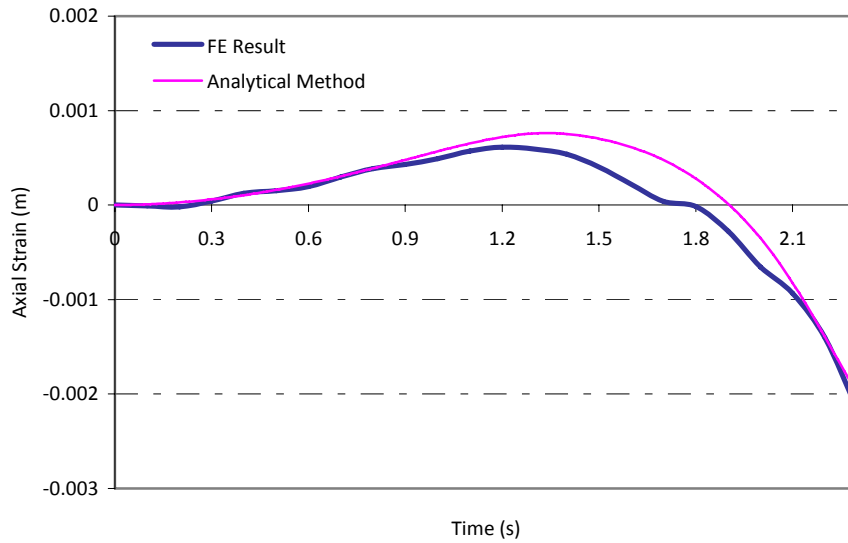


Figure 3.32 - Comparison of axial strain at the location of probe 2

Finally, it can be concluded that axial strain near the bottom of the tree can be accurately calculated by having the displacement of tree top and using the equation (3.19). Also, the displacement of tree top can be obtained from methods discussed in Chapter 2. The accuracy of the calculation of displacement of tree top and simplified dynamic model used in Chapter 2 is studied in Appendix B.

CHAPTER 4

SENSITIVITY STUDY OF THE CALCULATION OF CUT PIECE MOTION AND APPLIED FORCE

In Chapter 2, the motion function for the cut piece and induced apical loads due to the cutting process were formulated in a general case and calculated for a sample tree (Tree No.7). Since some calculations were based on assumed values for the parameters which were not measured in field experiments, the sensitivity of the calculations and results presented in Chapter 2 to these parameters has been studied in this chapter. The parameters which may affect the motion of the cut piece and induced cutting process forces that are studied in this chapter are:

- Initial rotation of cut piece
- Linear Velocity (V_{Δ})
- Height of tree trunk
- Mass of cut piece
- Diameter of tree trunk

4.1. Initial Rotation of Cut Piece

As discussed in Chapter 2, it is assumed that the cut piece has an initial rotation of θ_0 equals to 0.1 rad. This initial rotation results from the push of the worker to force the cut piece to fall during the cutting process of the tree. In this section, the motion of the cut piece and induced apical forces are calculated for initial rotations of 0.1rad and 0.52 rad. The value of 0.1rad (6°) is a reasonably small value to initiate the motion with, and 0.52rad (30°) is a high value for initial angle of rotation.

In Figure 4.1, 4.2, 4.3 and 4.4, the effect of initial rotation of cut piece on the motion of cut piece and force function is studied. The curves labeled with subscript 1 in the figures indicate the results of having an initial rotation equals to 0.52 rad (30°); the other curves (bold lines) in each plot represents the results of using the originally assumed value of 0.1 rad (6°) for initial angle of rotation, θ_0 .

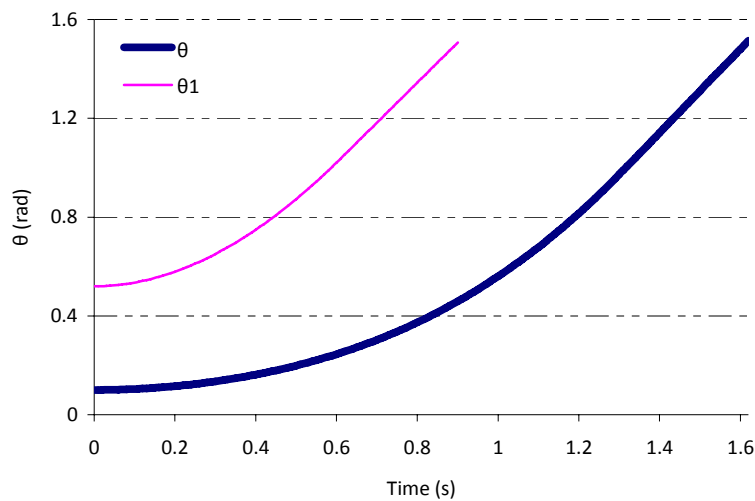


Figure 4.1-Variation of piece angle (θ) with time for two different initial rotations–Stages A, B and C

It is clear from Figure 4.1 that the higher initial value for θ results in decreasing the total time for stages A, B and C from 1.6 sec to 0.9 sec. However the angle of rotation of piece at the beginning of stage E does not change significantly.

Variation of apical force and displacement of top of tree with time are plotted in Figure 4.2 and Figure 4.3, respectively. Similarly, it is clear from the graphs that the whole cutting process time decreases by increasing the value of initial rotation angle of the piece. In addition, the maximum force and displacement of top of tree decrease between 15 and 20%.

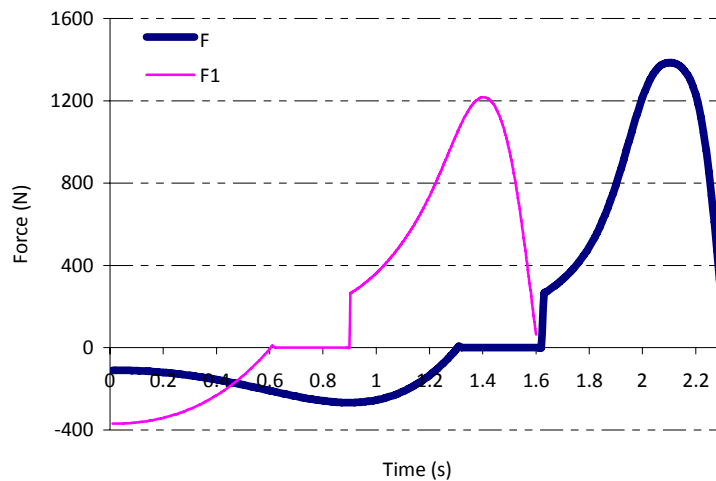


Figure 4.2 - Apical force induced during cutting process to the tree for two different initial rotations

In Figure 4.3, displacement of tree top is shown from the beginning of cutting process to the moment when the piece stops moving. Only the response of tree during this period is shown because the vibration of the tree, after the apical load ends, is simply free vibration.

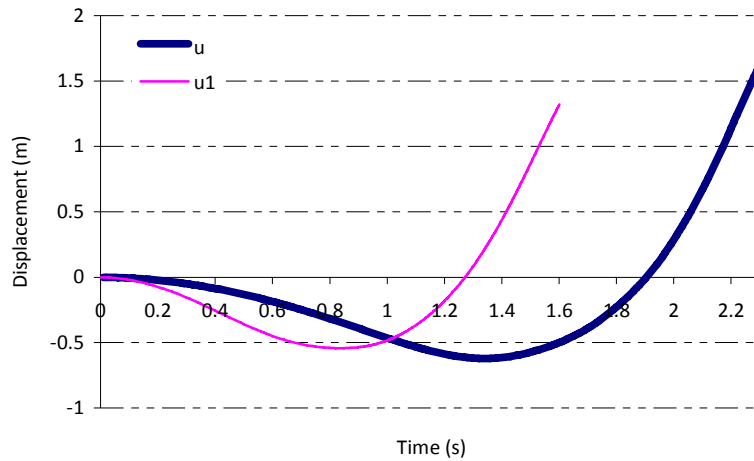


Figure 4.3 - Variation of displacement of tree top with time for two different initial rotations

The movement of the CG of the cut piece during stage D is illustrated in Figure 4.4. It can be seen in the figure that changing the initial rotation of piece from 0.1rad to 0.52rad does not significantly affect the motion of cut piece during stage D.

Relevant parameters of motion of the cut piece and force function during cutting process are listed and compared in Table 4.1. In Table 4.1, cells filled in gray represent the results for the model with initial rotation angle of $\theta_0=0.52$ rad (30°) and white cells contain previously calculated results for $\theta_0=0.1$ rad (6°).

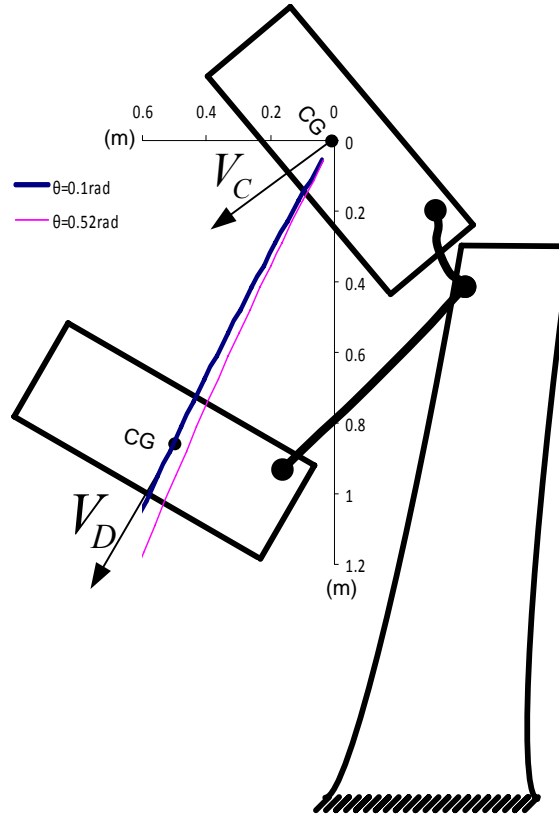


Figure 4.4 - Movement trajectory of the CG of the piece for two different initial rotations – Stage D

It can be concluded that changing the initial rotation of the cut piece does not change the piece motion, maximum force and displacement of tree top significantly. Changing initial rotation of piece from 0.1rad to 0.52rad increases maximum force and displacement of tree top 15% to 20%. Thus, approximating a value for initial rotation of cut piece does not result in significant differences and its accurate measurement is not needed. The only parameter which is significantly affected is the duration of the motion for stages A, B and C. It decreases by increasing the value of initial rotation angle of the piece.

Table 4.1 - Parameters of motion of the cut piece and applied force function during cutting process

PARAMETER \ STAGE		Initial condition	Release point	Beginning of stage E	Impact moment	Initial Rotation of Cut Piece (rad)
		Beginning of stage A	End of stage C	End of stage D	End of stage E	
Time (s)	t	0	1.31	1.62	2.31	0.10
		0	0.61	0.90	1.60	0.52
	Difference (%)	0	53	44	31	-
Piece angle (rad)	θ and β	$\theta = 0.10$	$\theta = 0.99$ $\beta = 2.15$	$\beta = 1.62$	$\beta = -0.1$	0.10
		$\theta = 0.52$	$\theta = 1.04$ $\beta = 2.08$	$\beta = 1.63$	$\beta = -0.1$	0.52
	Difference (%)	420	5	1	0	-
Angular velocity of piece (rad/s)	θ' and β'	$\theta' = 0$	$\theta' = 1.69$ $\beta' = -1.69$	$\beta' = -1.69$	$\beta' = -2.38$	0.10
		$\theta' = 0$	$\theta' = 1.62$ $\beta' = -1.62$	$\beta' = -1.62$	$\beta' = -2.71$	0.52
	Difference (%)	0	4	4	13	-
Horizontal deflection of trunk (m)	u	0	-0.62	-0.48	1.67	0.10
		0	-0.46	-0.53	1.32	0.52
	Difference (%)	0	26	10	21	-
Horizontal velocity of trunk (m/s)	u'	0	-0.11	0.92	4.41	0.10
		0	-0.75	0.23	4.20	0.52
	Difference (%)	0	581	75	5	-

4.2. Linear Velocity (V_{Δ})

As discussed in Chapter 2, it is assumed that during cutting process and after the release point there is a sliding motion of cut piece on top of the trunk edge causing it to develop a linear velocity of V_{Δ} which is the reason of forward moving of the cut piece while no horizontal force is being applied to the piece. Thus, just after the release instant, the linear velocity is V_{Δ} at one end and $V_{\Delta} + \omega_c \cdot L_p$ at the farther end of the piece (L_p is piece total length and ω_c is angular velocity an instant after release point). In this section, the effect of the parameter V_{Δ} on the motion of cut piece and force function after release from the top of tree is studied.

Linear velocity, V_{Δ} , is assumed to be 2m/s in Chapter 2 calculations. To study the effect of linear velocity, V_{Δ} , on the motion of cut piece and force function calculations, Chapter 2 analysis is done for V_{Δ} equals to 0m/s and 4m/s. These new values for V_{Δ} have a $\pm 100\%$ difference with previously assumed value of 2m/s. Since changing V_{Δ} only affects the motion of the tree and cut piece after releasing from the trunk, it does not affect the motion related to stages A, B and C.

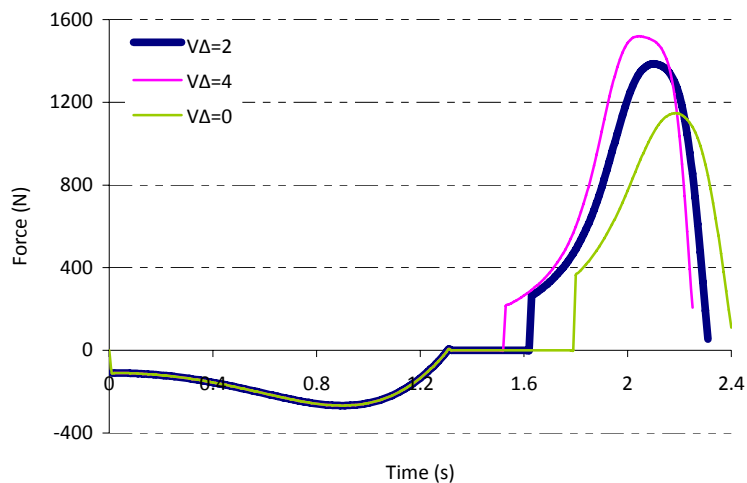


Figure 4.5- Apical force induced during cutting process to the tree

Figure 4.5 shows that increasing the value of V_{Δ} from 0m/s to 4m/s increases the maximum force applied to the tree during stage E of the cutting process. Also, as expected, increasing V_{Δ} decreases the cutting process time.

The tree top displacement during the cutting process is plotted in Figure 4.6. It is obvious from the graph that the maximum value of tree top displacement is not significantly affected by value of V_{Δ} .

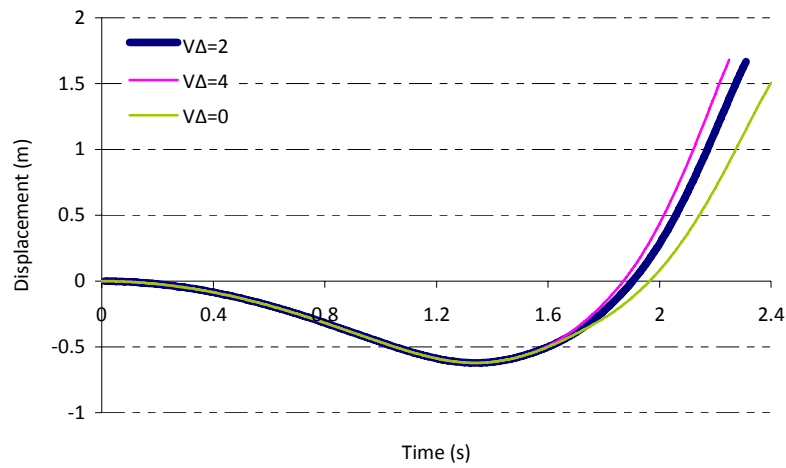


Figure 4.6 - Variation of displacement of tree top with time

Figure 4.7 indicates that the highest value of V_{Δ} (4 m/s) increases the horizontal movement of the cut piece

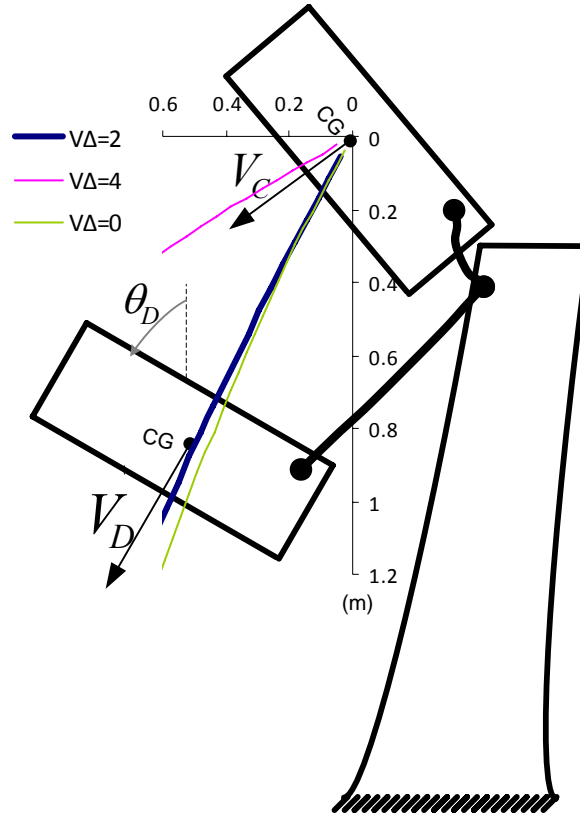


Figure 4.7 - Movement trajectory of the CG of the piece – Stage D

Table 4.2 summarizes the value each relevant parameter adopts as a result of various assumed values for V_{Δ} . The parameters related to stages A, B and C do not vary significantly by changing the value of V_{Δ} .

It can be concluded that assuming an approximate value for V_{Δ} does not significantly affect the displacement of tree top and force function, within reasonable values. Only the motion of the cut piece during Stage D is significantly dependant on the value of V_{Δ} . From Table 4.2, it can be seen that the maximum values of difference (30% to 40%) are occurred in calculating of velocity and displacement of tree top at the end of stage D.

Table 4.2 - Parameters of motion of the cut piece and applied force function during cutting process

PARAMETER \ STAGE		Initial condition	Release point	Beginning of stage E	Impact moment	V_d
		Beginning of stage A	End of stage C	End of stage D	End of stage E	
Time (s)	t	0	1.31	1.62	2.31	$V_d=2$
		0	1.31	1.52	2.25	$V_d=4$
		0	1.31	1.79	2.40	$V_d=0$
	Difference (%)	0	0	6	3	$V_d=4$
	Difference (%)	0	0	10	4	$V_d=0$
Piece angle (rad)	θ and β	$\theta = 0.10$	$\theta = 0.99$ $\beta = 2.15$	$\beta = 1.62$	$\beta = -0.1$	$V_d=2$
		$\theta = 0.10$	$\theta = 0.99$ $\beta = 2.15$	$\beta = 1.79$	$\beta = -0.1$	$V_d=4$
		$\theta = 0.10$	$\theta = 0.99$ $\beta = 2.15$	$\beta = 1.34$	$\beta = -0.1$	$V_d=0$
	Difference (%)	0	0	10	0	$V_d=4$
	Difference (%)	0	0	17	0	$V_d=0$
Angular velocity of piece (rad/s)	θ' and β'	$\theta' = 0$	$\theta' = 1.69$ $\beta' = -1.69$	$\beta' = -1.69$	$\beta' = -2.38$	$V_d=2$
		$\theta' = 0$	$\theta' = 1.69$ $\beta' = -1.69$	$\beta' = -1.69$	$\beta' = -2.43$	$V_d=4$
		$\theta' = 0$	$\theta' = 1.69$ $\beta' = -1.69$	$\beta' = -1.69$	$\beta' = -2.26$	$V_d=0$
	Difference (%)	0	0	0	2	$V_d=4$
	Difference (%)	0	0	0	5	$V_d=0$

PARAMETER		STAGE		Initial condition	Release point	Beginning of stage E	Impact moment	V_d
		Beginning of stage A	End of stage C	End of stage D	End of stage E			
Horizontal deflection of trunk (m)	u	0	-0.62	-0.48	1.67	$V_d=2$		
		0	-0.62	-0.56	1.68	$V_d=4$		
		0	-0.62	-0.29	1.50	$V_d=0$		
	Difference (%)	0	0	17	1	$V_d=4$		
	Difference (%)	0	0	40	10	$V_d=0$		
Horizontal velocity of trunk (m/s)	u'	0	-0.11	0.92	4.41	$V_d=2$		
		0	-0.11	0.64	5.03	$V_d=4$		
		0	-0.11	1.24	3.59	$V_d=0$		
	Difference (%)	0	0	30	14	$V_d=4$		
	Difference (%)	0	0	35	19	$V_d=0$		

4.3. Height of Tree Trunk

In this section, the effect of height of tree trunk is studied on the motion of the cut piece and induced force function. Height of tree No.7 used in Chapter 2 calculations is 15.52 m. Two other trees with 25% difference in height are analyzed in this section and their results are compared to study the effect of height of tree on response of the cut piece.

Varying height of tree trunk will change the dynamic properties of tree trunk. In Table 4.3, the variation of dynamic properties of tree as a function of height of tree trunk is shown. All other parameters like diameter, density and modulus of elasticity remain constant and equal to values measured for tree No.7 for these analyses.

Table 4.3 – Variation of dynamic properties of tree trunk with height

Height	K	M	C	f
m	N/m	Kg	N.s/m	Hz
10	2153	60	72	0.949
15.52 ²⁴	575	94	46	0.394
20	269	121	36	0.237

Values for height of tree trunk, M, K and C from Table 4.3 have been reentered in calculations following the procedures in Chapter 2 to find motion of the cut piece and applied force function during cutting process.

Figure 4.8 shows that the cut piece in the shorter tree, which is stiffer and lighter, rotates slowly and takes more time to get to the release time.

²⁴ Measured in tree No.7.

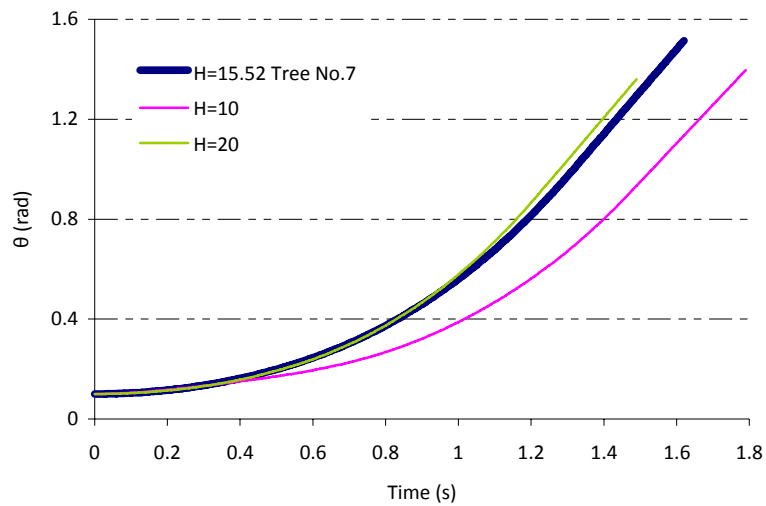


Figure 4.8- Variation of piece angle (θ) with time for three different tree heights – Stages A, B and C

Variation of apical force and displacement of tree top with time are plotted in Figure 4.9 and Figure 4.10, respectively. It is clear that for shorter tree trunks the maximum force during stage D of the cutting process is higher (Figure 4.9). Also the whole cutting process time decreases by increasing the height of the tree trunk.

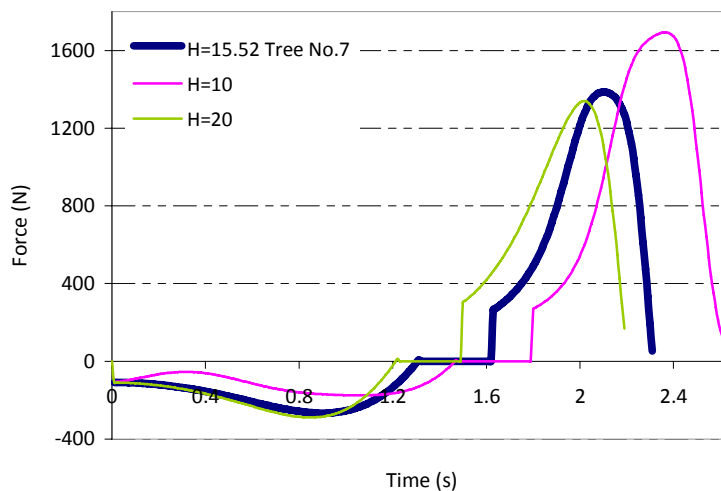


Figure 4.9 - Apical force induced during cutting process to the tree for three different tree heights

In Figure 4.10, displacement of tree top is shown from the beginning of cutting process to the moment when the cut piece impacts the tree. Figure 4.10 shows that for the shorter tree, which is stiffer and lighter, the displacement of top of the tree is smaller. Figure 4.11 shows movement trajectory of the CG of the cut piece during stage D.

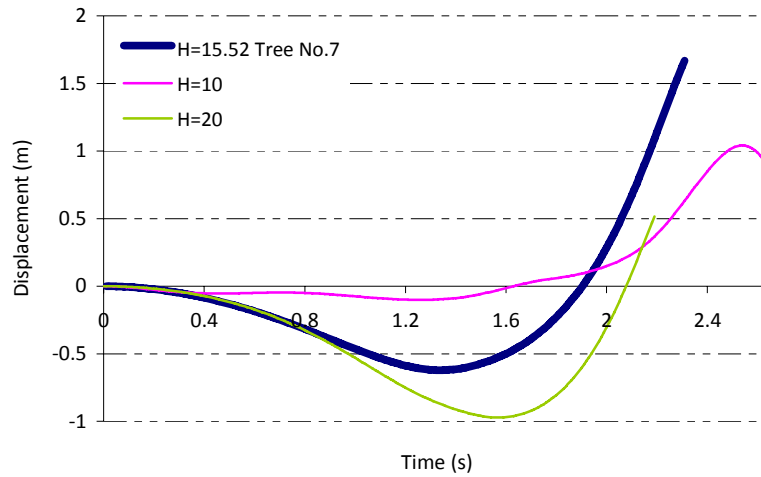


Figure 4.10 - Variation of displacement of tree top with time for three different tree heights

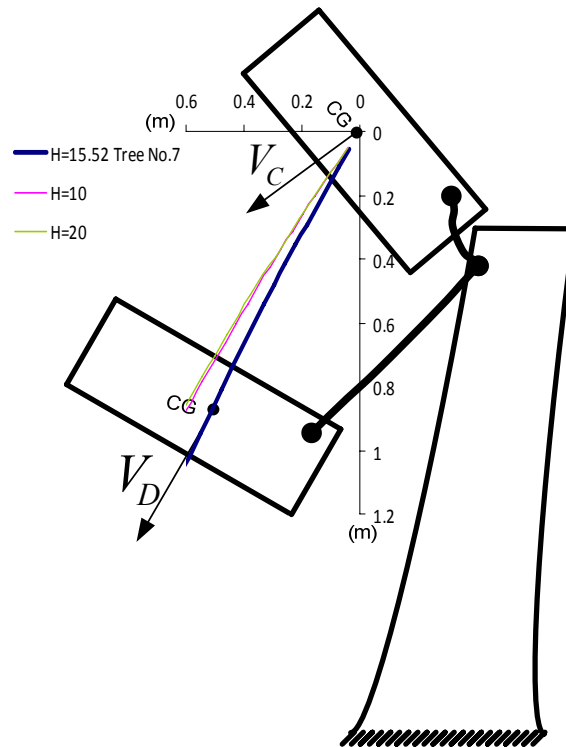


Figure 4.11 - Movement trajectory of the CG of the piece for three different tree heights – Stage D

Most of the parameters of motion of the cut piece and applied force function during cutting process are listed and compared in Table 4.4.

It can be concluded from the graphs that the height of the tree affects significantly the piece motion, force function and displacement of tree top. Thus accurate measurement of height of tree is needed to get precise results from Chapter 2 models. Also it is observed that, although for shorter tree trunks the maximum force is higher, the displacement of top of the tree is smaller.

To study the effect of height of the tree trunk on the maximum value of force function, the ratio of maximum force²⁵ vs. the ratio of height of the tree is plotted in Figure 4.12.

From Figure 4.12, it is obvious that, if height of the tree multiplies by 2, the maximum force will be decreased by factor of 0.78

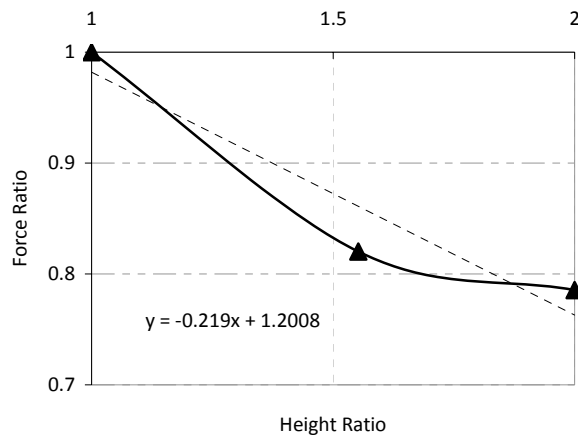


Figure 4.12 - Maximum force ratio vs. Height of tree ratio

$$^{25} \text{ Height Ratio} = \frac{H}{10m}, \quad \text{Force Ratio} = \frac{\text{Maximum Force (When height is } H)}{\text{Maximum Force (When height is } 10m)}$$

Table 4.4 - Parameters of motion of the cut piece and applied force function during cutting process

PARAMETER \ STAGE		Initial condition	Release point	Beginning of stage E	Impact moment	Height of tree (m)
		Beginning of stage A	End of stage C	End of stage D	End of stage E	
Time (s)	t	0	1.31	1.62	2.31	15.52 ²⁶
		0	1.47	1.79	2.65	10
		0	1.22	1.49	2.19	20
	Difference (%)	0	12	10	15	10
	Difference (%)	0	7	8	5	20
Piece angle (rad)	θ and β	$\theta = 0.10$	$\theta = 0.99$ $\beta = 2.15$	$\beta = 1.62$	$\beta = -0.1$	15.52
		$\theta = 0.10$	$\theta = 0.90$ $\beta = 2.24$	$\beta = 1.74$	$\beta = -0.1$	10
		$\theta = 0.10$	$\theta = 0.89$ $\beta = 2.25$	$\beta = 1.78$	$\beta = 0.02$	20
	Difference (%)	0	9	7	0	10
	Difference (%)	0	10	10	80	20

²⁶ Measured in tree No.7.

PARAMETER \ STAGE		Initial condition	Release point	Beginning of stage E	Impact moment	Height of tree (m)
		Beginning of stage A	End of stage C	End of stage D	End of stage E	
Angular velocity of piece (rad/s)	θ' and β'	$\theta' = 0$	$\theta' = 1.69$ $\beta' = -1.69$	$\beta' = -1.69$	$\beta' = -2.38$	15.52
		$\theta' = 0$	$\theta' = 1.54$ $\beta' = -1.54$	$\beta' = -1.54$	$\beta' = -1.49$	10
		$\theta' = 0$	$\theta' = 1.70$ $\beta' = -1.70$	$\beta' = -1.70$	$\beta' = -3.12$	20
	Difference (%)	0	9	9	37	10
	Difference (%)	0	1	1	31	20
Horizontal deflection of trunk (m)	u	0	-0.62	-0.48	1.67	15.52
		0	-0.07	0.06	0.86	10
		0	-0.77	-0.95	0.51	20
	Difference (%)	0	89	112	48	10
	Difference (%)	0	24	98	69	20
Horizontal velocity of trunk (m/s)	u'	0	-0.11	0.92	4.41	15.52
		0	0.34	0.21	-3.19	10
		0	-0.97	-0.39	4.69	20
	Difference (%)	0	400	78	172	10
	Difference (%)	0	782	142	6	20

4.4. Mass of Cut Piece

In this section, the effect of mass of cut piece is studied on the motion of cut piece and induced force function. Mass of cut piece for tree No.7 used in Chapter 2 calculations is 113.4 Kg. Two other analyses with 100% difference in mass of the cut piece are carried out in this section and their results are compared to study the effect of mass of the cut piece on response of the cut piece. Figure 4.13, 4.14 and 4.15 show the effect of mass of cut piece on response of the cut piece. Figure 4.13, 4.14 and 4.15 show the effect of mass of cut piece on the piece motion and force function.

It can be seen in Figure 4.13 that the lighter cut piece rotates slowly and takes more time to get to the release time.

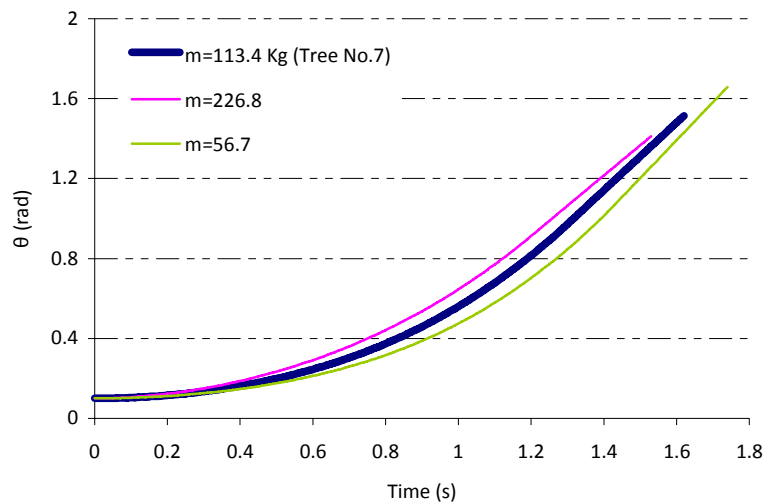


Figure 4.13 - Variation of piece angle (θ) with time for three different mass values–Stages A, B and C

Variation of apical force and displacement of tree top with time are plotted in Figure 4.14 and Figure 4.15, respectively. It is clear from Figure 4.14 that for heavier cut piece the maximum force during stage D is higher and variation is quite high.

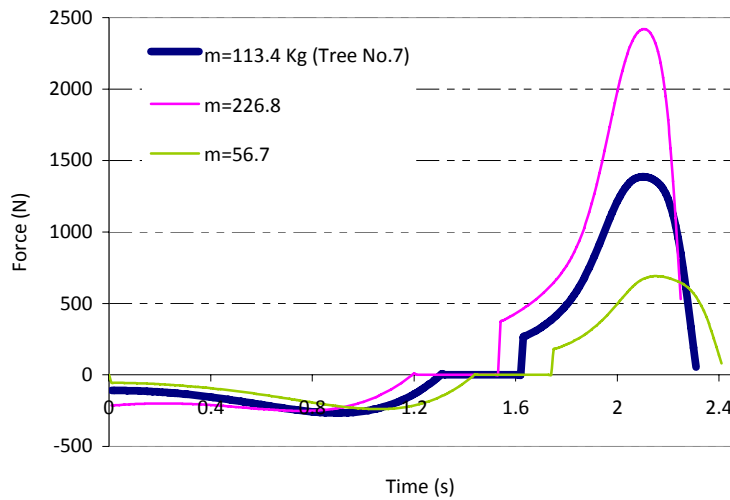


Figure 4.14 - Apical force induced during cutting process to the tree for three different mass values

In Figure 4.15, displacement of tree top is shown from the beginning of cutting process to the moment when the piece impacts the tree. It is clear from the graph that the lighter cut piece results in displacement of top of the tree to be smaller. Also, it can be seen in Figure 4.16 that heavier cut piece moves more in horizontal direction than lighter cut pieces.

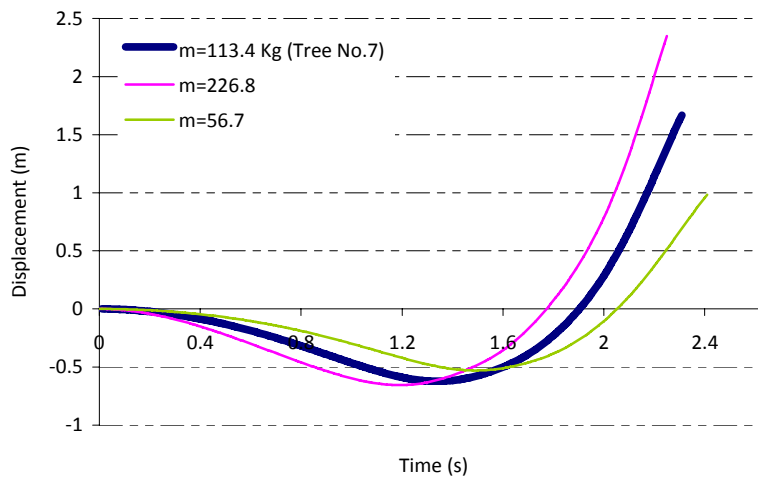


Figure 4.15 - Variation of displacement of tree top with time for three different mass values

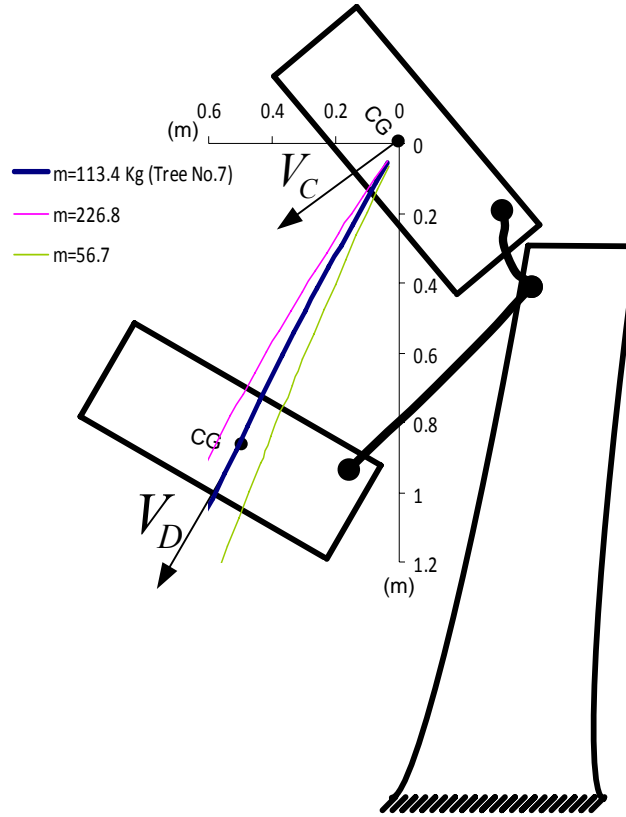


Figure 4.16 - Movement trajectory of the CG of the piece for three different mass values – Stage D

It can be seen in the graphs that the whole cutting process time is not being affected significantly by the mass of the cut piece but other parameters like force and displacement of tree top are. Relevant parameters describing motion of the cut piece and applied force function during cutting process are listed and compared in Table 4.5.

To study the effect of mass of the cut piece on maximum value of force function, the ratio of maximum force²⁷ vs. the ratio of mass of the cut piece is plotted in Figure 4.17

It is obvious from Figure 4.17 that, if the mass of the cut piece multiplies by 2, the maximum force will be exactly doubled. Also increasing mass of the cut piece by 4 times will increase the maximum force by a factor of 3.50.

$$^{27} \text{ Mass Ratio} = \frac{M}{56.7\text{Kg}} , \quad \text{Force Ratio} = \frac{\text{Maximum Force (When mass is } M)}{\text{Maximum Force (When mass is } 56.7\text{Kg)}}$$

Slope of the trendline of the curve (0.82) shows that the maximum force is affected by the mass of the cut piece more than height of the trunk.

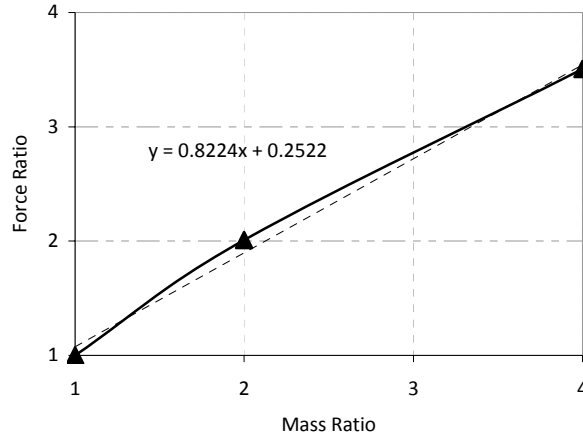


Figure 4.17 - Maximum force ratio vs. Mass of cut piece ratio

Table 4.5 - Parameters of motion of the cut piece and applied force function during cutting process

PARAMETER \ STAGE		Initial condition	Release point	Beginning of stage E	Impact moment	Mass of cut piece (Kg)
		Beginning of stage A	End of stage C	End of stage D	End of stage E	
Time (s)	t	0	1.31	1.62	2.31	113.4 ²⁸
		0	1.20	1.53	2.25	226.8
		0	1.44	1.74	2.41	56.7
	Difference (%)	0	8	5	3	226.8
	Difference (%)	0	10	7	4	56.7
Piece angle (rad)	θ and β	θ = 0.10	θ = 0.99 β = 2.15	β = 1.62	β = -0.1	113.4
		θ = 0.10	θ = 0.91 β = 2.23	β = 1.73	β = -0.1	226.8
		θ = 0.10	θ = 1.08 β = 2.06	β = 1.66	β = -0.05	56.7
	Difference (%)	0	8	7	0	226.8
	Difference (%)	0	9	2	50	56.7

²⁸ Measured in tree No.7.

PARAMETER \ STAGE		Initial condition	Release point	Beginning of stage E	Impact moment	Mass of cut piece (Kg)
		Beginning of stage A	End of stage C	End of stage D	End of stage E	
Angular velocity of piece (rad/s)	θ' and β'	$\theta' = 0$	$\theta' = 1.69$ $\beta' = -1.69$	$\beta' = -1.69$	$\beta' = -2.03$	113.4
		$\theta' = 0$	$\theta' = 1.51$ $\beta' = -1.51$	$\beta' = -1.51$	$\beta' = -2.85$	226.8
		$\theta' = 0$	$\theta' = 1.89$ $\beta' = -1.89$	$\beta' = -1.89$	$\beta' = -2.03$	56.7
	Difference (%)	0	10	10	40	226.8
	Difference (%)	0	11	11	0	56.7
Horizontal deflection of trunk (m)	u	0	-0.62	-0.48	1.67	113.4
		0	-0.65	-0.45	2.35	226.8
		0	-0.52	-0.43	0.98	56.7
	Difference (%)	0	5	6	41	226.8
	Difference (%)	0	16	10	41	56.7
Horizontal velocity of trunk (m/s)	u'	0	-0.11	0.92	4.41	113.4
		0	0.04	1.11	6.73	226.8
		0	-0.16	0.71	2.65	56.7
	Difference (%)	0	136	21	53	226.8
	Difference (%)	0	45	22	40	56.7

4.5. Diameter of Tree Trunk

In this section, the effect of diameter of tree trunk is studied on the motion of the cut piece and induced force function. Average diameter of tree No.7 used in Chapter 2 calculations is 21.4 cm. Two other trees with 20% difference in diameter are analyzed in this section and their results are compared to study the effect of diameter of tree trunk on response of the cut piece.

Varying diameter of tree trunk will change the dynamic properties of tree trunk. In Table 4.6, the variation of dynamic properties of tree as a function of diameter of tree trunk is shown. All other parameters like tree height, density and modulus of elasticity remain constant and equal to values measured for tree No.7 for these analyses.

Table 4.6 – Variation of dynamic properties of tree trunk with height

Average diameter	K	M	C	f
cm	N/m	Kg	N.s/m	Hz
17.83	278	65	26	0.328
21.4 ²⁹	575	94	46	0.394
25.68	1194	135	80	0.473

Values for diameter of tree trunk, M, K and C from Table 4.6 have been reentered in calculations following the procedure in Chapter 2 to find motion of the cut piece and applied force function during cutting process. In Figure 4.18, Figure 4.19, Figure 4.20 and Figure 4.21, the effect of diameter of tree trunk on the piece motion and force function is studied.

²⁹ Measured in tree No.7.

Figure 4.18 shows that the cut piece of the thicker tree which is stiffer rotates slowly and takes more time to get to the release time.

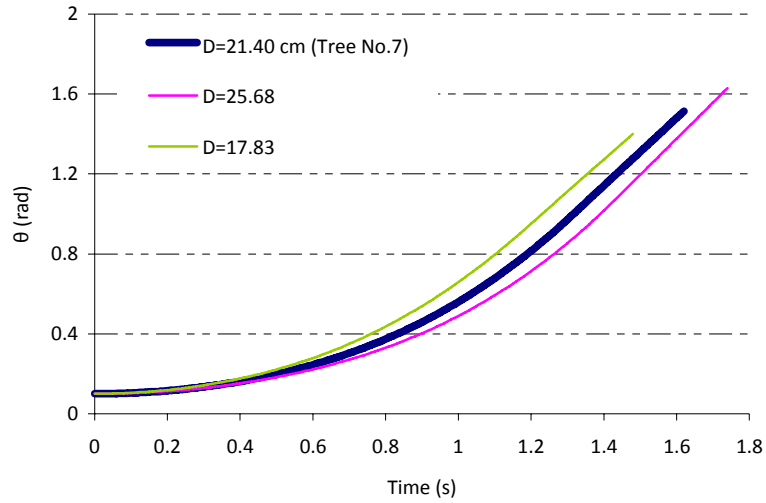


Figure 4.18 - Variation of piece angle (θ) with time for three different diameters – Stages A, B and C

Variation of apical force and displacement of tree top with time are plotted in Figure 4.19 and Figure 4.20, respectively. It is clear that for thicker tree trunks the maximum force during stage D of the cutting process is higher (Figure 4.19).

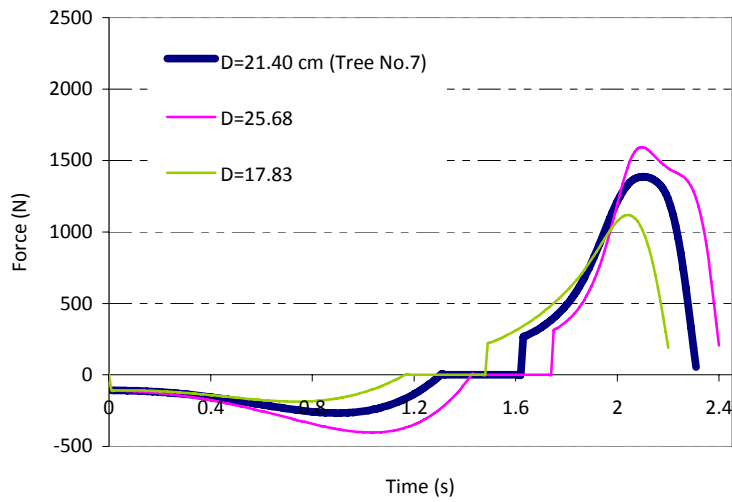


Figure 4.19 - Apical force induced during cutting process to the tree for three different diameters

In Figure 4.20, displacement of tree top is shown from the beginning of cutting process to the moment when the piece hits the tree. It is clear from the figure that for the thicker tree the displacement of top of the tree is smaller.

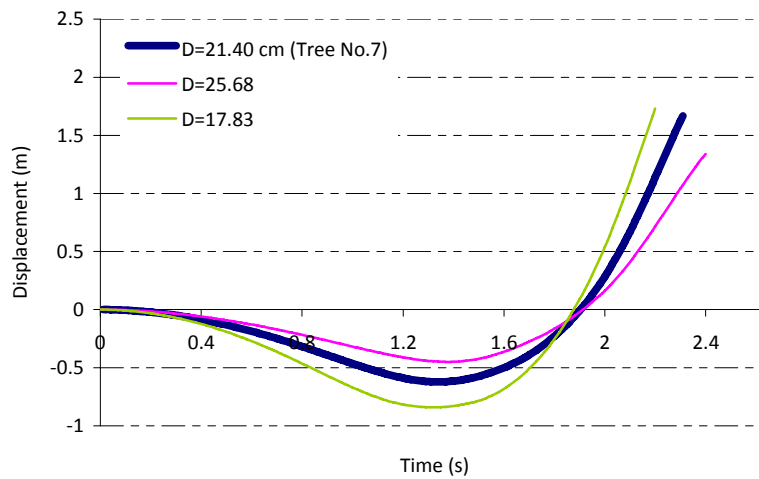


Figure 4.20 - Variation of displacement of tree top with time for three different diameters

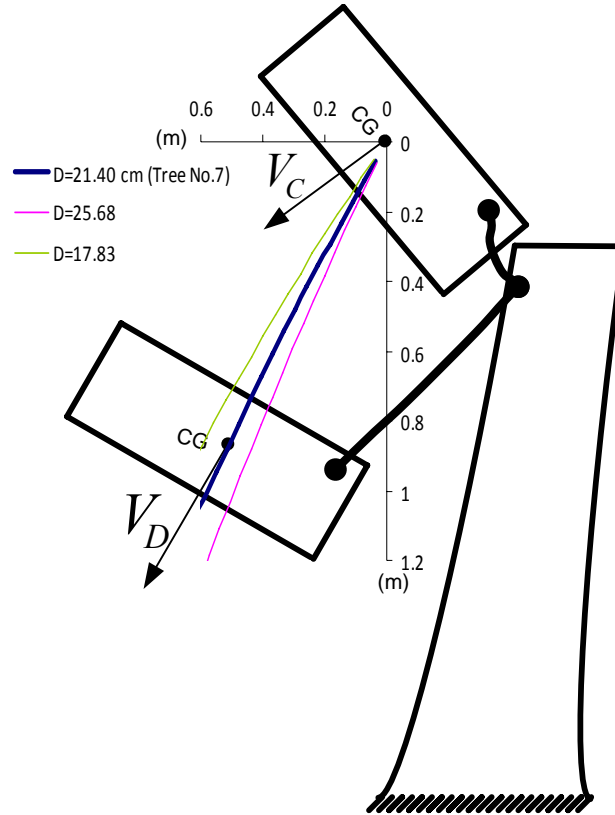


Figure 4.21 - Movement trajectory of the CG of the piece for three different diameters – Stage D

Also, it can be seen in Figure 4.21 that the cut piece of thicker tree moves less in horizontal direction. It can be concluded from the graphs that deflection of thinner tree under cutting process forces is more.

The effect of diameter of tree trunk on maximum value of force function has been studied by plotting the ratio of maximum force³⁰ vs. the ratio of diameter of the tree trunk in Figure 4.22.

It is obvious from Figure 4.22 that, increasing the diameter of tree will increase the maximum force by the same factor. Slope of the trendline of the curve (0.97) shows that

³⁰

$$\text{Diameter Ratio} = \frac{D}{17.83\text{cm}} , \quad \text{Force Ratio} = \frac{\text{Maximum Force (When diameter is } D)}{\text{Maximum Force (When diameter is 17.83cm)}}$$

the maximum force is affected by the diameter of the tree more than other parameters studied in this chapter. Thus the diameter of tree has to be measured accurately.

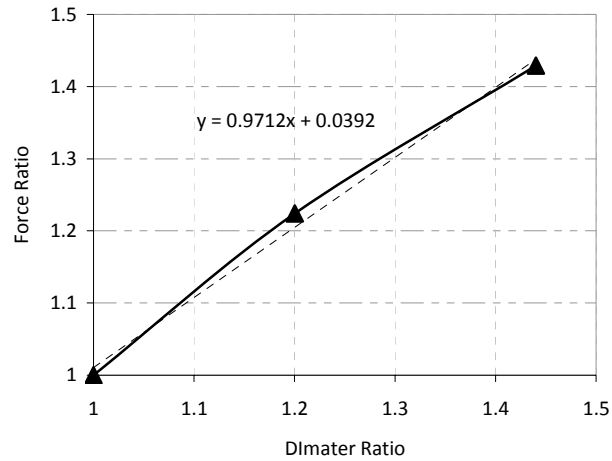


Figure 4.22 - Maximum force ratio vs. Diameter of tree ratio

Relevant parameters of motion of the cut piece and applied force function during cutting process are listed and compared in Table 4.7.

Table 4.7 - Parameters of motion of the cut piece and applied force function during cutting process

PARAMETER \ STAGE		Initial condition	Release point	Beginning of stage E	Impact moment	Average diameter (cm)
		Beginning of stage A	End of stage C	End of stage D	End of stage E	
Time (s)	t	0	1.31	1.62	2.31	21.4 ³¹
		0	1.44	1.74	2.40	25.68
		0	1.18	1.48	2.20	17.83
	Difference (%)	0	10	7	4	25.68
	Difference (%)	0	10	9	5	17.83
Piece angle (rad)	θ and β	$\theta = 0.10$	$\theta = 0.99$ $\beta = 2.15$	$\beta = 1.62$	$\beta = -0.1$	21.4
		$\theta = 0.10$	$\theta = 1.08$ $\beta = 2.06$	$\beta = 1.51$	$\beta = -0.1$	25.68
		$\theta = 0.10$	$\theta = 0.92$ $\beta = 2.22$	$\beta = 1.74$	$\beta = -0.05$	17.83
	Difference (%)	0	9	7	0	25.68
	Difference (%)	0	7	7	50	17.83

³¹ Measured in tree No.7.

PARAMETER \ STAGE		Initial condition	Release point	Beginning of stage E	Impact moment	Average diameter (cm)
		Beginning of stage A	End of stage C	End of stage D	End of stage E	
Angular velocity of piece (rad/s)	θ' and β'	$\theta' = 0$	$\theta' = 1.69$ $\beta' = -1.69$	$\beta' = -1.69$	$\beta' = -2.03$	21.4
		$\theta' = 0$	$\theta' = 1.81$ $\beta' = -1.81$	$\beta' = -1.81$	$\beta' = -1.76$	25.68
		$\theta' = 0$	$\theta' = 1.60$ $\beta' = -1.60$	$\beta' = -1.60$	$\beta' = -3.11$	17.83
	Difference (%)	0	7	7	13	25.68
	Difference (%)	0	5	5	53	17.83
Horizontal deflection of trunk (m)	u	0	-0.62	-0.48	1.67	21.4
		0	-0.44	-0.23	1.33	25.68
		0	-0.81	-0.79	1.73	17.83
	Difference (%)	0	29	52	20	25.68
	Difference (%)	0	30	65	4	17.83
Horizontal velocity of trunk (m/s)	u'	0	-0.11	0.92	4.41	21.4
		0	0.22	1.05	2.53	25.68
		0	-0.50	0.55	6.13	17.83
	Difference (%)	0	300	14	43	25.68
	Difference (%)	0	354	40	39	17.83

CHAPTER 5

CONCLUSION

The thesis presented the first research which studies tree dynamic behavior under apical forces generated during cutting process, while most of recent researches just studied effects of environmental loads on trees (Refer to Section 1.4 – Literature Review).

In the thesis, the motion function for the cut piece and forces due to cutting process were formulated in a general case and calculated for a sample tree. Displacement of tree top and axial strain near the bottom of the tree were two outputs of the research. The field measurements were used to assess the accuracy and validity of the schemed models and it was concluded by comparing the axial strain near the bottom of tree trunk that the proposed model gives a reasonable force function for cutting process.

The model proposed in this thesis was only tested for tree No.7 so the results and findings are limited to similar trees with tree No.7. To extrapolate these findings to a larger group of trees, the model has to be verified by more field measurements.

The unmodified FE model of tree trunk, modeled with geometry and material properties measured in the field, did not accurately represent the dynamic behavior of tree trunk. It was observed that the natural frequency of vibrations of real tree is higher than the frequency of vibrations of FE model. The parameters affecting dynamic properties of the tree are dimensions, density, modulus of elasticity, trunk-ground connection, and defects in the trunk. Thus, a parametric analysis was carried out to find how much error in measuring each of these parameters is required to cause the mentioned difference in natural frequency. The parametric analysis indicated that 11%, 31% and 71% error in

measuring the height of tree trunk, average diameter and modulus of elasticity, respectively, is adequate to create a 31% error in calculating natural frequency.

The effect of the defect size on the dynamic behavior of tree trunk was also studied and it was observed that frequencies of the first bending and the axial modes of vibration decrease with increasing defect length. But frequencies of the second and third modes of vibration behave differently. By studying the mode shapes of vibration of cantilever beam in Appendix I, it was concluded that the phenomenon may be originated from closeness of defect location and peak in the second and third mode shapes.

The dynamic analysis with loads calculated in Chapter 2 was done on unmodified and modified FE models in SAP2000. The axial strain at the bottom of tree in unmodified model indicates more than 30% difference with measurements. The difference in modified model is less than 20%.

The axial strain near tree bottom indicates that the most critical moment of cutting process is stage E where the maximum force is induced to the tree top. The stages A, B and C are not very critical since during these stages the cut piece cannot induce a large force to tree top.

Beam elements were used by Kerzenmacher (1997) and Niklas(1999) to model tree [1,6]. In this research, the ability of beam elements to model the tree under cutting forces was studied and it was also concluded that the simplified FE model meshed with 1.5m beam elements is a reasonably accurate simplification of the FE model meshed with 0.1m solid elements, and the simplification decreased the analysis running time from 10 seconds to 1 second. In addition, the analytical method proposed in the thesis to skip the

FE modeling (Refer to Section 3.3) can be used by an engineer who is inexperienced in FEM in order to avoid the complexities and errors that would come up in FEM.

Since proposed models in Chapter 2 were based on some assumed values for parameters which were not measured in field experiments, the sensitivity of results to these parameters is studied in Chapter 4. It was shown that the two unmeasured variables (initial rotation of the cut piece and V_{Δ}) do not affect the maximum force and response of tree significantly. So it is not critical to measure these two parameters precisely and rough numbers suggested in the thesis can be used.

The sensitivity analysis has been done for three other parameters: height of tree trunk, mass of cut piece and diameter of tree. It was observed that increasing the height of tree by one unit decreases maximum force by 0.21 unit (this value is called sensitivity factor). This value for other parameters is listed in Table 5.1.

Table 5.1 - Sensitivity of maximum force to each parameter³²

Height of tree trunk	-0.219
Mass of cut piece	0.822
Diameter of tree	0.971

It can be concluded that the diameter of tree has the most effect on the maximum force and response of tree so they have to be measured precisely. This finding was predictable because the diameter of tree has the most effect on the rigidity of the tree. If tree trunk is assumed to behave like a cantilever column, the rigidity of the column under horizontal

³² Indicates how much the maximum force will change by increasing each parameter by one unit.

force is proportional to EI/H^3 where I is $\frac{\pi r^4}{4}$ (r is radius). Thus rigidity of tree trunk is being affected by diameter of tree more than height and modulus of elasticity.

5.1. Future research on the topic

The research is very rare in the case of the variety of the topics it covers from modeling falling piece motion to studying dynamic properties of tree trunk, and finite element modeling. Hence, many extensions can be performed on it.

1) In this research the only available experiment data, explained in Section 1.5, is a set of data gathered from Red Pine trees during cutting process. The strain near the bottom of the tree was the only time history parameter recorded during these field measurements. Therefore performing more experiments and gathering more data such as displacement and acceleration at the top of the tree can be the next steps for future researches.

2) Obtaining a spectrum by running the proposed model in the thesis for hundreds of cases with different geometric and material properties. Proposed model in the thesis can be run for large number of trees and in each case the natural frequency of vibrations of tree and maximum displacement of tree top (or maximum axial strain near tree bottom) must be calculated. The data from these analyses can be used to make a spectrum which indicates maximum displacement of tree top (or maximum axial strain near tree bottom) vs. frequency. The spectrum provides a powerful tool for the arborist to predict the ultimate displacement and strains generated during cutting process.

APPENDIX A

CALCULATING M, K AND C OF THE TRUNK SIMPLIFIED MODEL

Tree horizontal deflections were obtained by modeling the trunk as a dynamic model consisting of a concentrated mass, linear spring, viscous damper and roller (Figure A-1). Now, to find mentioned modeling parameters, tree trunk is assumed to be a cantilever partial cone. Then M, K and C will be estimated using an assumed shape function and substituting it into equation of dynamic equilibrium for distributed mass and elasticity systems [18]. The equation of dynamic equilibrium can be reformulated conveniently by work or energy principle to get equations (A-1, A-2 and A-3).

$$M = \int_0^H m(z) \cdot \psi(z)^2 \cdot dz \quad (A-1)$$

$$K = \int_0^H EI(z) \cdot \psi''(z)^2 \cdot dz \quad (A-2)$$

$$C = 2 \cdot \xi \cdot \omega \cdot M \quad (A-3)$$

In which $m(z)$ is mass per unit length of trunk, $EI(z)$ is flexural rigidity, $\psi(z)$ is assumed shape function (Figure A-1-c) and z is shown in Figure A-1-b. The natural frequency of the system, ω , is calculated by equation (A-4).

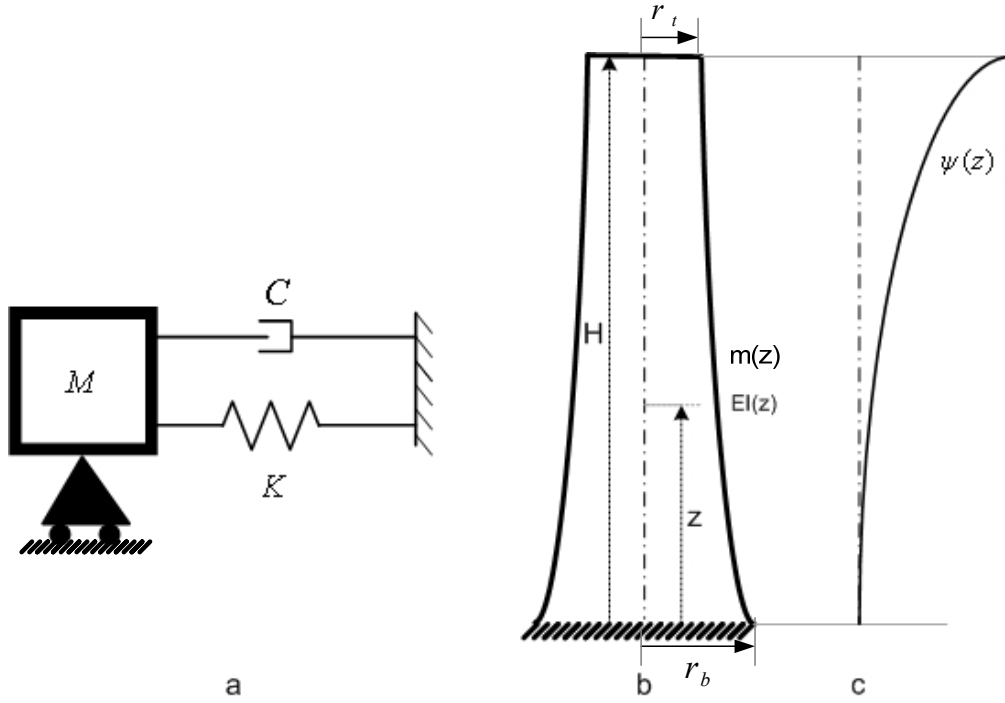


Figure A-1. Tree trunk simplified dynamic model

$$\omega = \sqrt{K/M} \quad (A-4)$$

The assumed shape function $\psi(z)$ for cantilever beam should satisfy boundary conditions $\psi(0)=0$ and $\psi'(0) = 0$ (Figure A-1-c). Shape function (A-5) fulfills these boundary conditions.

$$\psi(z) = 1 - \cos\left(\frac{\pi \cdot z}{2 \cdot H}\right) \quad (A-5)$$

The distributed properties, $m(z)$, $EI(z)$ are calculated by assuming that the trunk cross section varies linearly. The radius of the trunk in each section is calculated by applying geometric proportion rule.

$$r(z) = r_b + \frac{(r_t - r_b)}{H} z \quad (A-6)$$

In which subscripts b and t stand for bottom and top of trunk, respectively.

Then $r(z)$ is substituted in equations(A-7 and A-8) to obtain $m(z)$ and $EI(z)$. The tree modulus, E , is assumed to be constant along the trunk height.

$$m(z) = \rho \cdot \pi \cdot r(z)^2 \quad (A-7)$$

$$EI(z) = \frac{\pi}{4} r(z)^4 \cdot E \quad (A-8)$$

After substituting $m(z)$, $EI(z)$ and $\psi(z)$ into equations (A-1,A-2 and A-3), modeling parameters (M,K and C) are obtained. The damping ratio, ξ , was assumed equal to 0.10 (Refer to Section 1.5 for calculation of damping ratio).

APPENDIX B

STUDY OF THE MODELING OF TREE TRUNK AS A SIMPLIFIED DYNAMIC MODEL

In Chapter 2, the horizontal deflection of tree top was obtained by modeling the tree trunk as a dynamic model consisting of a concentrated mass, linear spring, viscous damper and roller (Figure B.1). Dynamic parameters of tree trunk were obtained modeling the tree trunk as cantilever truncated cone. Then M , K and C were estimated (in Appendix A) using an assumed shape function and equations of dynamic equilibrium for distributed mass and elasticity systems.

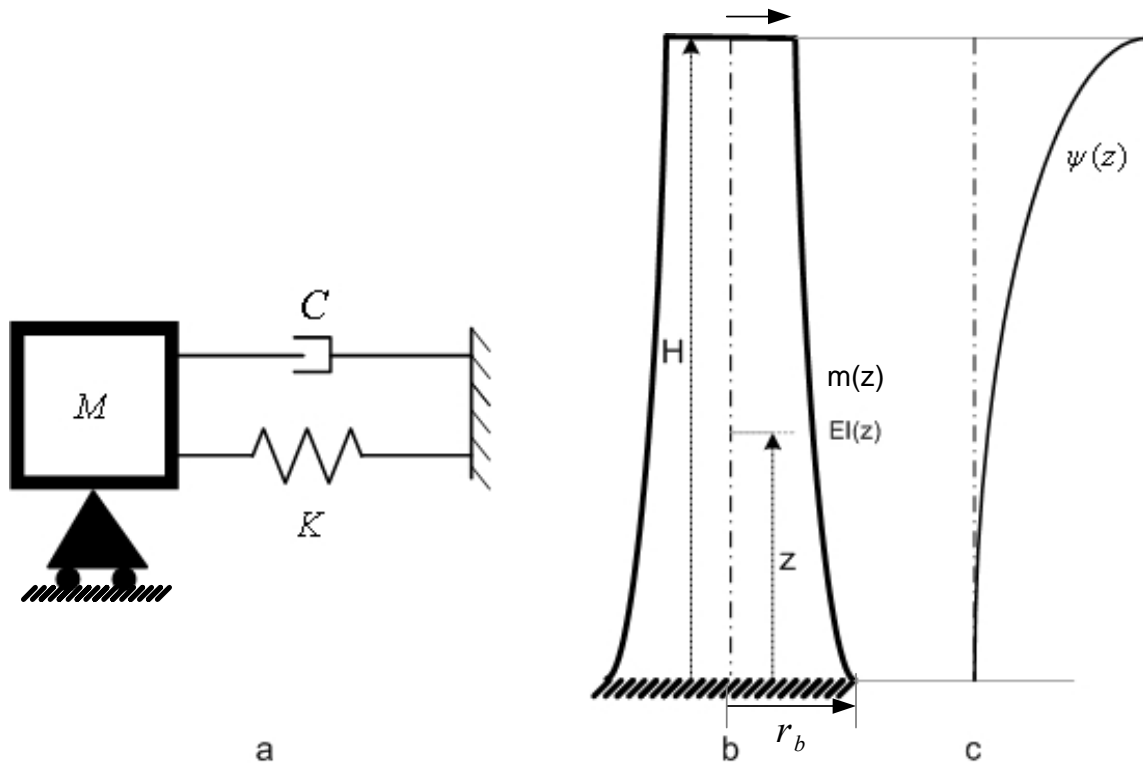


Figure B.1 - Simplified Model of Tree Trunk

This dynamic model is studied to find the accuracy of the simplification. Simplified dynamic model is solved numerically under various loading functions $F(t)$ using equation (B.1).

$$M \cdot \ddot{u} + C \cdot \dot{u} + K \cdot u = F(t) \quad (B.1)$$

Where u is the displacement of tree top.

To solve the simplified model numerically, C , M , K values for tree No.7 from Appendix A are substituted into equation (B.1) and the Runge-Kutta method is used to solve the equation numerically. This equation can be rewritten as discussed in Chapter 2 to be solved with the Runge Kutta method.

$$\ddot{u} = \frac{F(t) - C \cdot \dot{u} - K \cdot u}{M} \quad (B.2)$$

Table B.1 - Tree No.7 dynamic properties from Appendix A

Parameter	Value
Mass (Kg)	94.03
Spring Stiffness (N/m)	575.87
Damper Constant (N.s/m)	23.27
ξ	10 %
Frequency (Hz)	0.394

Then the FEM of Tree No.7 in SAP2000 with solid elements and radial meshing is used to find the tree top displacement under various apical loading functions. The response

using FEM is compared with the numerical solution of the model to study the accuracy of the simplified dynamic model of the tree.

The first load function used is a simple ramped force as plotted in Figure B.2. The frequency of the force function is one eighth of the natural frequency of the model.

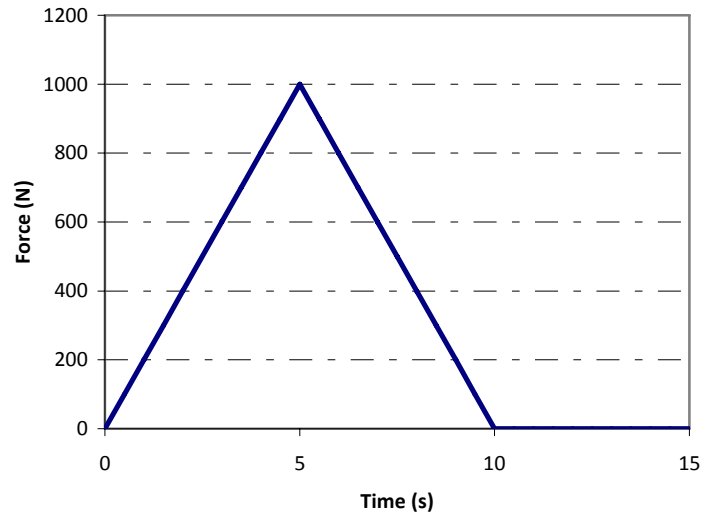


Figure B.2 - Applied force function

The displacement of tree top from FE model and simplified dynamic model are compared in Figure B.3.

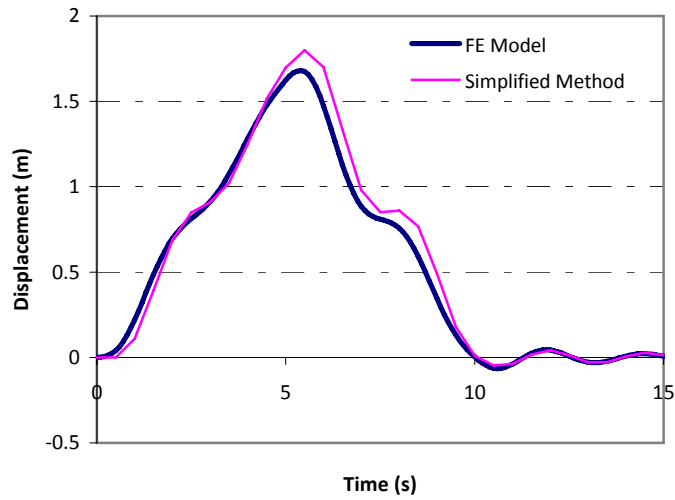


Figure B.3 - Displacement of tree top from FE model and Simplified dynamic model

The second force function sample is a sine shape function plotted in Figure B.4. The frequency of this force function is two times the natural frequency of the model (0.39 Hz).

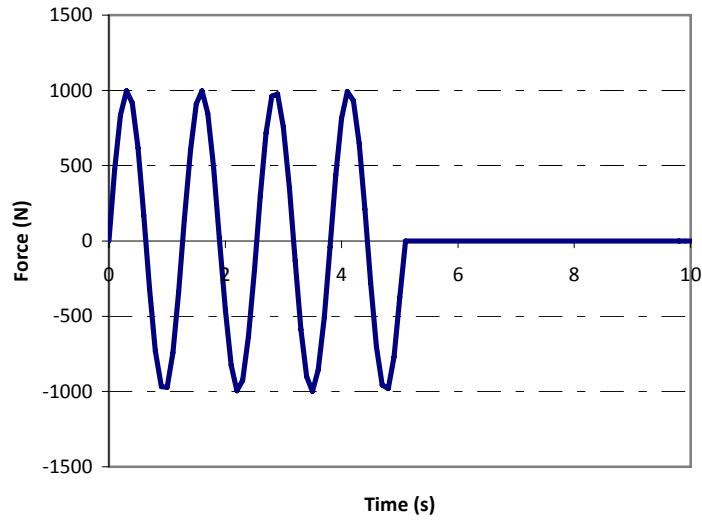


Figure B.4 - Applied force function

The displacement of tree top from FE model and simplified dynamic model are compared in Figure B.5.

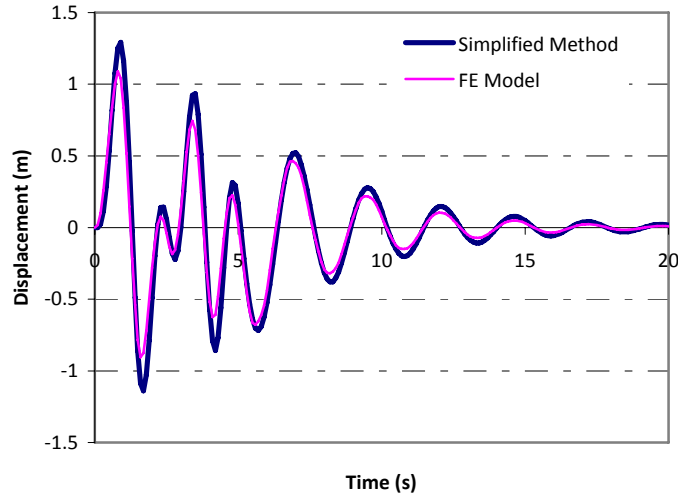


Figure B.5 - Displacement of tree top from FE model and Simplified dynamic model

The probable reasons for the slight differences observed in the results are:

- Single degree of freedom assumption in simplified method: the assumption results in having only one mode shape and completely neglecting effect of other vibration modes.
- It is assumed in simplified method that the shape of tree deflection

$$\text{is } \psi(z) = 1 - \cos\left(\frac{\pi \cdot z}{2 \cdot H}\right).$$

Finally, it can be concluded that assuming tree as a dynamic model consisting of a concentrated mass, linear spring and viscous damper is an accurate assumption. Also this study can verify the FE model because the proposed analytical model is based on a well accepted mechanical model.

APPENDIX C
PULLEY AND ROPE MODELING

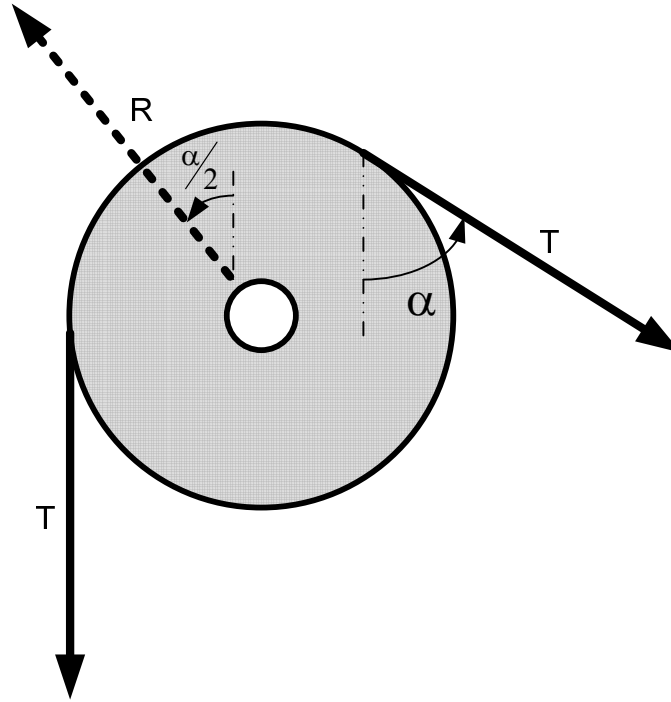


Figure C-1 - Pulley and rope

Friction between pulley and rope was assumed to be negligible. Thus the equation is obtained from static load equilibrium:

$$R = 2.T.\cos\left(\frac{\alpha}{2}\right) \quad (C-1)$$

Now, by substituting equation above into equation (C-2), p and q are obtained:

$$R = p \cdot T + q \quad (C-2)$$

$$p = 2.\cos\left(\frac{\alpha}{2}\right) \quad (C-3)$$

$$q = 0 \quad (C-4)$$

APPENDIX D

RUNGE KUTTA METHOD OF ORDER FOUR (RK4)³³

The Runge–Kutta methods are an important group of iterative numerical methods to estimate the solutions of ordinary differential equations. Runge–Kutta methods were formulated around 1900 by the German mathematicians C. Runge and M.W. Kutta.

Let a differential equation with boundary condition be specified as follows:

$$y' = f(t, y), \quad y(t_0) = y_0$$

Then, the Runge Kutta Method of Order Four (RK4) for mentioned problem is formulized by the following equations:

$$y_{n+1} = y_n + \frac{h}{6}(k_1 + 2k_2 + 2k_3 + k_4)$$

$$t_{n+1} = t_n + h$$

Where y_{n+1} is the RK4 approximation of $y(t_{n+1})$, and

$$k_1 = f(t_n, y_n)$$

$$k_2 = f\left(t_n + \frac{h}{2}, y_n + \frac{h}{2}k_1\right)$$

$$k_3 = f\left(t_n + \frac{h}{2}, y_n + \frac{h}{2}k_2\right)$$

$$k_4 = f(t_n + h, y_n + hk_3)$$

The Runge Kutta Method of Order Four (RK4) has the error per step of the order of h^5 , and the total accumulated error of the order of h^4 .

³³ Butcher, J. C. (1993). Numerical methods for ordinary differential equations.

APPENDIX E

LAGRANGIAN APPROACH

E.1. Summary of Lagrangian Approach³⁴

Lagrangian mechanics is a branch of classical mechanics and its equations are obtained by combining conservation of momentum with conservation of energy laws. Lagrangian mechanics was developed by Joseph Louis Lagrange in 1788. The Lagrangian is:

$$\Phi = \text{Kinetic Energy} - \text{Potential Energy}$$

And the Euler-Lagrange equation is:

$$\frac{d}{dt} \left(\frac{d}{d\dot{\alpha}} \Phi \right) - \frac{d}{d\alpha} \Phi = 0 \quad (\text{E-1})$$

$$\frac{d}{dt} \left(\frac{d}{d\dot{\beta}} \Phi \right) - \frac{d}{d\beta} \Phi = 0 \quad (\text{E-2})$$

Where α and β are degrees of freedom of system. It should be noted that the use of generalized coordinates may significantly simplify analysis of system.

E.2. Lagrangian Approach in Modeling of Stages A, B, C

$$\Phi = \frac{1}{2} M \dot{u}^2 + \frac{1}{2} m (\dot{u}^2 + d^2 \dot{\theta}^2 + 2.d \dot{u} \dot{\theta} \cos(\theta)) - \frac{1}{2} K u^2 - m.g.d \cos(\theta) - \int C \dot{u} du \quad (\text{E-3})$$

Now Lagrangian, Φ , should be differentiated with respect to main degrees of freedom like below.

$$\frac{d}{dt} \left(\frac{d}{d\dot{\theta}} \Phi \right) - \frac{d}{d\theta} \Phi = 0 \quad (\text{E-4})$$

³⁴ Torby, Bruce (1984). "Energy Methods". *Advanced Dynamics for Engineers*. HRW Series in Mechanical Engineering. United States of America: CBS College Publishing.

$$\frac{d}{dt} \left(\frac{d}{du} \Phi \right) - \frac{d}{du} \Phi = 0 \quad (\text{E-5})$$

Final result after doing above calculations is similar to the obtained equations from Newtonian approach:

$$\ddot{\theta}.d_{CG} + \ddot{u}.\cos(\theta) - g.\sin(\theta) = 0 \quad (\text{E-6})$$

$$\ddot{\theta}.d_{CG}.\cos(\theta) - \dot{\theta}^2.d_{CG}.\sin(\theta) + \ddot{u}.\left(\frac{M}{m} + 1\right) + \dot{u}.\frac{C}{M} + u.\frac{K}{M} = 0 \quad (\text{E-7})$$

E.3. Lagrangian Approach in Simplified Modeling of Stage E

$$\Phi = \frac{1}{2}.m.(\dot{x}^2 + \dot{y}^2) + \frac{1}{2}.I_c.\dot{\alpha}^2 + m.g.y \quad (\text{E-8})$$

Now Lagrangian, Φ , should be differentiated with respect to main degrees of freedom like below. It should be noticed that x and y should be substituted using equations (2.55 and (2.56) before doing below derivatives.

$$\frac{d}{dt} \left(\frac{d}{d\dot{\alpha}} \Phi \right) - \frac{d}{d\alpha} \Phi = 0 \quad (\text{E-9})$$

$$\frac{d}{dt} \left(\frac{d}{d\dot{\beta}} \Phi \right) - \frac{d}{d\beta} \Phi = 0 \quad (\text{E-10})$$

Final result after doing above calculations is:

$$\ddot{\alpha}.L + \ddot{\beta}.L_1.\cos(\alpha - \beta) + \dot{\beta}^2.L_1.\sin(\alpha - \beta) + g.\sin(\alpha) = 0 \quad (\text{E-11})$$

$$\ddot{\alpha}.L.\cos(\alpha - \beta) + \ddot{\beta}.\left(L_1 + \frac{J_c}{L_1}\right) - \dot{\alpha}^2.L_1.\sin(\alpha - \beta) + g.\sin(\beta) = 0 \quad (\text{E-12})$$

It can be justified easily that two above equations are the linear product of Newtonian results (Equations 2.60 and 2.61)

APPENDIX F

INFORMATION ABOUT RED PINE ³⁵

Red Pine is called *Pinus Resinosa*, Norway Pine, Eastern Red Pine, Pin Rouge and its origin is from some places in Canada and the following places in United States:

Connecticut, Illinois, Maine, Massachusetts, Michigan, Minnesota, New Hampshire, New Jersey, New York, Pennsylvania, Vermont, West Virginia, Wisconsin.

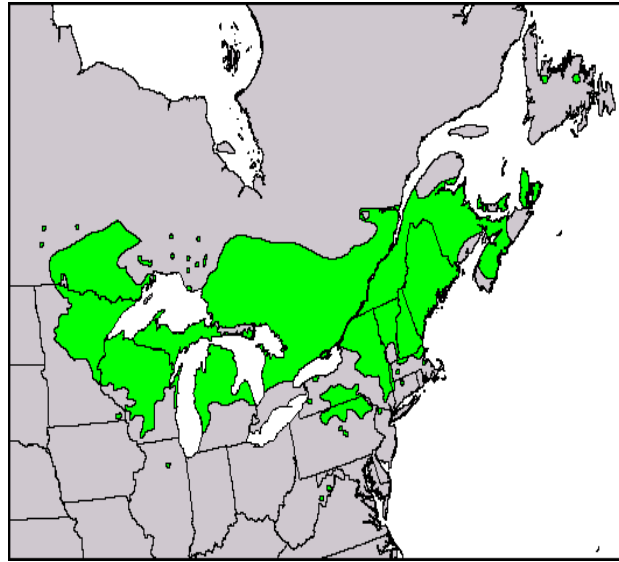


Figure F.1 (at left) – Old tree in Itasca State Park, Minnesota
Figure F.2 (at right) – Distribution map (USGS 1999)

Red pine has a smooth, straight, clear bole of little taper and an oval crown which is symmetric. The sizes are different and it can be from about 50 to 80 feet in height and 1 to 3 feet in diameter at breast height in developed trees. The crown is conical in the first years but tree getting older, the crown is becoming a narrow rounded dome. The name

³⁵ Reference: Gymnosperm database - <http://www.conifers.org>

“Red Pine” has derived from its thin, flaky and bright orange-red upper crown although it’s thick and gray-brown at the base of the tree.



Figure F-3 - Pollen cones of *Pinus resinosa* in spring

The wood can be used for poles, lumber, cabin logs, railway ties, post, pulpwood, and fuel and the tree is also used for landscaping also for snowbreaks, windbreaks, and Christmas trees.

The wood is hard and very useful and it’s easy to work with as it holds nails and screws well. Therefore it’s used for structural purposes as well as outdoor furniture and toys. Although trees can be injured or killed by disease, insects, animals, fire or weather, Red pine has fewer natural enemies than most other trees.



Figure F.4 - Old-growth red pine, Algoma Highlands, Ontario

APPENDIX G

TREE NO.7 MEASUREMENTS AND DATA

Available data from field measurements on tree No. 7 is listed in following table and is used during modeling.








Table G.1 – Field Measurement Data

Available Data		
Piece Mass (kg)	m	113.4
Piece Length (m)	L_P	6.10
Rope Length (m)	$L_{Rope\ or\ L}$	1
Distance to Center of Gravity of Piece (m)	$L_{CG\ or\ d_{CG}}$	2.77
Rotation Length (m)	L_I	2.06
Rotational Inertia / Piece Mass	J_C	3.101

For more information about measurements and experimental data see Section 1.5. Refer to Section 2.3 and Figure 2.28 where the listed variables were plotted.

APPENDIX H

TRUNK DEFECTS WHICH MAY CAUSE FAILURE³⁶

Decay	Canker
	
Flush cuts	Crack - Vertical
	
Lightning strike damage	Fire Damage
	
Insect Injury – only if related to failure	Mechanical injury – people or natural
	

³⁶ E.T. Smiley (2005), User manual of International Tree Failure Database, *USDA Forest Service*.

APPENDIX I

CODES WRITTEN IN C++

I.1. C++ code to solve stages A, B, C and D equations

The code is related to Sections 2.1 and 2.2.

```
#include <stdio.h>
#include <stdlib.h>
#include <math.h>
#define PI 3.14159265
#define N 4 /* Number of equations */
#define g 9.81 /* Gravity */
#define d 2.77 /* CG length */
#define K 575.988 /* Dummy Spring- K=575.988 */
#define m 113.4 /*Mass*/
#define m1 94.023 /*Dummy Mass- M=94.023*/
#define c 46.544 /*Dummy Damping- C=46.544*/
# define Vdelta 2
# define Wratio 1
# define L0 1 /*Rope Length*/
void RK4(double xin, double yin[], double yout[], double h);
void derivs(double xin, double yin[], double DY[]);
void RK42(double xin, double yin[], double yout[], double h);
void derivs2(double xin, double yin[], double DY[]);
int main(int argc, char *argv[])
{
int i = 0, NSTEP;
double h, TMIN, TMAX, TETA0, TETA0dot, TETA2dot0, U0, Udot0, U2dot0, Energy0, EnergyC0;
double yin[N], yout[N];
double *t, *TETA, *TETA0dot, *TETA2dot, *U, *Udot, *U2dot, *Energy, *EnergyC;
/* Initial Condition - Angles in Radian */
TMIN = 0;
TMAX = 3;
TETA0 = 0.1;
TETA0dot = 0;
TETA2dot0 = 0;
U0 = 0;
Udot0 = 0;
U2dot0 = 0;
Energy0 = 0;
EnergyC0 = 0;
h = 0.01;
NSTEP = int(1 + (TMAX - TMIN)/h);
/* Allocate memory for array */
t = (double *) malloc(NSTEP * sizeof(double));
TETA = (double *) malloc(NSTEP * sizeof(double));
TETA0dot = (double *) malloc(NSTEP * sizeof(double));
TETA2dot = (double *) malloc(NSTEP * sizeof(double));
U = (double *) malloc(NSTEP * sizeof(double));
Udot = (double *) malloc(NSTEP * sizeof(double));
```

```

U2dot = (double *) malloc(NSTEP*sizeof(double));
Energy = (double *) malloc(NSTEP*sizeof(double));
EnergyC = (double *) malloc(NSTEP*sizeof(double));
/* Stepsize */
for (i = 0; i < NSTEP; i++)
t[i] = TMIN + h*i;
/* Initial values */
TETA[0] = TETA0;
TETAAdot[0] = TETAAdot0;
TETA2dot[0] = TETA2dot0;
U[0] = U0;
Udot[0] = Udot0;
U2dot[0] = U2dot0;
Energy[0] = Energy0;
EnergyC[0] = EnergyC0;
/* Integration */
printf("%f %f %f %f %f %f %f %f %f\n", t[0], TETA[0], TETAAdot[0], TETA2dot[0], U[0], Udot[0],
U2dot[0], Energy[0], EnergyC[0]);
FILE * myfile;
myfile=fopen("ADt7p2.txt","w");
fprintf(myfile,"%f %f %f %f %f %f %f %f %f\n", t[0], TETA[0], TETAAdot[0], TETA2dot[0], U[0],
Udot[0], U2dot[0], Energy[0], EnergyC[0]);
for (i = 0; i < NSTEP - 1; i++)
{
yin[0] = TETA[i];
yin[1] = TETAAdot[i];
yin[2] = U[i];
yin[3] = Udot[i];
RK4(t[i], yin, yout, h);
TETA[i+1] = yout[0];
TETAAdot[i+1] = yout[1];
U[i+1] = yout[2];
Udot[i+1] = yout[3];
double A, B, C, D, E, F;
A = d;
B = cos(yout[0]);
C = -g*sin(yout[0]);
D = d*cos(yout[0]);
E = 1+m1/m;
F = K*yout[2]/m1+c*yout[3]/m1-d*sin(yout[0])*(yout[1]*yout[1]);
TETA2dot[i+1] = (-E*C+B*F)/(A*E-B*D);
U2dot[i+1] = (D*C-A*F)/(A*E-B*D);
Energy[i+1] =
0.5*m1*(yout[3]*yout[3])+0.5*m*(yout[3]*yout[3]+d*d*yout[1]*yout[1]+2*d*yout[1]*yout[3]*B) ;
EnergyC[i+1]=EnergyC[i]+c*(Udot[i+1]+Udot[i])*(U[i+1]-U[i])/2;
printf("%f %f %f %f %f %f %f %f %f\n", t[i+1], TETA[i+1], TETAAdot[i+1], TETA2dot[i+1], U[i+1],
Udot[i+1], U2dot[i+1], Energy[i+1], EnergyC[i+1]);
fprintf(myfile,"%f %f %f %f %f %f %f %f %f\n", t[i+1], TETA[i+1], TETAAdot[i+1], TETA2dot[i+1],
U[i+1], Udot[i+1], U2dot[i+1], Energy[i+1], EnergyC[i+1]);
if ( m1*U2dot[i+1]+K*U[i+1]+c*Udot[i+1]>=0.0) {
break;
}
}
int j ;
j=i+1;
double Vcx, Vcy, Vdx, Vdy, X, Y, Lx, Ly, L, AL, BET;

```



```

{
k1[i] = h*DY[i];
yt[i] = yin[i] + 0.5*k1[i];
}
derivs2(xh, yt, DYt);
for (i = 0; i < N; i++)
{
k2[i] = h*DYt[i];
yt[i] = yin[i] + 0.5*k2[i];
}
derivs2(xh, yt, DYt);
for (i = 0; i < N; i++)
{
k3[i] = h*DYt[i];
yt[i] = yin[i] + k3[i];
}
derivs2(xin + h, yt, DYt);
for (i = 0; i < N; i++)
{
k4[i] = h*DYt[i];
yout[i] = yin[i] + k1[i]/6. + k2[i]/3. + k3[i]/3. + k4[i]/6.;
}
return;
}
void derivs(double xin, double yin[], double DY[])
{
double A, B, C, D, E, F;
A = d;
B = cos(yin[0]);
C = -g*sin(yin[0]);
D = d*cos(yin[0]);
E = 1+m1/m;
F = K*yin[2]/m1+c*yin[3]/m1-d*sin(yin[0])*(yin[1]*yin[1]);
DY[0] = yin[1];
DY[1] = (-E*C+B*F)/(A*E-B*D);
DY[2] = yin[3];
DY[3] = (D*C-A*F)/(A*E-B*D);
return;
}
void RK4(double xin, double yin[], double yout[], double h)
{
/* Runge-Kutta*/
int i;
double hh, xh, DY[N], DYt[N], yt[N], k1[N], k2[N], k3[N], k4[N];
hh = 0.5*h;
xh = xin + hh;
derivs(xin, yin, DY);
for (i = 0; i < N; i++)
{
k1[i] = h*DY[i];
yt[i] = yin[i] + 0.5*k1[i];
}
derivs(xh, yt, DYt);
for (i = 0; i < N; i++)
{
k2[i] = h*DYt[i];

```

```

yt[i] = yin[i] + 0.5*k2[i];
}
derivs(xh, yt, DYt);
for (i = 0; i < N; i++)
{
k3[i] = h*DYt[i];
yt[i] = yin[i] + k3[i];
}
derivs(xin + h, yt, DYt);
for (i = 0; i < N; i++)
{
k4[i] = h*DYt[i];
yout[i] = yin[i] + k1[i]/6. + k2[i]/3. + k3[i]/3. + k4[i]/6.;
}
return;
}

```


I.2. C++ code to solve stage E equations

The code is related to Section 2.3.

```
#include <stdio.h>
#include <stdlib.h>
#include <math.h>
#define PI 3.14159265
#define N 6 /* Number of equations */
#define g 9.81 /* Gravity */
#define L 1.0 /* Rope length */
#define L1 2.06 /* Rotation length */
#define L2 3.06 /* DF center */
#define Jc 3.101 /* Rotational Inertia/mass */
#define K 575.988 /* Dummy Spring- K */
#define q 0 /* Reaction=pT+q */
#define p 1. /* Reaction=pT+q */
#define m 113.4 /*Mass*/
#define m1 94.023 /*Dummy Mass- M*/
#define c 46.544 /*Dummy Damping- C*/
void RK4(float xin, float yin[], float yout[], float h);
void derivs(float xin, float yin[], float DY[]);
int main(int argc, char *argv[])
{
    int i = 0, NSTEP;
    float h, TMIN, TMAX, ALFA0, V0, BETA0, BETA2dot0, W0, U0, Udot0, U2dot0, ALFA2dot0,
        Tension0, Energy0, Reaction0;
    float yin[N], yout[N];
    float *t, *ALFA, *BETA, *V, *W, *U, *Udot, *U2dot, *BETA2dot, *ALFA2dot, *Tension, *Energy,
        *Reaction, EnergyC;
    /* Initial Condition - Angles in Radian */
    TMIN = 1.62;
    TMAX = 4.0;
    ALFA0 = 0.20615;
    V0 = 0;
    ALFA2dot0 = 0;
    BETA0 = 1.6258;
    W0 = 0;
    BETA2dot0 = 0;
    U0 = -0.482377;
    Udot0 = 0.923031;
    U2dot0 = 0;
    Tension0 = 0;
    Energy0 = 0;
    EnergyC=0;
    Reaction0 = 0;
    NSTEP = 1001;
    /* Allocate memory for array */
    t = (float *) malloc(NSTEP*sizeof(float));
    ALFA = (float *) malloc(NSTEP*sizeof(float));
    V = (float *) malloc(NSTEP*sizeof(float));
    ALFA2dot = (float *) malloc(NSTEP*sizeof(float));
    BETA = (float *) malloc(NSTEP*sizeof(float));
    W = (float *) malloc(NSTEP*sizeof(float));
    BETA2dot = (float *) malloc(NSTEP*sizeof(float));
```

```

U = (float *) malloc(NSTEP*sizeof(float));
Udot = (float *) malloc(NSTEP*sizeof(float));
U2dot = (float *) malloc(NSTEP*sizeof(float));
Tension = (float *) malloc(NSTEP*sizeof(float));
Energy = (float *) malloc(NSTEP*sizeof(float));
Reaction = (float *) malloc(NSTEP*sizeof(float));
/* Stepsize */
h = (TMAX - TMIN)/(NSTEP - 1.0);
for (i = 0; i < NSTEP; i++)
t[i] = TMIN + h*i;
/* Initial values */
ALFA[0] = ALFA0;
V[0] = V0;
ALFA2dot[0] = ALFA2dot0;
BETA[0] = BETA0;
W[0] = W0;
BETA2dot[0] = BETA2dot0;
U[0] = U0;
Udot[0] = Udot0;
U2dot[0] = U2dot0;
Tension[0] = Tension0;
Energy[0] = Energy0;
Reaction[0] = Reaction0;
/* Integration */
printf("%f %f %f %f %f %f %f %f %f %f %f %f %f %f\n", t[0], ALFA[0], V[0], ALFA2dot[0], BETA[0],
W[0], BETA2dot[0], U[0], Udot[0], U2dot[0], Tension[0], Energy[0], Reaction[0]);
FILE * myfile;
myfile=fopen("output.txt","w");
fprintf(myfile,"%f %f %f %f %f %f %f %f %f %f %f %f %f %f\n", t[0], ALFA[0], V[0], ALFA2dot[0],
BETA[0], W[0], BETA2dot[0], U[0], Udot[0], U2dot[0], Tension[0], Energy[0], Reaction[0]);
for (i = 0; i < NSTEP - 1; i++)
{
yin[0] = ALFA[i];
yin[1] = V[i];
yin[2] = BETA[i];
yin[3] = W[i];
yin[4] = U[i];
yin[5] = Udot[i];
float A1, A2, A3, A4, B1, B2, B3, B4, B5, C1, C2, C3, C4, C5, C6, C7, C8, C9, E1, E2, E3, F1, F2, F3;
A1 = L*cos(yin[0]);
A2 = -L*sin(yin[0]);
B1 = L1*cos(yin[2]);
B2 = -L1*sin(yin[2]);
C1 = 1+(m1*sin(yin[0])/(p*m*sin(yin[0])));
C2 = c/(p*m);
C3 = K/(p*m);
E1 = (-q*sin(yin[0])/(p*m));
A3 = L*sin(yin[0]);
A4 = L*cos(yin[0]);
B3 = L1*sin(yin[2]);
B4 = L1*cos(yin[2]);
C4 = -m1*cos(yin[0])/(p*m*sin(yin[0]));
C5 = -c*cos(yin[0])/(p*m*sin(yin[0]));
C6 = -K*cos(yin[0])/(p*m*sin(yin[0]));
E2 = (q*cos(yin[0])/(p*m))+g;
B5 = Jc/L1;

```

```

C7 = -m1*sin(yin[0]-yin[2])/(p*m*sin(yin[0]));
C8 = -c*sin(yin[0]-yin[2])/(p*m*sin(yin[0]));
C9 = -K*sin(yin[0]-yin[2])/(p*m*sin(yin[0]));
E3 = (q*sin(yin[0]-yin[2])/(p*m));
F1 = -(yin[1]*yin[1]*A2-(yin[3]*yin[3])*B2-(yin[5])*C2-yin[4]*C3-E1;
F2 = -(yin[1]*yin[1]*A4-(yin[3]*yin[3])*B4-(yin[5])*C5-yin[4]*C6-E2;
F3 = -(yin[5])*C8-yin[4]*C9-E3;
RK4(t[i], yin, yout, h);
ALFA[i+1] = yout[0];
V[i+1] = yout[1];
BETA[i+1] = yout[2];
W[i+1] = yout[3];
U[i+1] = yout[4];
Udot[i+1] = yout[5];
ALFA2dot[i+1] = (1/(-A1*B3*C7+A1*B5*C4+A3*B1*C7-A3*B5*C1))*(-
    F1*B3*C7+F1*B5*C4+F2*B1*C7-F2*B5*C1-F3*B1*C4+F3*B3*C1);
BETA2dot[i+1] = (1/(-A1*B3*C7+A1*B5*C4+A3*B1*C7-A3*B5*C1))*(A3*C7*F1-
    A1*C7*F2+A1*C4*F3-A3*C1*F3);
U2dot[i+1] = (1/(-A1*B3*C7+A1*B5*C4+A3*B1*C7-A3*B5*C1))*(-A3*B5*F1+A1*B5*F2-
    A1*B3*F3+A3*B1*F3);
Tension[i+1] = -
    (m*(g+ALFA2dot[i+1]*L*sin(ALFA[i+1])+BETA2dot[i+1]*L1*sin(BETA[i+1]))+(V[i+1]*V[i+1])*L
    *cos(ALFA[i+1]))/(W[i+1]*W[i+1]*L1*cos(BETA[i+1]))/cos(ALFA[i+1]);
EnergyC=EnergyC+c*(Udot[i+1]+Udot[i])*(U[i+1]-U[i])/2;
Energy[i+1] =
    EnergyC+0.5*m*((Udot[i+1]+L*V[i+1]*cos(ALFA[i+1])+L1*W[i+1]*cos(BETA[i+1]))*(Udot[i+1]+
    L*V[i+1]*cos(ALFA[i+1])+L1*W[i+1]*cos(BETA[i+1]))+(L*V[i+1]*sin(ALFA[i+1])+L1*W[i+1]*s
    in(BETA[i+1]))*(L*V[i+1]*sin(ALFA[i+1])+L1*W[i+1]*sin(BETA[i+1]))+Jc*W[i+1]*W[i+1])-
    m*g*(L*cos(ALFA[i+1])+L1*cos(BETA[i+1]))+0.5*m1*Udot[i+1]*Udot[i+1]+0.5*K*U[i+1]*U[i+
    1]);
Reaction[i+1] = p*Tension[i+1]+q;
printf("%f %f %f %f %f %f %f %f %f %f %f %f %f %f %f %f %f %f %f %f %f %f", t[i+1], ALFA[i+1], V[i+1], ALFA2dot[i+1],
    BETA[i+1], W[i+1], BETA2dot[i+1], U[i+1], Udot[i+1], U2dot[i+1], Tension[i+1], Energy[i+1],
    Reaction[i+1]);
fprintf(myfile, "%f %f %f %f %f %f %f %f %f %f %f %f %f %f %f %f %f %f %f %f %f %f", t[i+1], ALFA[i+1], V[i+1],
    ALFA2dot[i+1], BETA[i+1], W[i+1], BETA2dot[i+1], U[i+1], Udot[i+1], U2dot[i+1], Tension[i+1],
    Energy[i+1], Reaction[i+1]);
}
fclose(myfile);
return 0;
}
void derivs(float xin, float yin[], float DY[])
{
float A1, A2, A3, A4, B1, B2, B3, B4, B5, C1, C2, C3, C4, C5, C6, C7, C8, C9, E1, E2, E3, F1, F2, F3;
A1 = L*cos(yin[0]);
A2 = -L*sin(yin[0]);
B1 = L1*cos(yin[2]);
B2 = -L1*sin(yin[2]);
C1 = 1+(m1*sin(yin[0])/(p*m*sin(yin[0])));
C2 = c/(p*m);
C3 = K/(p*m);
E1 = (-q*sin(yin[0])/(p*m));
A3 = L*sin(yin[0]);
A4 = L*cos(yin[0]);
B3 = L1*sin(yin[2]);
B4 = L1*cos(yin[2]);

```

```

C4 = -m1*cos(yin[0])/(p*m*sin(yin[0]));
C5 = -c*cos(yin[0])/(p*m*sin(yin[0]));
C6 = -K*cos(yin[0])/(p*m*sin(yin[0]));
E2 = (q*cos(yin[0])/(p*m))+g;
B5 = Jc/L1;
C7 = -m1*sin(yin[0]-yin[2])/(p*m*sin(yin[0]));
C8 = -c*sin(yin[0]-yin[2])/(p*m*sin(yin[0]));
C9 = -K*sin(yin[0]-yin[2])/(p*m*sin(yin[0]));
E3 = (q*sin(yin[0]-yin[2])/(p*m));
F1 = -(yin[1]*yin[1])*A2-(yin[3]*yin[3])*B2-(yin[5])*C2-yin[4]*C3-E1;
F2 = -(yin[1]*yin[1])*A4-(yin[3]*yin[3])*B4-(yin[5])*C5-yin[4]*C6-E2;
F3 = -(yin[5])*C8-yin[4]*C9-E3;
DY[0] = yin[1];
DY[1] = (1/(-A1*B3*C7+A1*B5*C4+A3*B1*C7-A3*B5*C1))*(-F1*B3*C7+F1*B5*C4+F2*B1*C7-
F2*B5*C1-F3*B1*C4+F3*B3*C1);
DY[2] = yin[3];
DY[3] = (1/(-A1*B3*C7+A1*B5*C4+A3*B1*C7-A3*B5*C1))*(A3*C7*F1-A1*C7*F2+A1*C4*F3-
A3*C1*F3);
DY[4] = yin[5];
DY[5] = (1/(-A1*B3*C7+A1*B5*C4+A3*B1*C7-A3*B5*C1))*(-A3*B5*F1+A1*B5*F2-
A1*B3*F3+A3*B1*F3);
return;
}
void RK4(float xin, float yin[], float yout[], float h)
{
/* Runge-Kutta*/
int i;
float hh, xh, DYt[N], DYt[N], yt[N], k1[N], k2[N], k3[N], k4[N];
hh = 0.5*h;
xh = xin + hh;
derivs(xin, yin, DY);
for (i = 0; i < N; i++)
{
k1[i] = h*DY[i];
yt[i] = yin[i] + 0.5*k1[i];
}
derivs(xh, yt, DYt);
for (i = 0; i < N; i++)
{
k2[i] = h*DYt[i];
yt[i] = yin[i] + 0.5*k2[i];
}
derivs(xh, yt, DYt);
for (i = 0; i < N; i++)
{
k3[i] = h*DYt[i];
yt[i] = yin[i] + k3[i];
}
derivs(xin + h, yt, DYt);
for (i = 0; i < N; i++)
{
k4[i] = h*DYt[i];
yout[i] = yin[i] + k1[i]/6. + k2[i]/3. + k3[i]/3. + k4[i]/6.;
}
return;
}

```

BIBLIOGRAPHY

- [1] KERZENMACHER T. and GARDINER B. (1997). "A Mathematical Model to Describe the Dynamic Response of a Spruce Tree to the Wind", *Trees-Structure and Function*, 12(6), 385-394.
- [2] GARDINER B. (1989). "Mechanical Characteristics of Sitka spruce", *Forestry Commission*, 24.
- [3] BRUCHERT F., SPECK O., SPATZ H.C. (2003). "Oscillations of Plants' Stems and Their Damping: Theory and Experimentation", *Philos Trans R Soc Lond B Biol Sci.*, 358(1437), 1487–1492.
- [4] SPATZ H.C., BRUCHERT F. (2007). "Multiple resonance damping or how do trees escape dangerously large oscillations?" *American Journal of Botany*, 94, 1603-1611.
- [5] YUNG C., FRIDLEY, R.B. (1975). "Simulation of Vibration of Whole Tree System Using Finite Element".
- [6] NIKLAS K.J, SPATZ H.C. (1999). "Methods for Calculating Factors of Safety for Plant Stems", *Journal of Experimental Biology*, 202(23), 3273-3280.
- [7] SPECK O., SPATZ H.C. (2004). "Damped oscillations of the Giant Reed *Arundo Donax*", *American Journal of Botany*, 91, 789-796.
- [8] SPATZ H.C., SPECK O. (2002). "Oscillation Frequencies of Tapered Plant Stems", *American Journal of Botany*, 89, 1-11.

- [9] MOORE J.R., MAGUIRE D.A. (2008). "Simulating the Dynamic Behavior of Douglas-Fir Tree under Applied Load by Finite Element Method", *Tree Physiology*, 28(1), 75-83.
- [10] MOORE J.R., MAGUIRE D.A. (2004). "Natural Sway Frequencies and Damping Ratios of Trees", *Trees-Structure and Function*, 18(2), 195-203.
- [11] MILNE R. (1991). "Dynamics of Swaying of Picea-Sitchensis", *Tree Physiology*, 9(3), 383-399.
- [12] JAMES R.K., HARITOS N., ADES K.P. (2006). "Mechanical Stability of Trees under Dynamic Loads", *American Journal of Botany*, 96, 1454-1461.
- [13] PELTOLA H. (1996). "Swaying of Trees in Response to Wind and Thinning in a Stand of Scots Pine", *Boundary-Layer Meteorology*, 77(3), 285-304.
- [14] QUEIROZ D. et al. (2000). "Vibration Analysis of Coffee Tree by Using Finite Element Analysis". *ASAE Annual International Meeting*, 9(12), 1-21.
- [15] JONSSON M.J., FOETZKI A., KALBERER M., LUNDSTROM T., AMMANN W., STOCKLI V. (2007). "Natural Frequencies and Damping Ratios of Norway Spruce", *Trees-Structure and Function*, 21(5), 541-548.
- [16] SPATZ H.C., ZEBROWSKI J. (2001). "Oscillation Frequencies of Plant Stems with Apical Loads", *Planta*, 214(2), 215-219.
- [17] SMILEY E.T., MATHENY N., and CLARK J. (2006) *International Tree Failure Database: User Manual*.
- [18] CHOPRA A.K. (1995) *Dynamics of Structures*, Prentice Hall, NJ2001.

[19] *Reducing Hazard in the Urban Forest*, the California Tree Failure Report Program (CTFRP), 1993-1994.

[20] JOHNSON W.D. (1981), "Tree Hazards: Recognition and Reduction in Recreation Sites", *Region Tech. Rept.*, R2.

[21] YEHB. T., HARTZ J. AND BROWN C. B. (1971) *Damping Sources in Wood Structures*.

[22] BISHOP R. E. D., JOHNSON D. C (1979) *the Mechanics of Vibration*, University Press.

[23] KANE B., BRENA S., AUTIO W. (2009). "Forces and Stresses Generated During Rigging Operations", *Arboriculture & Urban Forestry*, 35(2), 68-74.